

3. SITE 1262¹

Shipboard Scientific Party²

INTRODUCTION

Site 1262 (proposed Site WALV-12A) is located in the Angola Basin near the base of the northwestern flank of Walvis Ridge. At a water depth of 4759 m, the site is 500 and 200 m deeper than the previously drilled Deep Sea Drilling Project (DSDP) Site 527 to the south and Site 523 to the southwest, respectively. Drilling at Site 527 yielded a 341-m section of Neogene, Paleogene, and Maastrichtian sediment (Moore, Rabinowitz, et al., 1984), whereas drilling at Site 523 retrieved a 150-m section of Neogene and upper Paleogene sediment (Hsü, LaBrecque, et al., 1984). Sediments vary from clays to carbonate-rich oozes and chalks. The Pliocene–Pleistocene section consists of nannofossil oozes and extends to <100 meters below seafloor (mbsf). The Oligocene–Miocene sequence, yielding carbonate-poor clays, is condensed and contains an unconformity. The Paleocene–Eocene sequence recovered at Site 527 appears complete and consists of nannofossil oozes and chalks and a clay layer. However, only a portion of the Paleocene/Eocene Thermal Maximum (PETM), including a 70-cm-thick clay layer, was recovered at Site 527 (Thomas and Shackleton, 1996; Thomas et al., 1999). A continuous Cretaceous/Paleogene (K/P) boundary was also recovered at Site 527. The basal *Parvularugoglobigerina eugubina* Zone in the Tertiary is well represented (25 cm), and faunas are well preserved. The sediments immediately above basement are of late Maastrichtian age. Site 527 was rotary cored and, as a consequence, recovery was poor (25%–75%) and much of the core suffered from severe drilling disturbance, particularly the unlithified Neogene and Paleogene oozes.

Our main objective for this site was the recovery of undisturbed sediments recording critical intervals in the early Cenozoic, specifically the K/P boundary and subsequent recovery of biota following the mass extinction, the PETM, and the period of global cooling and growth of polar ice caps across the Eocene/Oligocene (E/O) boundary into the earli-

¹Examples of how to reference the whole or part of this volume.

²Shipboard Scientific Party addresses.

est Oligocene (early Oligocene Glacial Maximum). We planned to recover 100% of the sedimentary section in multiple holes to establish a cyclostratigraphy and develop an astronomically tuned timescale. We aimed to fully document events across the critical intervals as well as short-lived events such as the mid-Paleocene biotic event (PBE) and episodes of climate fluctuation during the early Eocene Climatic Optimum. Site 1262 forms the deep anchor of the Leg 208 depth transect and is located close to the calcite compensation depth (CCD) in the present ocean, making the site most suitable to document fluctuations in the depth of the CCD.

We chose a location where the Neogene section is thin (~100 m) to facilitate recovery of the entire Paleogene section using the advanced piston corer (APC) rather than the extended core barrel. To this end, Site 1262 was positioned in a perched basin filled with ~230 m of sediments (common depth point 2775 on line GeoB 01-035) (Figs. F1, F2). Seismic profiles revealed two distinct packages of reflectors in the basin, a thin upper package (0–100 ms two-way traveltimes [TWT] below seafloor) with a series of closely spaced sharp reflectors and a thicker lower package of weaker reflectors than in the upper package (100–280 ms TWT below seafloor) (Fig. F3). Based on Site 527, the upper package was interpreted as a condensed interval of Neogene calcareous oozes and clays and the lower package is interpreted as upper Maastrichtian to lower Eocene calcareous oozes and chalks. Two prominent reflectors dissect the lower package. The upper reflector (140 ms TWT below seafloor) was interpreted to represent the Paleocene/Eocene (P/E) boundary, whereas the deeper reflector (220 ms TWT below seafloor) was interpreted to represent the K/P boundary contact. Using an average velocity of 1.8 m/ms, the depths of these target reflectors were estimated to be 114 and 181 mbsf, respectively.

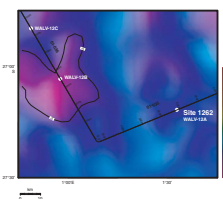
As anticipated, coring at Site 1262 yielded sediments deposited just above or below the CCD over most of the Cenozoic, and the APC system produced much better recovery and less distorted core than that obtained with the rotary coring system during the drilling of Site 527 (see “[Site 1262](#),” p. 13, in “Site Summaries” in the “Leg 208 Summary” chapter). The upper Maastrichtian and Paleocene–lower Eocene sections are moderately expanded, and both the P/E and K/P boundaries were recovered by APC drilling in multiple holes at ~127 and ~195 mbsf, respectively, with no obvious coring disturbance. Both critical intervals appear to be stratigraphically complete, and both exhibit distinct lithologic cycles and thus are suitable for high-resolution studies.

OPERATIONS

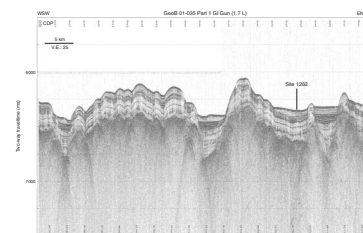
Rio de Janeiro Port Call and Transit to First Site

Leg 208 began when the first line was passed ashore in Rio de Janeiro, Brazil, at 1720 hr on 6 March 2003. Incoming scientific and technical personnel encountered numerous difficulties with Brazilian immigration authorities regarding visa declarations. Most of these incidents were resolved locally with the assistance of the ship’s agent. In two separate incidents involving a total of seven people, personnel were required to leave Brazil and reenter. Routine port call activities proceeded at a slow tempo. Several barge deliveries of potable water, tested for biological and chemical contamination by the ship’s doctor, were needed and were released into the ship’s potable water system. Frozen sediment

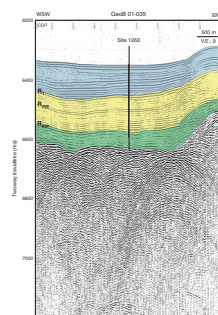
F1. Locations of Site 1262 and alternate sites, p. 25.



F2. Line GeoB 01-035 and Site 1262 in a perched basin, p. 26.



F3. Line GeoB 01-035 and Site 1262 with reflector ages, p. 27.



samples from Leg 207 were kept on board because Brazilian authorities stated that it would “take a minimum of 30 days” before the specimens would be released for shipment.

The last line was released from the pier at 0721 hr on 14 March. After clearing the harbor entrance, the captain initiated turning maneuvers to evaluate the tracking ability of the very small aperture tunnel antenna. Additional personnel aboard for this acceptance test departed the vessel at 1047 hr, and the ~2500-nmi journey to the first site of Leg 208 began. The first week of the transit was characterized by a moderate southeasterly swell through which the vessel negotiated easily as it headed almost directly east to Walvis Ridge. By 18 March, the vessel had traveled 1220 nmi at an average speed slightly more than 11 kt. By the early morning of 19 March, easterly winds had increased to force 4 and eventually grew to force 6. As the sea and swell started to build, waves breaking over the bow began to inundate the bridge deck. The speed of the vessel fell below 9 kt as the vessel was pelted by rain and wind gusts exceeding 30 kt. During the evening of 22 March, the captain reduced propeller revolutions from 140 to 120 rpm to lessen vessel pitch and roll. The speed then fell below 7 kt. Later in the evening, the shafts were again back to 140 rpm as the weather gradually abated and the speed gradually increased above 8 kt.

The vessel approached the coordinates of proposed Site WALV-12A using the Global Positioning System and was on site on 24 March at 1300 hr. The 2455-nmi transit from Rio de Janeiro to the first site of Leg 208 required 239.0 hr (9.96 days) at an average speed of 10.2 kt. The corrected precision depth recorder depth was 4776.4 m relative to the top of the dual elevator stool on the rig floor, or 4776.4 meters below rig floor (mbrf). The bottom-hole assembly (BHA) (see “[Operations](#),” p. 1, in the “Explanatory Notes” chapter) was made up, and all the tubulars were measured during the initial deployment of the drill string. A cleaning plug was pumped down the string to remove rust, and the slow-circulating-rate parameters were established prior to deploying the first core barrel.

Site 1262

Coring intervals, times, nominal recovery rates, core barrels that required drillover to be released from the sediment, and the deployments of the Advanced Piston Corer Temperature (APCT) tool, Tensor core orientation tool, and nonmagnetic core barrel are listed in Table [T1](#).

Hole 1262A was initiated with the APC at 0340 hr on 25 March, with the bit placed at 4770 mbrf. The first core was recovered with a full barrel, and the nominal seafloor depth for Hole 1262A is therefore defined at 4770.0 mbrf (~6 m below the more accurate seafloor estimate in Hole 1262B). When the core winch operator attempted to recover Core 208-1262A-15H (133.0–142.5 mbsf), the aft coring wire parted just above the rope socket, leaving the core barrel in the outer core barrel of the BHA. The barrel was successfully recovered with the forward coring line using a “fishing assembly” made up of the lower section of an APC barrel and a rotary core barrel coring shoe. The salvaging of the core barrel required several hours, and coring subsequently advanced to 161.5 mbsf. During an attempt to recover the core barrel containing Core 208-1262A-18H from the sediment following a full stroke of the APC, one of the core barrel connections failed after the application of only 60,000 lb. The failed part was the male threaded connection between two 5-ft core barrel sections used to replace a 10-ft nonmagnetic core

[T1. Coring summary, p. 61](#)

barrel damaged during the previous leg. The failure left most of the APC barrel (and a full core liner) at the bottom of the hole, making further coring impossible. Hole 1262A was therefore ended prematurely; the inventory of nonmagnetic APC assemblies was reduced to one.

The vessel was offset 20 m north, and Hole 1262B was initiated with the APC at 1450 hr on 26 March. In an attempt to obtain a good mudline core and a stratigraphic overlap with the initial hole, the bit was positioned at 4762 mbrf, or 8 m shallower than the initial bit position for Hole 1262A. A reliable mudline core was obtained, containing 6.91 m of nannofossil ooze. The seafloor depth inferred by the recovery of the initial core was 4764.6 mbrf, or 4753.6 meters below sea level (mbsl). Piston coring advanced without incident to the target depth of 209.9 mbsf. The bit was pulled free of the seafloor at 2125 hr on 27 March, and the vessel was offset 20 m north for Hole 1262C.

Hole 1262C was initiated at 2140 hr and drilled ahead with a wash barrel to 90 mbsf, where coring was initiated. Piston coring deepened the hole to the target depth of 212.5 mbsf. Coring in this hole was used to fill gaps in the stratigraphic record. Adjustments were made in the firing depth of Cores 208-1262C-4H (4.0-m advance), 7H (7.5-m advance), and 11H (6.5-m advance) to maintain overlaps with the previous holes.

The cored interval for the site was 493.9 m, and the recovered interval was 502.5 m (average nominal recovery = 101.7%). The total drilled interval was 90 m.

Four downhole temperature measurements (Hole 1262A: 0–143 mbsf) and one bottom water temperature measurement (Hole 1262B) with the APCT yielded an initial temperature gradient estimate of 5.3°C/100 m.

The routine recovery of the drill string was suspended for 1.5 hr for slipping and cutting of the drilling line. The beacon was recovered; the drilling equipment was secured; and the vessel proceeded to the next site at 0530 hr on 29 March.

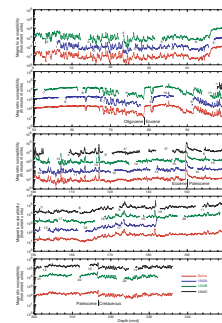
COMPOSITE DEPTH

Magnetic susceptibility (MS) and sediment lightness (L^*) data collected from Holes 1262A, 1262B, and 1262C at 2.5-cm intervals were used to construct the composite section for Site 1262. The MS measurements were primarily used for core-to-core correlation and to construct the composite section (Fig. F4). The depth offsets that define the composite section for Site 1262 are given in Table T2.

The composite data show that the cores from Site 1262 provide a continuous sequence down to 236.4 meters composite depth (mcd), the total depth of Hole 1262C (Core 208-1262C-14H; upper Maastrichtian). The MS data from the multisensor track (MST) were affected by reduced core diameter at the base of Section 208-1262C-12H-7. MS point-sensor measurements taken on the archive half were therefore used to confirm the correlation of this interval. Following construction of the composite depth section for Site 1262, a single spliced record was assembled from the aligned core intervals from all three holes (Table T3).

Cores that had been significantly stretched, squeezed, or disturbed by the coring process were not used for the splice. Without a stretch or squeezing correction, all points within each core are offset equally. As a result, most of the cycles are not perfectly aligned between holes (e.g., at ~12, ~22, ~38, ~110, ~173, and ~182 mcd in Fig. F4). Thus, the mcd

F4. MS data, p. 28.



T2. Composite depth scale, p. 62.

T3. Splice tie points, p. 63.

values of the different holes will approximate but not precisely correspond to the same stratigraphic horizon in alternate holes.

The P/E boundary interval in the composite was taken from Core 208-1262B-15H (140.17 mcd), and the K/P boundary interval in the composite was taken from Core 208-1262C-13H (216.75 mcd). The Site 1262 splice (Table T3) can be used as a guide to sample a single sedimentary sequence between 0 and 236 mcd and was used to plot other data sets from this site. The mcd to mbsf growth factors for Holes 1262A, 1262B, and 1262C were 11%, 11%, and 13%, respectively (Fig. F5).

LITHOSTRATIGRAPHY

Three holes were cored at Site 1262. Hole 1262A was cored to a depth of 182.4 mcd (162.0 mbsf); Hole 1262B was cored to 232.9 mcd (209.7 mbsf); and Hole 1262C was washed to 97.8 mcd (90.0 mbsf) and cored to 236.9 mcd (213.0 mbsf). The major lithologies recovered include nannofossil ooze, foraminifer-bearing nannofossil ooze, foraminifer-nannofossil ooze, clay-bearing nannofossil ooze, clayey nannofossil ooze, and clay. Minor lithologies include volcanic ash-bearing nannofossil ooze and hematite-bearing clay. Combining measurements of MS, natural gamma radiation (NGR), and L* with smear slide analysis, we have divided this sequence into three major lithostratigraphic units, with two units further subdivided based on minor lithologic variation (Table T4). In addition to the description of these lithostratigraphic subdivisions, we provide descriptions of the P/E and K/P boundary lithologies.

Description of Lithostratigraphic Units

Unit I

Interval: Sections 208-1262A-1H-1 through 4H-CC; Sections 208-1262B-1H-1 through 6H-3, 52 cm

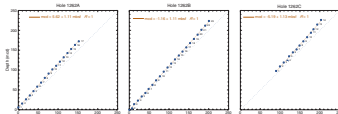
Depth: Hole 1262A: 0.0–38.6 mbsf (6.0–46.1 mcd); Hole 1262B: 0.0–43.9 mbsf (0.0–45.8 mcd)

Age: Pleistocene to Miocene

Lithology: nannofossil ooze and foraminifer-bearing nannofossil ooze

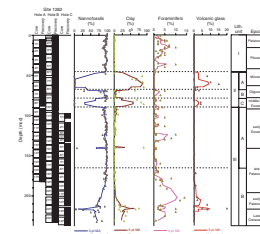
Unit I consists primarily of nannofossil ooze that varies slightly in the relative abundance of associated skeletal components, organic content, and clay content (Fig. F6). MS and NGR are low, and L* is high, reflecting a high average carbonate content of 89 wt% (Figs. F7, F8, F9). The color varies throughout from brown and very pale brown to light gray in 10- to 50-cm bands and likely reflects differences in clay, organic content, and carbonate production or preservation. Other than these features, bedding is largely absent. The boundaries between color bands are generally diffuse, reflecting moderate to pervasive bioturbation. In the upper part of this unit, oscillations in sediment color may record the variable dissolution of carbonate during glacial-interglacial cycles of the Pliocene–Pleistocene (i.e., typical Atlantic-type carbonate cycles). These decimeter-scale cycles are well expressed in signals of both MS and L* (Fig. F10A). Porosity decreases, whereas bulk density and compressional wave (P-wave) velocity increase slightly downcore in Unit I (Figs. F11,

F5. Mbsf vs. mcd plots, p. 29.

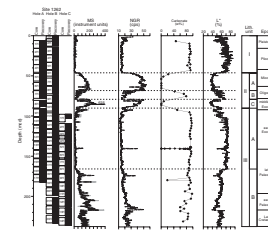


T4. Lithostratigraphic subdivisions, p. 64.

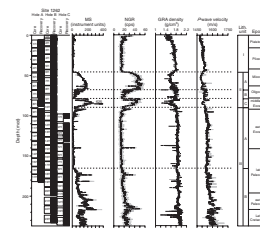
F6. Smear slide components, p. 30.



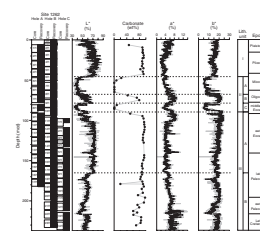
F7. MS, NGR, carbonate content, and L*, p. 31.



F8. MS, NGR, GRA bulk density, and P-wave velocity data, p. 32.



F9. Lightness, carbonate content, and chromaticity, p. 33.



F12A, F13A), reflecting sediment consolidation. In general, densities and *P*-wave velocities determined with the MST correlate well with the discrete sample measurements (Figs. **F12B, F13B**), indicating that the cores have not been severely disturbed during the splitting process. In addition, porosity is negatively correlated with bulk density, whereas *P*-wave velocity and grain density are positively correlated with bulk density (Fig. **F12C, F12D, F12E**).

Unit II

Interval: Sections 208-1262A-5H-1 through 8H-CC; intervals 208-1262B-6H-3, 52 cm, through 10H-4, 120 cm

Depth: Hole 1262A: 38.0–74.0 mbsf (47.0–88.0 mcd); Hole 1262B: 43.9–82.6 mbsf (45.8–90.0 mcd)

Age: Miocene to middle Eocene

Lithology: clay, ash-bearing clay, nannofossil clay, nannofossil ooze, and clayey nannofossil ooze

Unit II consists of upper and lower clay-rich subunits separated by a middle subunit of nannofossil ooze. Subunit IIA is composed of clay, ash-bearing clay, and nannofossil clay; Subunit IIB is an intermediate interval of nannofossil ooze and clayey nannofossil ooze; Subunit IIC is a thick interval of clay, ash-bearing clay, and nannofossil clay.

Subunit IIA

Interval: Sections 208-1262A-5H-1 through 6H-CC; interval 208-1262B-6H-3, 52 cm, through 8H-4, 85 cm

Depth: Hole 1262A: 38.0–57.7 mbsf (47.0–68.4 mcd); Hole 1262B: 43.9–63.3 mbsf (45.8–68.1 mcd)

Age: Miocene to Oligocene

Lithology: clay, ash-bearing clay, and nannofossil clay

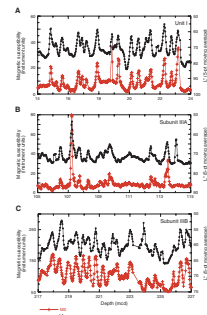
The most common lithology of Subunit IIA is a dark gray to brown clay, containing variable amounts of nannofossils, altered volcanic ash, and rare foraminifers (Fig. **F6**). The generally uniform color of this unit limits determination of bioturbation, but where color gradients exist, bioturbation appears moderate to extensive. Scattered oxide grains (2–25 μm), zeolites, and volcanic ash and shards are present locally as accessory components. MS and NGR values are high, and carbonate is virtually absent (Fig. **F7**).

The contact between Unit I and Subunit IIA is marked by sharp breaks in physical properties that reflect the change from a carbonate-to clay-rich lithology. Bulk density, grain density, carbonate content, L* (Fig. **F14A**), and seismic velocity (Figs. **F11, F13A**) decrease downhole as the nannofossil ooze grades into carbonate-poor clay (Fig. **F14A, F14B**). The correlation of bulk density with porosity, grain density, and *P*-wave velocity sensor (PWS3) measurements with the Hamilton Frame probe (Fig. **F12C–E**) suggests that sediment bulk density is controlled primarily by the degree of compaction. The chromaticity ratio (a^*/b^*) increases dramatically at the boundary as a result of relative clay abundance (Fig. **F14C**).

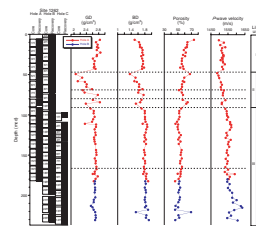
Subunit IIB

Interval: Sections 208-1262A-7H-1 through 7H-CC; interval 208-1262B-8H-4, 85 cm, through 9H-4, 10 cm

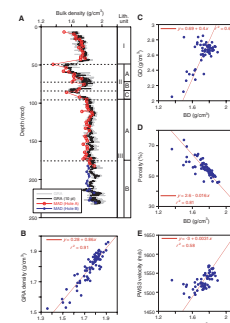
F10. Cycles observed in MS and L*, p. 34.



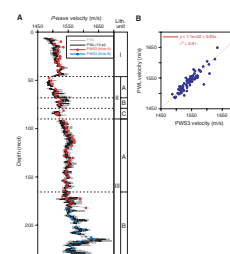
F11. Grain density, bulk density, porosity, and *P*-wave velocity, p. 35.



F12. Physical property measurements, p. 36.



F13. *P*-wave velocities, p. 37.



Depth: Hole 1262A: 57.0–66.8 mbsf (68.4–78.2 mcd); Hole 1262B: 63.3–72.0 mbsf (68.1–78.9 mcd)

Age: Oligocene

Lithology: nannofossil ooze, foraminifer-bearing nannofossil ooze, and clayey nannofossil ooze.

Subunit IIB is light brown to gray nannofossil ooze and foraminifer-bearing nannofossil ooze alternating with medium brown to gray clayey nannofossil ooze. This subunit is higher in nannofossil, carbonate, and sediment L* and lower in MS and NGR than Subunits IIA and IIC (Figs. F6, F7). Subunit IIB has slightly higher bulk density and P-wave velocity than Subunit IIA (Figs. F8, F12A, F13A), resulting from a higher carbonate content. Some foraminifer-rich intervals have sharp, irregular basal contacts with the underlying clay and fine upward into nannofossil ooze (Fig. F15). In contrast to the sharp basal contact, the upper contact of these carbonate intervals is bioturbated, forming a gradual contact with overlying, relatively dark nannofossil clay. We interpret these sequences as fine-grained carbonate turbidites in a clay-dominated sedimentary regime. This interpretation is supported by biomarkers of Paleocene and Eocene age for the basal coarser-grained sediments compared to Oligocene–Miocene biostratigraphic ages for finer-grained sediment above and below.

The E/O boundary, although not clearly defined at this site (see “[Eocene/Oligocene Boundary Interval \(75–81 mcd\)](#),” p. 10, in “[Biostratigraphy](#)”), occurs in an interval containing the base of Subunit IIB and the upper part of Subunit IIC. Section 208-1262B-9H-4 (Fig. F16) highlights upcore lithologic transition of clay-rich lithologies characterized by high MS and NGR and low L* (Subunit IIC) to calcareous foraminifer- and nannofossil-rich lithologies characterized by low MS and NGR and high L* (Subunit IIB). This lithologic transition represents our best approximation of the E/O boundary.

Subunit IIC

Interval: Sections 208-1262A-8H-1 through 8H-CC; interval 208-1262B-9H-4, 10 cm, through 10H-4, 120 cm

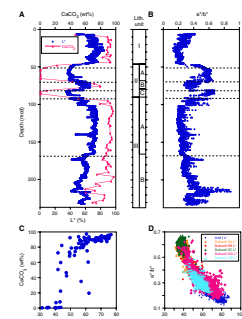
Depth: Hole 1262A: 66.5–74.0 mbsf (80.5–88.0 mcd); Hole 1262B: 72.0–82.6 mbsf (78.9–90.0 mcd)

Age: late Eocene to middle Eocene

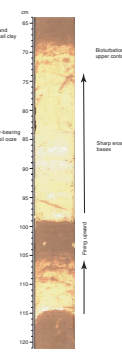
Lithology: clay, ash-bearing clay, and nannofossil clay

Subunit IIC is lithologically similar to Subunit IIA and is composed primarily of dark gray to brown clay with intervals of light brown nannofossil ooze. A prominent 2-cm volcanic ash layer was recovered at 85.25 mcd in intervals 208-1262A-8H-5, 6–8 cm (71.2 mbsf), and 208-1262B-10H-1, 93–94 cm (77.83 mbsf). This ash layer contains abundant clear volcanic glass shards, suggesting a felsic volcanic origin; some have been altered to clays by devitrification and weathering. The ash layer is marked by a large spike (625 instrument units) in the MS record (Fig. F7). Subunit IIC is distinguished from Subunit IIB above and Subunit IIIA below by its higher MS and NGR values and lower carbonate content and L* (Figs. F7, F8, F9, F12A).

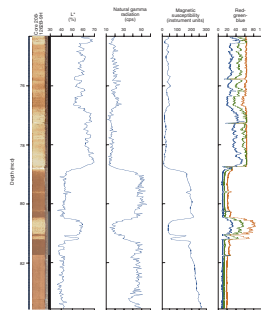
F14. Color reflectance data, p. 38.



F15. Turbidites and gravity flows, p. 39.



F16. Digital image, L*, RGB, MS, and NGR across the E/O boundary, p. 40.



Unit III

Interval: Sections 208-1262A-9H-1 through 17H-CC; interval 208-1262B-10H-4, 120 cm, through 23H-CC; Sections 208-1262C-1H-1 through 14H-CC

Depth: Hole 1262A: 76.0–162.0 mbsf (91.2–182.4 mcd); Hole 1262B: 82.6–209.7 mbsf (90.0–232.9 mcd); Hole 1262C: 90.0–213.0 mbsf (97.8–236.9 mcd)

Lithology: nannofossil ooze and clayey nannofossil ooze

Unit III is a carbonate-rich lithology with low MS and NGR signals, similar to lithostratigraphic Unit I (Fig. F7). We have divided Unit III into two subunits based on the abundance of clay and volcanic ash (Fig. F6). Subunit IIIA is a nannofossil ooze with very minor clay and ash components; Subunit IIIB shows a progressive downcore increase in clay and ash. Although petrographically gradual, this increase in clay is associated with a distinct increase in the MS and NGR values (Figs. F7, F8) and a decrease in sediment L* (Figs. F7, F9, F14A).

Subunit IIIA

Interval: Sections 208-1262A-9H-1 through 16H-2, 60 cm; intervals 208-1262B-10H-4, 120 cm, through 17H-CC; intervals 208-1262C-1H-1 through 8H-3, 13 cm

Depth: Hole 1262A: 76.0–144.6 mbsf (91.2–165.6 mcd); Hole 1262B: 82.6–152.7 mbsf (90.0–166.3 mcd); Hole 1262C: 90.0–152.1 mbsf (97.8–165.1 mcd)

Age: middle Eocene to late Paleocene

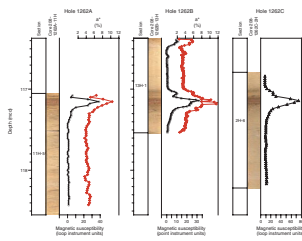
Lithology: nannofossil ooze

Subunit IIIA is a 75-m-thick interval of relatively pure nannofossil ooze (92.4 wt% carbonate) with low MS and NGR values and high L* (Fig. F7). The subunit has lower porosity and higher bulk density and P-wave velocity than Units I and II (Figs. F11, F12A, F13A). Color oscillates from light gray brown to medium gray on the decimeter to meter scale and covaries with changes in MS (Fig. F10B). Based on the gradational nature of most contacts between these colors and the occasional preservation of burrow traces, we interpret this interval as moderately bioturbated. Moreover, large rounded or irregular pinkish white blebs (1–3 cm in diameter) are present throughout this unit. These blebs, which may be associated with burrowing, often have a halo of small brown to black opaque grains interpreted to be Mn oxides and Fe oxides based on reflected-light observations in smear slides. Pyrite was not commonly observed in these sediments, which is in agreement with interstitial water chemistry that shows little evidence of sulfate reduction (see “Geochemistry,” p. 19).

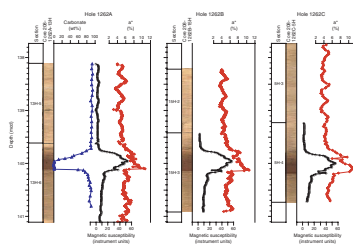
Subunit IIIA consists almost entirely of nannofossil ooze with the exception of a thin clayey horizon at ~117.3 mcd and 30–40 cm of clay-rich sediment directly above the P/E boundary (Figs. F17, F18). The layer at 117.3 mcd comprises ~20 cm of reddish clay-bearing nannofossil ooze containing abundant fragments of volcanic ash. This horizon exhibits a distinctive positive spike in MS and chromaticity a*.

The P/E boundary was recovered in three holes at ~140.2 mcd (Sections 208-1262A-13H-6, 50 cm, at 122 mbsf; 208-1262B-15H-3, 74 cm, at 127.84 mbsf; and 208-1262C-5H-4, 95 cm, at 127.95 mbsf) and is marked by an abrupt contact between nannofossil ooze and dusky red hematite and ash-bearing clay (Fig. F18). Bioturbation is nearly absent

F17. Digital image, a*, and MS of the clay horizon, p. 41.



F18. Digital image, carbonate, MS, and red-green chromaticity across the P/E boundary, p. 42.



in the 10 cm above the contact and then increases as sediment grades into nannofossil ooze above. Nannofossil-rich horizons in the underlying Paleocene sequence are firmer and approach chalk, whereas Eocene sediments are uniformly soft and unlithified. The P/E boundary is interpreted as a horizon formed in response to a severe dissolution event at Site 1262 (4753 m water depth) as expressed by a decrease in carbonate content (see “[Geochemistry](#),” p. 19), a decrease in L^* , and increases in NGR and MS (Figs. [F18](#), [F19](#)). The structure of the MS signal is nearly identical for all three holes (Fig. [F20](#)).

Subunit IIIB

Interval: Sections 208-1262A-16H-2, 60 cm, through 17H-CC; Sections 208-1262B-18H-1 through 23H-CC; interval 208-1262C-8H-3, 13 cm, through 14H-CC

Depth: Hole 1262A: 144.6–162.0 mbsf (165.6–182.4 mcd); Hole 1262B: 152.9–209.7 mbsf (168.0–232.9 mcd); Hole 1262C: 152.1–213.0 mbsf (165.1–236.9 mcd)

Age: late Paleocene to Maastrichtian

Lithology: clayey nannofossil ooze

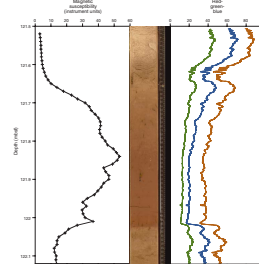
Subunit IIIB has a greater abundance of clay than Subunit IIIA and exhibits a greater range of minor lithologies, including nannofossil ooze, foraminifer-bearing nannofossil ooze, clay-bearing to clayey nannofossil ooze, foraminifer- and nannofossil-bearing clay, and ash-bearing clay. The upper part of Subunit IIIB is typically very uniform, lacks the thin layers (5–10 cm) of light-colored nannofossil oozes that are sporadic in Subunit IIIA, and is generally darker (perhaps reflecting the increased clay content). MS, NGR, and *P*-wave velocity are higher in Subunit IIIB than in Subunit IIIA (Figs. [F7](#), [F13A](#)). Variations in sediment lightness are negatively correlated with MS and display distinct cyclicity (Fig. [F10C](#)), representing a potential sedimentologic response to orbital forcing.

In Subunit IIIB, clay content increases downhole where the major lithology, a medium brown clayey nannofossil ooze and ash-bearing clay, is interbedded and intermixed with a reddish brown nannofossil ooze directly above the K/P boundary. We recovered the K/P boundary from two holes at ~216.6 mcd (Sections 208-1262B-22H-4, 137 cm, at 195.53 mbsf and 208-1262C-13H-2, 68 cm, at 195.68 mbsf). The boundary marks an abrupt lithologic transition from underlying carbonate-rich, clay-bearing nannofossil ooze with foraminifers and nannofossil-bearing and foraminifer-bearing clays above (Fig. [F21](#)). Across the boundary, clay content, MS, and NGR values increase (Figs. [F6](#), [F7](#)).

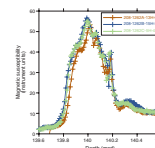
BIOSTRATIGRAPHY

Pleistocene through upper Maastrichtian sediments were recovered at Site 1262. Pliocene–Pleistocene assemblages show considerable reworking, and the Miocene through upper middle Eocene section yields calcareous microfossils strongly affected by carbonate dissolution as well as reworking. Lower Eocene and older sediments contain well-preserved calcareous assemblages. Shipboard examination of calcareous nannofossils and planktonic foraminifers permitted preliminary zonal and stage assignments (Fig. [F22](#); Tables [T5](#), [T6](#)). Benthic foraminifers place the sequence at lower abyssal depths during the late Paleocene through Pleistocene and at upper abyssal depths during the Cretaceous

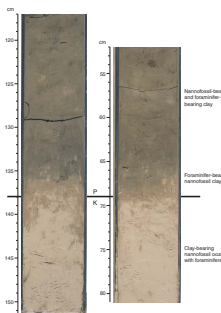
F19. MS and color variations across the P/E boundary, p. 43.



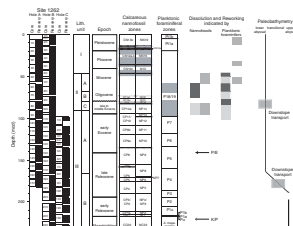
F20. MS across the P/E boundary, p. 44.



F21. K/P boundary, Holes 1262B and 1262C, p. 45.



F22. Planktonic foraminiferal and calcareous nannofossil biozonations, p. 46.



T5. Selected calcareous nannofossil datums, p. 65.

T6. Selected planktonic foraminiferal datums, p. 67.

through early Paleocene. Biochronological ages plotted against mcd delineate overall sedimentation rates (Fig. F23) (see “Age Model and Mass Accumulation Rates,” p. 23).

Calcareous Nannofossils

Calcareous nannofossil assemblages were examined in the core catcher samples of all holes, and additional samples were inspected in numerous cores. Age and depth estimates of key biostratigraphic markers are shown in Table T5; a distribution chart showing the results from the core catcher samples is reported in Table T7.

Nannofossils are present in varying concentrations and states of preservation. In Cores 208-1262A-1H through 3H and Cores 208-1262B-1H through 5H, the assemblages have abundant nannofossils with good preservation. Sections 208-1262A-5H-CC and 6H-CC and 208-1262B-6H-CC, 7H-CC, and 9H-CC are barren. In sediments below 96 mcd (Cores 208-1262A-9H through 17H, 208-1262B-10H through 23H, and 208-1262C-1H through 14H), nannofossil assemblages are abundant, diverse, and generally well preserved, although nannofossils show varying degrees of dissolution and overgrowth.

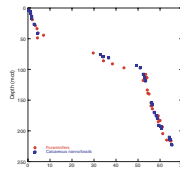
Pleistocene–Oligocene (0–78 mcd)

The Pleistocene–Oligocene sequence (Core 208-1262A-1H through Section 7H-4 and Cores 208-1262B-1H through 9H) is characterized by slumps, turbidite layers, and thick intervals barren of calcareous nannofossils, making recognition of most nannofossil events of this time interval difficult. Moreover, assemblages are affected by reworking that increased anomalies in the biostratigraphic succession. On the basis of limited biostratigraphic data obtained from intermittent fossiliferous intervals, sediments from Cores 208-1262A-1H through 4H and Core 208-1262B-1H through Section 6H-2 were deposited during the Pleistocene–Pliocene. Lower Pliocene and upper Miocene nannofossil assemblages (Cores 208-1262A-5H and 208-1262B-6H) were extensively reworked and contain lower Miocene–Oligocene contaminants. Sediments in Cores 208-1262A-6H and 208-1262B-7H through 8H are barren of nannofossils, except for discrete layers that contain mixed assemblages of reworked Eocene forms.

Eocene/Oligocene Boundary Interval (75–81 mcd)

The carbonate-bearing sediments in the stratigraphic interval between 75 and 81 mcd (Cores 208-1262A-7H through 8H and 208-1262B-9H) were sampled to investigate the Eocene–Oligocene transition, including the uppermost occurrences of the last Paleogene representatives of rosette-shaped discoasters, *Discoaster saipanensis* and *Discoaster barbadiensis*. Nannofossil assemblages of Zones CP16 and CP15 (NP22, NP21, and NP20) straddle the Eocene–Oligocene transition. The boundary between Subzones CP16c and CP16b (NP22/NP21: top of *Ericsonia formosa* range) is distinct in both holes, whereas the uppermost occurrences (top [T]) of *D. saipanensis* and *D. barbadiensis* were recorded together and define the boundary between Subzone CP16a and Zone CP15 (NP21/NP20). The “cool-water taxon” *Isthmolithus recurvus* (Martini, 1971), whose range straddles the E/O boundary interval (from Zones CP16 through CP15; NP22 through NP19), is rare and has a discontinuous occurrence in Cores 208-1262A-8H and 7H and 208-1262B-

F23. Summary of sedimentation rates, p. 47.



T7. Range and abundance of calcareous nannofossils, p. 68.

9H. Major components of the lowermost Oligocene–uppermost Eocene assemblage are *Reticulofenestra umbilicus*, *Reticulofenestra dictyoda*, *Dicyococcites* spp., and *Coccolithus eopelagicus*. The absence of peaks in abundance of *Ericsonia obruta*, which characterize the E/O transition, suggests that this transition is incomplete at Site 1262.

Eocene (78–130 mcd)

The interval from 78 to 96 mcd (Sections 208-1262A-8H-1 through 9H-3 and 208-1262B-9H-6 through 10H-CC) is placed in the upper and middle Eocene. Assemblages characteristic of Zones CP15 to CP11 (NP19 to NP13) are recognized, but nannofossils are present in scattered samples only. From 84 to 94 mcd, assemblages belonging to Zones CP14, CP13, and CP12 (NP16, NP15, and NP14) are present along with common *Sphenolithus* spp., *Chiasmolithus* spp., *Nannotetra* spp., and reworked lower Eocene species.

Nannofossils are abundant throughout the interval from 96 to 140 mcd. The uppermost part of this interval is in Zone CP11 (upper part of NP12) in the lower Eocene (Cores 208-1262A-9H, 208-1262B-11H, and 208-1262C-1H). Preservation varies from good to moderate, with overgrowths on discoasterids and dissolution of other forms. The main marker species for the lower Eocene zones are present (Table T7), including abundant *Tribrachiatus orthostylus*, *Discoaster lodoensis*, *Sphenolithus radians*, rare *Discoaster multiradiatus*, and common *Discoaster diastypus*. Most of the lower Eocene nannofossil zonal boundaries (from NP14/NP13 through NP12/NP11) have been recognized. In the Walvis Ridge region, *Toweius crassus* (marker of the CP11/CP10 boundary) seems to have a different stratigraphic range than indicated in the standard zonations; its range extends into Zone CP9 and was not used for the biozonation.

Paleocene/Eocene Boundary Interval (130–150 mcd)

Specimens belonging to the *Rhomboaster-Tribrachiatus* plexus are poorly preserved because of calcite recrystallization. They are present in Sample 208-1262A-13H-6, 25 cm, just above the benthic extinction event (BEE), but their distribution is not continuous in the overlying sediments, indicating that the lineage from *Rhomboaster-Tribrachiatus* to *T. orthostylus* is not fully represented at Site 1262. Overgrown specimens belonging to the *Rhomboaster-Tribrachiatus* plexus hindered identification of *Tribrachiatus contortus* and *Tribrachiatus bramlettei*. Thus, the boundaries between Subzones CP9b and CP9a (NP11/NP10) and between Subzone CP9a and Zone CP8 (NP10/NP9) could not be confidently recognized. The Subzone CP9b/CP9a (NP11/NP10) boundary is approximated by the appearance of *S. radians*. The genus *Fasciculithus* shows a distinct decrease in abundance in the uppermost part of its range. Fasciculiths are relatively common in the uppermost Paleocene but decrease in abundance, whereas *Zygrhablithus bijugatus* increases in abundance between Samples 208-1262A-13H-6, 10 cm, and 13H-6, 25 cm, just above the BEE. The uppermost occurrence of fasciculiths is between Samples 208-1262A-13H-4, 43 cm, and 13H-4, 60 cm. The reversal in relative abundances of the genera *Fasciculithus* and *Zygrhablithus* is prominent and easy to recognize and is observed just above the BEE. A similar “relative abundance reversal” between the genera *Fasciculithus* and *Rhomboaster* has been reported at equatorial Pacific Sites 1220 and 1221 (Lyle, Wilson, Janecek, et al., 2002) and may be correlative.

Paleocene (140–219 mcd)

Paleocene assemblages are generally diverse and moderately preserved because of slight dissolution of placoliths and some overgrowth on discoasterids. Important components of the assemblages are *Toweius* spp., *Coccolithus pelagicus*, *Prinsius* spp., *Chiasmolithus* spp., *Cruciplacolithus* spp., *Heliolithus* spp., and *Ericsonia* spp. Most of the key elements for the biostratigraphic classification of the interval from 153 to 219 mcd (Cores 208-1262A-14H through 17H, 208-1262B-16H through 22H, and 208-1262C-6H through 12H) were recorded with few exceptions (Table T7). The bottom of *Heliolithus kleinpellii* indicates the presence of the PBE between Samples 208-1262A-17H-2, 129 cm, and 17H-3, 34 cm, 208-1262B-18H-5, 40 cm, and 18H-5, 140 cm, and 208-1262C-9H-1, 150 cm, and Section 9H-CC. The marker of the Zonal CP7/CP6 boundary, *Discoaster nobilis*, was difficult to recognize because of overgrowth. The lowermost occurrence (bottom [B]) of *Ellipsolithus macellus* appears to be diachronous because its lowermost persistent occurrence is recorded in Zone CP5 (NP6), thereby preventing recognition of the Zonal CP3/CP2 (NP4/NP3) boundary.

Upper Cretaceous–Lower Paleocene Boundary Interval (211–232 mcd)

The K/P boundary interval is marked by a mass extinction of Cretaceous nannofossil taxa, together with a significant increase in abundance of *Thoracosphaera* spp., the B of *Biantholithus sparsus* (Sample 208-1262B-22H-4, 133 cm), and the co-occurrence of *Markalius inversus* and *Cyclagelosphaera reinhardtii*. These events are followed uphole by the appearance of new taxa such as *Cruciplacolithus primus* (64.8 Ma) and *Cruciplacolithus tenuis* s.s. (64.5 Ma). At Site 1262, the B of *C. tenuis* s.s. is between Samples 208-1262B-22H-2, 72 cm, and 22H-3, 33 cm, at an estimated depth of 213.79 mcd. The B of *C. primus* is between Samples 208-1262B-22H-3, 73 cm, and 22H-3, 130 cm, at an estimated depth of 214.45 mcd. An uppermost Maastrichtian nannofossil assemblage (Zone CC26) is present near the bottom part of the Site 1262 sedimentary succession. The B of *Micula prinsii* in Zone CC26 is recorded between Section 208-1262B-22H-CC and Sample 23H-1, 40 cm, at an estimated depth of 222.86 mcd.

Planktonic Foraminifers

Planktonic foraminifers were examined in all core catcher samples from Holes 1262A and 1262B, as well as at a higher resolution across the P/E and K/P boundary intervals (see Tables T6, T8).

Pleistocene–Oligocene (0–78 mcd)

Pleistocene assemblages preserved in Cores 208-1262A-1H and 208-1262B-1H through 2H (0.62–12.31 mcd) consist of a mixture of well-preserved subtropical and temperate planktonic foraminifers. The uppermost part of Core 208-1262B-1H may contain Holocene sediments, but this was not possible to confirm. Common species are *Globorotalia crassaformis*, *Globorotalia truncatulinoides*, *Globorotalia tumida*, *Globorotalia ungulata*, *Globoconella inflata*, *Globigerinoides ruber*, *Globigerinoides sacculifer*, *Globigerina falconensis*, *Globigerina (Zeoglobigerina) rubescens*, *Globigerinella siphonifera*, *Hirsutella scitula*, and *Neogloboquadrina pachy-*

T8. Range and abundance of planktonic foraminifers, p. 74.

derma (dextral). The T of *Globorotalia tosaensis* (base of Subzone Pt1b; 0.65 Ma) is in Sample 208-1262B-1H-4, 62–64 cm (~4.65 mcd). The base of Subzone Pt1a (~2.02 Ma) is used to approximate the Pliocene/Pleistocene boundary and is placed at ~19.20 mcd (Sample 208-1262A-1H-2, 62–64 cm, and Section 208-1262B-2H-CC). The lower portion of the Pleistocene (Section 208-1262A-1H-6) has been extensively reworked (Table T8).

Many of the tropical/subtropical age-diagnostic taxa used to subdivide the upper Miocene–Pliocene interval are missing from the section because of temperate environmental conditions. Preservation is variable, ranging from poor to good (Table T8). A reliable biozonation could not be constructed because of pervasive reworking, but specimens transitional between *Globoconella conomiozea* and *Globoconella puncticulata* (i.e., *Globoconella sphericomiozea*) are present in Section 208-1262B-5H-CC, providing a loose approximation for the Miocene/Pliocene boundary at ~43 mcd. The depth of the *G. crassaformis* lowermost occurrence (48.66 mcd) plots as an outlier along the age-depth curve, suggesting that this datum is diachronous (Fig. F23).

The interval from Sections 208-1262A-4H-CC through 6H-CC (40–68 mcd) contains a condensed upper Miocene through upper Oligocene section. Assemblages from this stratigraphic interval are very poorly preserved because of intense carbonate dissolution and fragmentation; only thick-shelled taxa resistant to dissolution were found intact (Table T8). The presence of robust *Sphaeroidinellopsis disjuncta* and *Globigerina druryi/Globigerina nepenthes* indicates a middle Miocene age for Section 208-1262A-5H-CC (56.83 mcd). Some carbonate-rich turbidite layers in Cores 208-1262A-5H and 6H contain well-preserved middle Eocene taxa (e.g., *Acarinina bullbrooki*). The stratigraphic position of the Oligocene/Miocene boundary could not be discerned, and the upper Oligocene may be missing (Fig. F22).

Section 208-1262A-7H-CC (77.92 mcd) is loosely constrained to the lower Oligocene based on the co-occurrence of *Subbotina angiporoides*, *Catapsydrax unicavus*, *Globorotaloides suteri*, and *Chiloguembelina cubensis*. Test preservation in these assemblages remains relatively poor, with only thick-shelled dissolution-resistant taxa present.

Eocene/Oligocene Boundary Interval (78–88 mcd)

The E/O boundary transition was not recognized at the core catcher sampling resolution. Intense carbonate dissolution and a dearth of tropical marker taxa hindered precise age determination for Section 208-1262A-8H-CC (87.68 mcd), but the co-occurrence of *Globigerinatheka* spp. and *Acarinina* spp. and the absence of *Morozovella aragonensis* restricts the age of this sample to the middle Eocene (foraminiferal Zones P12–P14). Thus, the entire upper Eocene is highly condensed or contains unconformities confined to an interval that is only ~10 m thick.

Lower Eocene (~90–140 mcd)

Preservation improves downhole as lower Eocene planktonic foraminiferal assemblages are better preserved than those in the overlying units. The presence of *M. aragonensis* and the absence of such common middle Eocene taxa as *A. bullbrooki* and *Acarinina spinuloinflata* constrain Section 208-1262A-9H-CC (100.84 mcd) to Zones P7 and P8. The scarcity of *Morozovella formosa*—a critical marker species—prevents a

more precise biostratigraphic assignment for Section 208-1262A-9H-CC, although Zone P7 (52.30–50.80 Ma) is more consistent with the co-occurring calcareous nannoflora (Fig. F22).

Planktonic foraminifers in Sections 208-1262A-10H-CC through 12H-CC (111–142 mcd) are moderately to well preserved and are assigned to Zone P6; subdivision of this zone was precluded by the absence of *M. formosa*. The diverse assemblages are largely dominated by species belonging to the genus *Acarinina* with subordinate numbers of morozovellids, subbotinids, globanomaliniids, chiloguembelinids, and igorinids. Relatively large specimens of *Chiloguembelina* sp. are present in Section 208-1262B-12H-CC (115.69 mcd).

Paleocene/Eocene Boundary Interval (139.5–142 mcd)

Samples were taken at ~10-cm spacings across the P/E boundary interval in Core 208-1262A-13H. In general, the *Morozovella velascoensis* group is poorly represented in the P/E boundary interval at Site 1262 (Table T8). The T of *M. velascoensis* is provisionally placed in Sample 208-1262A-13H-5, 138–139 cm (139.49 mcd). The stratigraphic range of *M. velascoensis* typically extends well into the lowermost Eocene, but at Site 1262, its range is abbreviated primarily because of suboptimal ecological conditions. Samples 208-1262A-13H-5, 138–139 cm (139.49 mcd), through 13H-6, 19–20 cm (139.80 mcd), contain abundant moderately preserved planktonic foraminifers. Primary constituents of these assemblages are *Morozovella subbotinae*, *Morozovella aequa*, *Acarinina solidoensis*, *Acarinina coalingensis*, chiloguembelinids, *Globanomalina australiformis*, and subbotinids.

The overall abundance and preservation of planktonic foraminifers declines downhole to the P/E boundary. Samples 208-1262A-13H-6, 30–31 cm (139.91 mcd), and 43–44 cm (140.04 mcd), are from a clay-rich layer that contains few planktonic foraminifers. These depauperate assemblages are moderately preserved and consist of diminutive acarininids, subbotinids, and morozovellids. Sample 208-1262A-13H-6, 57 cm (140.18 mcd), also from the clay layer, yields an assemblage composed of relatively small acarininids, morozovellids, chiloguembelinids, and rare *G. australiformis*. Unlike other low- to mid-latitude P/E boundary intervals, the Site 1262 record contains very few *M. velascoensis* and/or related “excursion” taxa (e.g., Kelly et al., 1996); only one specimen of *Morozovella allisonensis* was found.

Uppermost Paleocene Sample 208-1262A-13H-6, 95 cm (140.56 mcd), and Section 13H-CC (142.08 mcd) from below the clay layer contain moderately preserved foraminifers that exhibit a relatively high degree of fragmentation. The presence of rare, diminutive forms of *M. velascoensis* places these two samples in Zone P5.

Upper Paleocene (140–193.5 mcd)

Preservation among upper Paleocene assemblages is variable but generally moderate. The top of Zone P4, as delimited by the T of *Globanomalina pseudomenardii*, falls between Sections 208-1262B-15H-CC and 16H-CC at an estimated depth of ~151 mcd (Fig. F22). The bottom of Zone P4, as delimited by the B of *G. pseudomenardii*, falls between Sections 208-1262B-18H-CC and 19H-CC at an estimated depth of ~183 mcd. The B of *M. velascoensis* occurs between Sections 208-1262B-18H-CC and 19H-CC at an estimated depth of ~183 mcd. The boundary between the upper and lower Paleocene (Danian) is correlative to the base

of Subzone P3a and is denoted by the B of *Morozovella angulata*, which occurs between Sections 208-1262B-19H-CC and 20H-CC at an estimated depth of ~193.5 mcd.

Upper Cretaceous–Lower Paleocene Boundary Interval (193.5–217 mcd)

Core catcher samples bracketing the K/P boundary were supplemented by sampling from Core 208-1262B-22H. Assemblages are generally well preserved, although the Maastrichtian faunas exhibit varying degrees of etching and dissolution. The base of Zone P2 is placed between Sections 208-1262B-20H-CC and 21H-CC and is thereby constrained to ~204.5 mcd. Zone P2 is underlain conformably by Subzone P1c, which is estimated to extend from ~204.64 mcd to ~214.62 mcd (Fig. F22). Planktonic foraminifers in this expanded P1c–P2 interval are well preserved.

“Dwarfed” assemblages from Subzones P1a and P1b are generally well preserved and consist primarily of diminutive forms belonging to the following taxa: *Praemurica taurica*, *Parasubbotina pseudobulloides*, *Globanomalina archeocompressa*, *Globanomalina planocompressa*, *Globoconus daubjergensis*, *Eoglobigerina eobulloides*, and *Guembelitria cretacea*. The base of Subzone P1b, as delimited by the B of *Subbotina triloculinoidea*, is tentatively placed at 216 mcd (Fig. F22).

The zonal boundary between Subzone P1a and Zone P α is located between Samples 208-1262B-22H-4, 86 cm, and 22H-4, 115 cm, at an estimated depth of ~216 mcd. Large reworked specimens of Maastrichtian foraminifers are present in Zone P α , whereas Zone P0 was not recognized in the Hole 1262B K/P boundary section. The presence of *Abathomphalus mayaroensis* and *Contusotruncana contusa* in Sample 208-1262B-22H-4, 144 cm (216.58 mcd), signifies the Maastrichtian. Thus, the K/P boundary (Fig. F22) is situated between Samples 208-1262B-22H-4, 134 cm (216.48 mcd), and 22H-4, 144 cm (216.58 mcd).

Benthic Foraminifers

Core catcher samples from Hole 1262A were semiquantitatively investigated for benthic foraminifers, as were core catchers from Hole 1262B for intervals not recovered in Hole 1262A and additional samples around critical intervals (Table T9).

In most samples, benthic foraminifers are rare and strongly outnumbered by planktonic foraminifers, with the exception of samples in which strong dissolution has affected the foraminiferal assemblages. In these samples, benthic foraminifers are common, but planktonic foraminifers are mostly absent, and there is a residue of fish debris (Sections 208-1262A-7H-CC, 8H-CC, 16H-CC, and 17H-CC and interval 208-1262C-9H-1, 145–157 cm). These samples contain evidence of down-slope transport. Sections 208-1262A-6H-CC and 208-1262B-9H-CC and Sample 208-1262A-13H-6, 43–44 cm, are barren.

Benthic foraminiferal assemblages from Site 1262 indicate deposition at lower abyssal depths (>3000 m) for Sections 208-1262B-1H-CC through 17H-CC (0–166 mcd). Assemblages in samples from 166 through 188 mcd (Sections 208-1262B-17H-CC through 19H-CC) indicate deposition at transitional upper to lower abyssal depths (e.g., Alegret and Thomas, 2001), and assemblages below 188 mcd indicate lowermost upper abyssal depths (~3000 m).

T9. Selected benthic foraminifers, p. 80.

The mudline sample and core catcher samples down through interval 208-1262A-4H-CC (46 mcd) contain faunas similar to those presently living in the Walvis Ridge area (Mackensen et al., 1995; Schmiedl et al., 1997), with rare *Epistominella exigua* and *Alabaminella weddellensis* (phytodetritus-consuming species). Assemblages are dominated by *Nuttallides umbonifera*, an indicator of the presence of Antarctic Bottom Water, which has been argued to be present to the north of Walvis Ridge below depths of ~4200 m (Schmiedl et al., 1997). *Cibicidoides wuellerstorfi* is rare between 0 and 36 mcd. Other common species include *Pullenia* spp., *Oridorsalis umbonatus*, *Stainforthia complanata*, and *Globocassidulina subglobosa*.

Assemblages in Sections 208-1262A-5H-CC (56.83 mcd) through 208-1262B-9H-CC (83.94 mcd) are difficult to interpret because of strong dissolution, leaving only solution-resistant forms and signs of downslope transport of large, heavy-shelled taxa.

Section 208-1262A-9H-CC (100.84 mcd) through Sample 13H-6, 30–31 cm (139.91 mcd), generally contain rare benthic foraminifers because of very high planktonic to benthic ratios. The faunas are similar to those described at other abyssal sites in the South Atlantic Ocean (Clark and Wright, 1984; Müller-Merz and Oberhänsli, 1991; Thomas and Shackleton, 1996), with common to abundant small smooth-walled species belonging to the genera *Abyssamina*, *Quadriflorina*, and *Clinapertina* and common to abundant *Nuttallides truempyi*. Other taxa commonly present include *Tappanina selmensis*, *Siphogenerinoides brevispinosa*, and *Aragonina aragonensis* (none of the three are more abundant than a few percent), various species of *Gyroidinoides*, laevidentalinid and pleurostomellid taxa, *Anomalinoides spissiformis*, *Nonion hawaiiense*, and *O. umbonatus*. The species richness fluctuates, with the abundance of various abyssaminid taxa inversely correlated to species richness. The lowest species richness and a high relative abundance of *Abyssamina poagi* occur in the lower part of the interval and in Sample 208-1262C-2H-6, 35–36 cm (117.14 mcd), in a reddish clay layer.

The major extinction of benthic foraminifers at the end of the Paleocene (BEE) occurs between Sample 208-1262A-13H-6, 57–58 cm (140.18 mcd), and barren Sample 208-1262A-13H-6, 43–44 cm (140.04 mcd). Faunas in the lowermost nonbarren samples (i.e., immediately after the extinction) have very low species richness and are dominated by small thin-walled specimens of *N. truempyi* and various species of *Abyssamina*, *Clinapertina*, and *Quadriflorina*, as at DSDP Site 527 (Thomas and Shackleton, 1996). The uppermost sample below the extinction has a very diverse fauna with a typical upper Paleocene assemblage, but all specimens are diminutive.

Samples between 208-1262A-13H-6, 57–58 cm, through 15H-CC (140–162 mcd) contain a typical preextinction Paleocene highly diverse abyssal assemblage, with common *Stensioeina beccariiformis*, *Cibicidoides hyphalus*, *Pullenia coryelli*, *Bulimina thanetensis*, *Aragonina velascoensis*, large agglutinative taxa such as *Clavulinoides amorphus*, *Clavulinoides trilatera*, *Marssonella oxycona*, as well as large smooth-walled *Gyroidinoides* species such as *Gyroidinoides beisseli* and *Gyroidinoides globosus*, all of which had their last appearance during the extinction. In this interval, *S. brevispinosa* and *Rectobulimina carpentierae* are present in most samples and their relative abundances are highly variable. Lower bathyal indicator species are absent.

The assemblages change gradually in species composition in the interval between Sections 208-1262B-17H-CC and 19H-CC (166–188 mcd), with *Abyssamina* and *Clinapertina* species as well as *B. thanetensis*

becoming less common downhole and *Nuttallinella florealis* and *Nuttallinella* sp. becoming more common. At the bottom of this interval, *Spiroplectammina dentata* has its local uppermost occurrence, as does *Nuttallinella coronula* and *Tritaxia havanensis*. Benthic foraminiferal assemblages changed at about this time at ODP Sites 689 and 690 at Maud Rise (Thomas, 1990), but at Site 1262, the faunal changes might be the result of a change in paleodepth from upper abyssal in the lower part of the section to lower abyssal in its upper parts.

The benthic foraminiferal assemblages below 188 mcd closely resemble assemblages in the Velasco Formation in Mexico, where many of the species present at Site 1262 were first described (see review in Alegret and Thomas, 2001). Assemblages across the K/P boundary (Samples 208-1262B-22H-4, 134–135 cm, and 22H-CC; 216.50–221.75 mcd) document that benthic foraminifers at Site 1262 do not suffer significant extinction, as is observed at many other sites. The uppermost occurrences of *Angulogerina szajnochae* and *Praebulimina reussi* occur close to the K/P boundary in the preliminary data, but it is not well documented whether these species disappeared globally at that time.

PALEOMAGNETISM

Drilling and Core Orientation

All cores from Hole 1262A were recovered using two nonmagnetic core barrels. One of the nonmagnetic core barrels was damaged at the base of Hole 1262A, so Hole 1262B and all subsequent holes during Leg 208 were drilled using the remaining nonmagnetic core barrel every other core. The odd-numbered cores were recovered with the nonmagnetic barrel, and the even-numbered cores were recovered with a regular steel barrel. After the first core barrel had to be drilled over (see Table T1; “Operations,” p. 2), only regular steel barrels were deployed. No obvious differences were observed in the magnetic data between sediments retrieved with the nonmagnetic core barrel and those retrieved with the regular steel barrel.

All cores were oriented with the Tensor tool with the exception of Cores 208-1262A-4H through 7H and 208-1262B-16H through 21H. In these cases, the Tensor tool did not record the time and Tensor tool data from these cores should be viewed with caution.

Archive-Half Measurements

The archive halves of 54 cores from Holes 1262A, 1262B, and 1262C were measured in the pass-through magnetometer. Natural remanent magnetization (NRM) was measured on all cores. Most cores were demagnetized at 10 and 15 mT. A few cores were demagnetized only at 15 mT to speed the core flow through the core laboratory. Sections that clearly suffered from severe drilling disturbance were either not measured or were measured only at 15 mT.

As many of the sediments were very soft and easily deformed, a test was made to determine if splitting the cores was contributing to noise in the data. One core section (208-1262A-33H-1) was measured at 0, 10, and 15 mT before splitting. The results were compared with those from the archive half, which was demagnetized at 15 mT. No significant differences in the data were found, and all of the remaining cores were split and measured as usual. Note that many cores were much more

soupy than the one tested, and it remains possible that these cores were affected by the splitting.

A strong drilling overprint in the downhole direction was observed in the data from nearly all the cores but was largely removed in most cases by demagnetization to 10 mT (Fig. F24). Test Sections 208-1262A-14H-6 (reversed) and 208-1262B-5H-3 (normal) were demagnetized up to 25 mT. It was concluded that 15 mT is sufficient to remove most of the overprint and to determine the characteristic polarity of the sediment without compromising the magnetization of the cores for future study.

Remanent Magnetization Intensity

Intensities of initial remanent magnetization (prior to alternating-field [AF] demagnetization) in sediments were mostly on the order of 10^{-2} to 10^{-1} A/m (Fig. F25). Intensity values after AF demagnetization to 15 mT (and removal of the overprint) were typically an order of magnitude lower. A considerable increase in the component between 0 and 10 mT was observed in Cores 208-1262A-5H through 9H and 17H. High-intensity spikes at the top of each core are interpreted as representing coring-induced magnetization and/or contaminants from the core barrel.

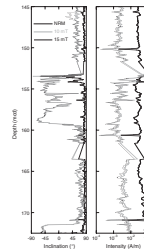
Depositional remanent magnetization (DRM) following demagnetization to 15 mT ($\text{DRM}_{15 \text{ mT}}$), DRM normalized by initial susceptibility ($n\text{DRM}_{15 \text{ mT}}$), and differential DRM between 10 and 15 mT ($d\text{DRM}_{10-15 \text{ mT}}$) curves for Hole 1262A are plotted in Figure F26. The variations in $n\text{DRM}_{15 \text{ mT}}$ and $d\text{DRM}_{10-15 \text{ mT}}$ normalized by susceptibility ($nd\text{DRM}_{10-15 \text{ mT}}$) display very similar trends, indicating that the ferromagnetic coercivity fraction of 10–15 mT may play a role as a proxy of relative paleointensity.

Magnetostratigraphy

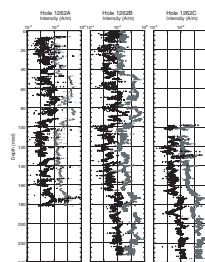
Magnetostratigraphy is generally interpretable in the nannofossil ooze units. The record is more difficult to interpret in the clay units, which are characterized by much slower sediment accumulation rates and possibly multiple hiatuses in the Neogene. Although the signal in the clay units appears to be well resolved and some features correlate well between holes, no chron identifications have been made in the clay units.

Preliminary chron identifications for the three holes are shown in Figure F27, and age-depth tie points are given in Table T10. In the Pliocene–Pleistocene section, the Brunhes (C1n), Jaramillo (C1r.1n), and Cobb Mountain events appear to be quite well defined and agree with both the biostratigraphy and cyclostratigraphy. Chron C2n appears to be well resolved in Hole 1262B only, but its location is constrained by the nannofossil datum Subzone CN13a assemblage (1.7–1.8 Ma) from 16.01 to 17.22 mcd (see “**Biostratigraphy**,” p. 9; Table T5). Several other short normal events are also evident in the Matuyama reversed polarity period and may correlate with the Reunion and other short events observed elsewhere. Whereas the top of Chron C2An appears quite clearly in sediments from both Holes 1262A and 1262B, the base (3.596 Ma) is less well defined, especially for Hole 1262B. The base of Chron C2An is placed in a core gap in Hole 1262A at ~36 mcd. This

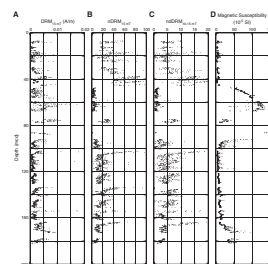
F24. Inclination and intensity data, Hole 1262B, p. 48.



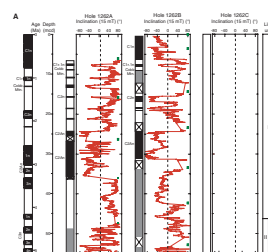
F25. Downhole variation in intensities, 0- and 15-mT demagnetization, p. 49.



F26. Downhole variations in DRM, $n\text{DRM}$, $nd\text{DRM}$, and MS, p. 50.



F27. Magnetostratigraphic interpretation, p. 51.



T10. Magnetostratigraphic age-depth tie points, p. 84.

depth corresponds with the base of the nannofossil datum Subzone CN12aB assemblage (2.83–3.66 Ma) at 35.7 mcd.

The nannofossil ooze unit corresponding to lithostratigraphic Sub-unit IIB is characterized by predominantly reversed polarity and appears to correlate to Chron C12r. Chron C13n (33.058–33.545 Ma) is placed at the base of this unit and is nicely bracketed by nannofossil datums with the T of *E. formosa* (32.9 Ma) above and *D. saipanensis* (34.0 Ma) below.

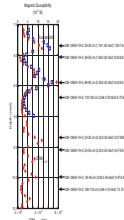
The next oldest identifiable chronos are in the Eocene, and although this part of the record is not well resolved for any of the holes, the top of Chron C23n (50.778 Ma) is tentatively placed at ~93 mcd. This reversal appears to be relatively distinct in Hole 1262A sediments (Fig. F27B), and the depth roughly agrees with the B of *Discoaster sublodoensis* (49.3 Ma) and the T of *T. orthostylus* (51.0 Ma). The base of Chron C24n (53.347 Ma) appears to be resolved only for Hole 1262C at ~120 mcd. Again, this depth roughly agrees with those of the top of nannofossil datum *D. multiradiatus* (53.0 Ma), the B of *S. radians* (53.3 Ma), and the B of *T. orthostylus* (53.4 Ma) from Hole 1262B. Confirmation of this reversal awaits shore-based analysis of discrete samples.

Chrons C25n through C28n are clearly seen and agree well between all holes (Fig. F27D). The base of Chron C29n (64.745 Ma) above the K/P boundary appears to fall in a Hole 1262C core break and is not well resolved for Hole 1262B. The reversal from Chron C29r to C29n is placed at ~215 mcd, based largely on the eccentricity cycles seen in the MS data for Hole 1262B, which put the reversal at ~300 k.y. above the K/P boundary.

Rock Magnetic Studies

A number of fluctuations in MS are seen in Hole 1262A. These features are strongly correlated with characteristic magnetic remanence ($DRM_{15\text{ mT}}$) (Fig. F28) as well as lithologic variations. Preliminary rock magnetic tests were performed on discrete samples associated with MS peaks in the interval 7.8–10.2 mcd from the working half. In most cases, the characteristic component is readily isolated after removal of a low-coercivity component by 15-mT demagnetization. Based on isothermal remanent magnetization (IRM) acquisition and backfield IRM analysis, magnetite is the most dominant ferromagnetic mineral in the sediments over this short interval. Grain size is identified as single domain or pseudosingle domain based on the median destructive fields (MDF) of anhysteretic remanent magnetization (ARM) and IRM (peaks: $MDF_{ARM} = 20.06 \pm 0.06$ mT, $MDF_{IRM} = 21.83 \pm 0.71$ mT; troughs: $MDF_{ARM} = 21.07 \pm 0.12$ mT, $MDF_{IRM} = 20.07 \pm 0.07$ mT). The magnetic behavior of samples from both peaks and troughs is very similar, indicating that magnetite concentration is the primary control on DRM and MS fluctuations.

F28. Discrete sample positions, p. 56.



(C₂–), propane (C₃), and propene (C₃₌) were detected in three samples from the top of Hole 1262B and near the bottom of Hole 1262A, showing low C₁/C₂ ratios; however, the concentration of these gases never exceeded 10 ppmv.

Interstitial Water Chemistry

Interstitial water from 20 samples was collected at Site 1262: 14 from Hole 1262A (13.5–179.0 mcd), 4 from Hole 1262B (4.5–231.0 mcd), and 2 from Hole 1262C (201.4–210.2 mcd). The samples from the three holes were taken to constitute a single depth profile using the composite depth scale. However, slight differences in lithology may cause minor breaks in concentration-depth gradients of some chemical parameters. Chemical constituents were determined according to the procedures outlined in “Geochemistry,” p. 23, in the “Explanatory Notes” chapter. Results of the chemical analyses are presented in Table T12.

T12. Pore water analyses, p. 86.

pH, Salinity, Alkalinity, Chloride, and Sodium

The pH of pore waters at Site 1262 ranges from 7.4 to 7.6 (average = 7.50 ± 0.06) (Table T12). All pH values are lower than the average seawater value of 8.1, and the general trend is a decrease with depth. Salinity typically ranges from 34.0 to 35.5, although an anomalous value of 37.0 was recorded at 128.5 mcd.

Alkalinity decreases slightly from 2.6 mM in the shallowest sample at 4.5 mcd to 2.3 mM at 231.0 mcd (Fig. F29A). The maximum alkalinity of 2.9 mM occurs at 54.4 mcd; the average alkalinity through this interval is 2.50 ± 0.15 mM. Below ~150 mcd, alkalinity values vary more than those in the upper 150 m.

The chloride concentrations generally increase with depth from a minimum value of 565 mM (13.5 mcd) to 574 mM (210.2 mcd) (Fig. F29B) (mean = 564 ± 18 mM). Several samples in this interval contain lower chloride values (527 mM at 43.5 mcd and 550 mM at 201.4 mcd). The highest value (577 mM) occurs at 170.9 mcd.

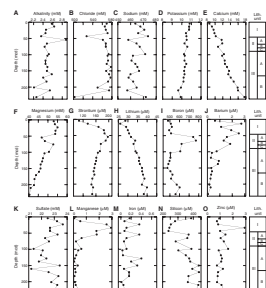
Sodium concentrations are more variable than those of chloride, with values ranging from 457 to 474 mM (Fig. F29C). The sodium profile does not exhibit any significant downcore trend or correlation to changes in chloride concentration.

Potassium, Calcium, Magnesium, Strontium, and Lithium

Site 1262 downcore trends in potassium, calcium, and magnesium are consistent with those resulting from exchange with basaltic basement at depth (Gieskes, 1981), with potassium and magnesium decreasing and calcium increasing slightly with depth (Fig. F29D, F29E, F29F). Pore water potassium concentrations decrease slightly from 10.8 mM (4.5 mcd) to 9.9 mM (231.0 mcd) (Fig. F29D). Calcium values increase from 8.5 mM (4.5 mcd) to 17.6 mM (231.0 mcd) (Fig. F29E). The magnesium profile (Fig. F29F) is characterized by a general decrease with depth, from 53.0 mM in the shallowest sample (4.5 mcd) to 40.4 mM at the base of the section (231.0 mcd).

Strontium concentrations increase from 110 µM (4.5 mcd) to 194 µM (54.4 mcd). Below this depth, strontium values decrease to 146 µM (231.0 mcd), indicating removal of strontium at depth (Fig. F29G). The slight convex-upward nature of the upper part of the strontium pore water profile suggests that some carbonate dissolution has occurred in

F29. Chemical constituents in interstitial waters, p. 57.



the upper ~75 mcd of the sediment column (e.g., Baker et al., 1982). In general, lithium concentrations increase gradually from 29 μM in the shallowest sample (4.5 mcd) to 40 μM toward the base of the section (210.2 mcd) (Fig. F29H). The increase with depth suggests a source of lithium from the sediment or underlying basement rock into the pore waters.

Boron and Barium

Boron values exhibit a slight increase with depth, from 468.6 μM (4.5 mcd) to 530.9 μM (231.0 mcd) (Fig. F29I). Superimposed on this trend is a peak to 757.1 μM (65.7 mcd). Values decrease back to 499.2 μM at 103.4 mcd. Pore water barium concentrations increase from 0.6 μM to 2.5 μM over the depth interval from 4.5 to 13.5 mcd (Fig. F29J) then decrease downcore to a value of 0.04 μM at the bottom of the section (231.0 mcd).

Sulfate, Manganese, and Iron

The pore water profile at Site 1262 is characterized by a general downhole decrease in sulfate from 4.5 to ~140 mcd (Fig. F29K). The relatively high concentrations of sulfate (mean = $22.54 \pm 0.65 \text{ mM}$) reflect the very low organic matter content of the sedimentary section recovered at Site 1262 (see “[Carbonate and Organic Carbon](#),” p. 22, in “[Sediment Geochemistry](#)”). The manganese pore water profile exhibits a broad maximum extending from 23.2 to 54.4 mcd (Fig. F29L) and reaching values up to 2.9 μM . The mean concentration above and below this interval is $0.26 \pm 0.21 \mu\text{M}$. The peak concentrations may be consistent with slightly enhanced reduction of manganese oxides; however, there is no subsequent increase in reduced iron below this manganese peak that would indicate enhanced microbial reduction. The base of the dissolved manganese peak also corresponds to the upper portion of a lithologic boundary between carbonate ooze above ~45 mcd and clay below (see “[Lithostratigraphy](#),” p. 5).

Pore water concentrations of dissolved iron are typically low and invariant throughout the interval analyzed (Fig. F29M). The mean iron concentration is $0.15 \pm 0.12 \mu\text{M}$. Given the relatively high pore water sulfate and lack of elevated iron concentrations throughout the interval, anaerobic microbial activity was probably not sufficiently intense to cause reduction of Fe(III) to Fe(II).

Silicon and Zinc

Pore water silicon concentrations (Fig. F29N) decrease from the shallowest value of 385 μM (4.5 mcd) to 239 μM (43.5 mcd) then increase to 369 μM (54.4 mcd). The remainder of the profile is variable with a slight overall silicon increase to 412 μM (231.0 mcd). Zinc concentrations from Site 1262 pore waters were low and relatively constant, ranging from 0.9 to 1.4 μM (Fig. F29O). One sample (33.8 mcd) yielded a concentration of 2.9 μM , but this is most likely an anomalous value.

Summary of Interstitial Water Chemistry

The Site 1262 pore water profiles described above are dominated by the diffusional gradient between seawater and basalt of the underlying basement. This relationship is demonstrated in the potassium, calcium,

and magnesium profiles. Little evidence of enhanced microbial influence exists in these profiles, as is reflected in the sulfate, manganese, and iron profiles.

Sediment Geochemistry

Carbonate and Organic Carbon

Carbonate determinations by coulometry were made for a total of 134 samples from Site 1262, 11 from Hole 1262A, 21 from Hole 1262B, and 2 from Hole 1262C (Table T13). Samples were selected to provide a measure of the carbonate content in different lithostratigraphic units (Fig. F30A) and to assess the influence of carbonate content on L*. High-resolution samples (every 2–5 cm) were also taken to assess the change in carbonate content across the P/E boundary (Fig. F30B). The carbonate values in Unit I are ~90 wt%, except for one anomalous value of 46 wt%. Carbonate contents in Subunit IIA are very low (mean = 4.3 wt%). Subunit IIB contains higher carbonate contents (mean = 68.1 wt%), whereas Subunit IIC values increase downsection from 8 to 93 wt%. Subunit IIIA is characterized by high carbonate contents (mean = 92.4 wt%). Values of Subunit IIIB sediments are lower and more variable, ranging from 20 to 97 wt%. High-resolution carbonate determinations across the P/E boundary section of Hole 1262A (Fig. F30B) reveal a gradual decline in carbonate content below the clay interval from ~85 wt% above 140.31 mcd to ~77 wt% at 140.16 mcd. Between 140.13 and 140.11 mcd, the carbonate content drops from >70 to <1 wt%. Carbonate contents of <1 wt% persist from 140.11 mcd uphole until 139.96 mcd (15 cm). From 139.93 to 139.51 mcd, carbonate contents rise to >90 wt%.

Elemental analysis of carbon indicates generally low concentrations of organic matter from Site 1262 sediments (Table T13). Several of the samples analyzed contained organic carbon concentrations slightly greater than zero, with values ranging from 0.0 to 0.3 wt%. Eleven samples yielded conspicuously high organic carbon values, most likely attributable to analytical artifacts and error (i.e., subtracting inorganic carbon values obtained by coulometry from total carbon values obtained by combustion to calculate organic carbon). None of the analyzed samples contained measurable nitrogen.

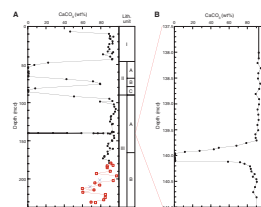
Extractable Hydrocarbons

Extraction of organic matter was attempted on several sample residues after squeezing interstitial water. Analyzable amounts of extracts were obtained from carbonate-rich interval 208-1262B-1H-3, 145–150 cm (4.5 mcd), and clay-rich intervals 208-1262A-6H-5, 145–150 cm (65.6 mcd), and 8H-2, 145–150 cm (83.4 mcd). Carbonate-rich sediments from intervals 208-1262A-12H-5, 140–150 cm (128.5 mcd), and 13H-4, 140–150 cm (138.0 mcd), did not yield hydrocarbons detectable with the gas chromatography–mass spectrometry selective detector (GC-MSD).

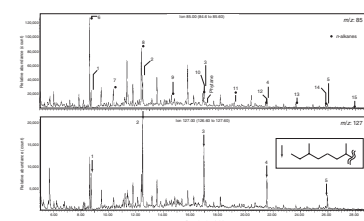
Total ion chromatography indicates that the aliphatic hydrocarbon fraction of interval 208-1262B-1H-3, 145–150 cm, is dominated by *n*-alkanes of algal origin. In contrast, the aliphatic fraction of clay-rich interval 208-1262A-8H-2, 145–150 cm, contains branched isoprenoids, specifically anteiso-alkanes against *n*-alkanes (Fig. F31), suggesting a cyanobacterial contribution to the sedimentary organic matter. No long-

T13. Calcium carbonate and total and organic carbon, p. 87.

F30. Carbonate contents vs. composite depth, p. 58.



F31. Gas chromatogram, p. 59.



chain alkanes indicative of terrestrial input were detected. Compounds identified with the GC-MSD are listed in Table T14.

AGE MODEL AND MASS ACCUMULATION RATES

A 236.4-mcd-thick (213.0 mbsf) Maastrichtian (~66 Ma) to Pleistocene pelagic sediment sequence was recovered at Site 1262. A total of 66 biostratigraphic datums and 23 magnetostratigraphic datums (Table T15) were selected to construct an age-depth model for this site (Table T16; Fig. F32). Linear sedimentation rates (LSRs), total mass accumulation rates (MARs), and carbonate MARs were calculated at 1-m.y. intervals (see “Age Model and Mass Accumulation Rates,” p. 33, in the “Explanatory Notes” chapter).

Age-Depth Model

The main objective of Site 1262 was to recover a complete and well-resolved upper Maastrichtian to lower Eocene section, and the site was chosen to yield this critical stratigraphic interval at a relatively shallow burial depth. The sediment section at Site 1262 is therefore characterized by significant condensed intervals and unconformities throughout the upper lower Eocene to the lower upper Miocene section (51–7 Ma; 94–44 mcd). Biostratigraphic and magnetic reversal data are in general agreement for the Maastrichtian to lowermost Eocene section and the uppermost Miocene to Pleistocene section (Fig. F32). In the younger interval, the age-depth model relies primarily on paleomagnetic and nannofossil data. Below 94 mcd, we relied primarily (although not exclusively) upon calcareous nannofossil datums to define the age-depth model. The most significant discrepancy between nannofossil and planktonic foraminiferal datums exists in the condensed middle to upper Eocene interval. Apparent discrepancies in the upper Paleocene probably result from the lower resolution of shipboard studies and possible lack of intercalibration.

Linear Sedimentation and Mass Accumulation Rates

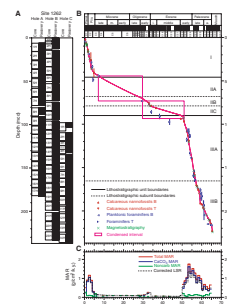
LSRs range between <1 and 14 m/m.y., and total MARs range from <0.1 to 1.8 g/cm²/k.y. Total MAR fluctuations essentially represent variations in carbonate MAR. LSRs and carbonate MARs show a broad peak from 65 to 50 Ma with the greatest values at 54–53 Ma and a second peak from 5 to 0 Ma with the greatest values at 2–3 Ma. Noncarbonate MARs averaged over 1-m.y. intervals are generally low (<0.2 g/cm²/k.y.) throughout the section, and the small fluctuations may be within the analytical uncertainty of the data. The Paleocene–Eocene sediment record is characterized by carbonate-poor intervals of a few centimeters to several decimeters in thickness (see “Lithostratigraphy,” p. 5, and “Geochemistry,” p. 19). These short-term carbonate dissolution events are smoothed out in our MAR record as a result of our 1-m.y. sampling of the age-depth model, dictated by the limited resolution of the shipboard age-depth control points and density and carbonate data.

T14. GC-MSD hydrocarbon peaks, p. 89.

T15. Age-depth model, LSRs, and MARs, p. 90.

T16. Datum levels, p. 92.

F32. Core recovery, age-depth model, and LSR and MAR, p. 60.



REFERENCES

- Alegret, L., and Thomas, E., 2001. Upper Cretaceous and lower Paleogene benthic foraminifera from northeastern Mexico. *Micropaleontology*, 47:269–316.
- Baker, P.A., Gieskes, J.M., and Elderfield, H., 1982. Diagenesis of carbonates in deep-sea sediments—evidence from $\text{Sr}^{2+}/\text{Ca}^{2+}$ ratios and interstitial dissolved Sr^{2+} data. *J. Sediment. Petrol.*, 52:71–82.
- Cande, S.C., and Kent, D.V., 1995. Revised calibration of the geomagnetic polarity timescale for the Late Cretaceous and Cenozoic. *J. Geophys. Res.*, 100:6093–6095.
- Clark, M.W., and Wright, R.C., 1984. Paleogene abyssal foraminifers from the Cape and Angola basins, South Atlantic Ocean: DSDP 73. In Hsü, K.J., LaBrecque, J.L., et al., *Init. Repts. DSDP*, 73: Washington (U.S. Govt. Printing Office), 459–480.
- Gieskes, J.M., 1981. Deep-sea drilling interstitial water studies: implications for chemical alteration of the oceanic crust, layers I and II. In Warme, J.E., Douglas, R.G., and Winterer, E.L. (Eds.), *The Deep Sea Drilling Project: A Decade of Progress*. Spec. Publ.—Soc. Econ. Paleontol. Mineral., 32:149–167.
- Hsü, K.J., LaBrecque, J.L., et al., 1984. *Init. Repts. DSDP*, 73: Washington (U.S. Govt. Printing Office).
- Kelly, D.C., Bralower, T.J., Zachos, J.C., Premoli Silva, I., and Thomas, E., 1996. Rapid diversification of planktonic foraminifera in the tropical Pacific (ODP Site 865) during the Late Paleocene Thermal Maximum. *Geology*, 24:423–426.
- Lourens, L.J., Hilgen, F.J., Laskar, J., Shackleton, N.J., and Wilson, D., in press. The Neogene period. In Gradstein, F.M., Ogg, J., and Smith, A.G. (Eds.), *A Geological Time Scale 2004*: Cambridge (Cambridge Univ. Press).
- Lyle, M.W., Wilson, P.A., Janecek, T.R., et al., 2002. *Proc. ODP Init. Repts.*, 199 [CD-ROM]. Available from: Ocean Drilling Program, Texas A&M University, College Station, TX 77845-9547, USA.
- Mackensen, A., Schmiedl, G., Harloff, J., and Giese, M., 1995. Deep-sea foraminifera in the South Atlantic Ocean: ecology and assemblage generation. *Micropaleontology*, 41:342–358.
- Martini, E., 1971. Standard Tertiary and Quaternary calcareous nannoplankton zonation. In Farinacci, A. (Ed.), *Proc. 2nd Int. Conf. Planktonic Microfossils Roma*: Rome (Ed. Tecnosci.), 2:739–785.
- Moore, T.C., Jr., Rabinowitz, P.D., et al., 1984. *Init. Repts. DSDP*, 74: Washington (U.S. Govt. Printing Office).
- Müller-Merz, E., and Oberhänsli, H., 1991. Eocene bathyal and abyssal benthic foraminifera from a South Atlantic transect at 20–30°S. *Palaeogeogr., Palaeoclimatol., Palaeoecol.*, 83:117–171.
- Schmiedl, G., Mackensen, A., and Müller, P.J., 1997. Recent benthic foraminifera from the eastern South Atlantic Ocean: dependence on food supply and water masses. *Mar. Micropaleontol.*, 32:249–287.
- Thomas, D.J., Bralower, T.J., and Zachos, J.C., 1999. New evidence for subtropical warming during the Late Paleocene Thermal Maximum: stable isotopes from Deep Sea Drilling Project Site 527, Walvis Ridge. *Paleoceanography*, 14:561–570.
- Thomas, E., 1990. Late Cretaceous through Neogene deep-sea benthic foraminifers (Maud Rise, Weddell Sea, Antarctica). In Barker, P.F., Kennett, J.P., et al., *Proc. ODP, Sci. Results*, 113: College Station, TX (Ocean Drilling Program), 571–594.
- Thomas, E., and Shackleton, N., 1996. The Palaeocene–Eocene benthic foraminiferal extinction and stable isotope anomalies. In Knox, R.W.O'B., Corfield, R.M., and Dunay, R.E. (Eds.), *Correlation of the Early Paleogene in Northwest Europe*. Geol. Soc. Spec. Publ., 101:401–441.

Figure F1. *Meteor* Cruise M49/1 track chart showing the location of Site 1262 (proposed Site WALV-12A) and alternate Sites WALV-12B and WALV-12C along lines GeoB 01-035 and GeoB 01-036.

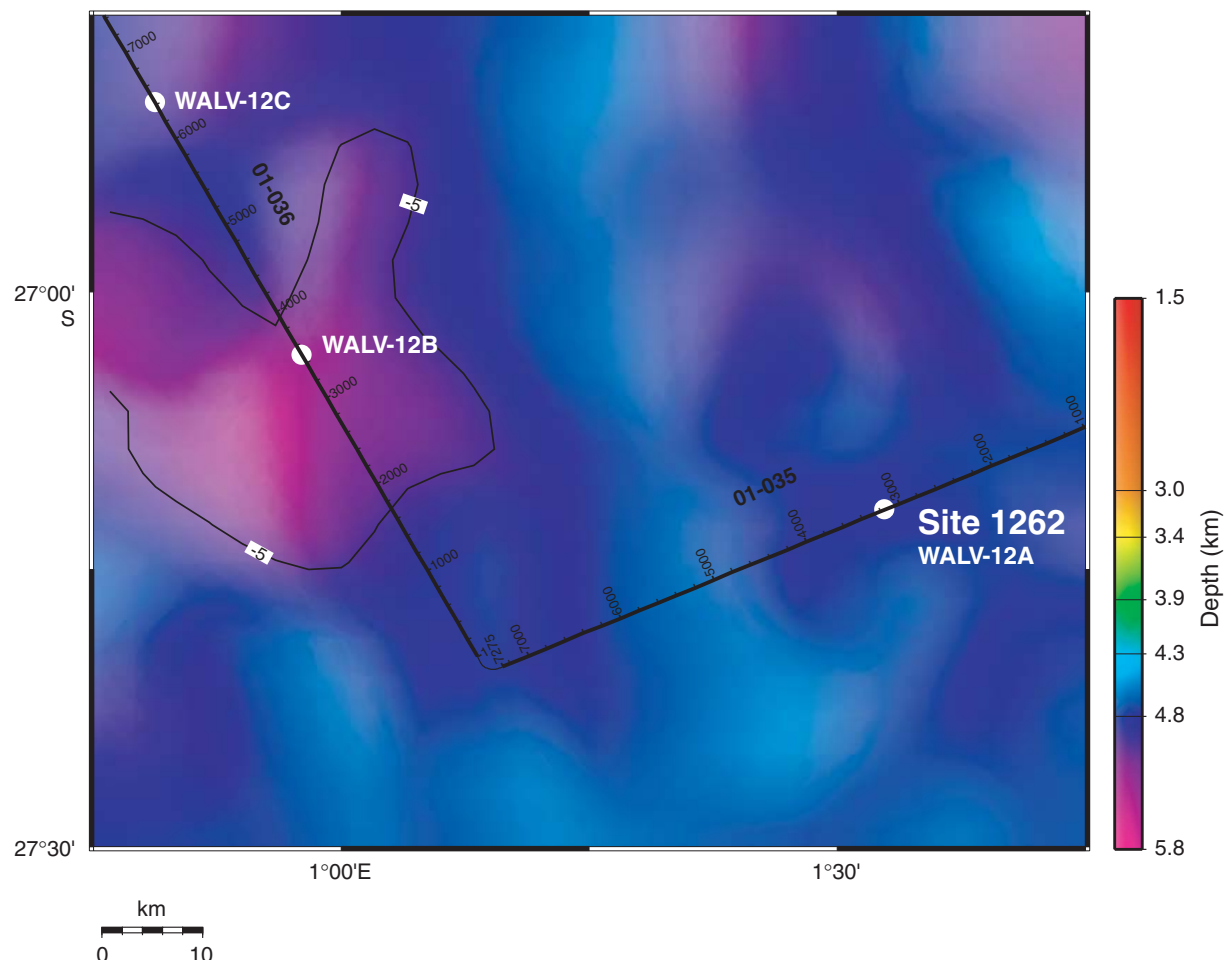


Figure F2. Line GeoB 01-035 (Part 1) and Site 1262 in a perched basin. GI = generated injection. CDP = common depth point. V.E. = vertical exaggeration.

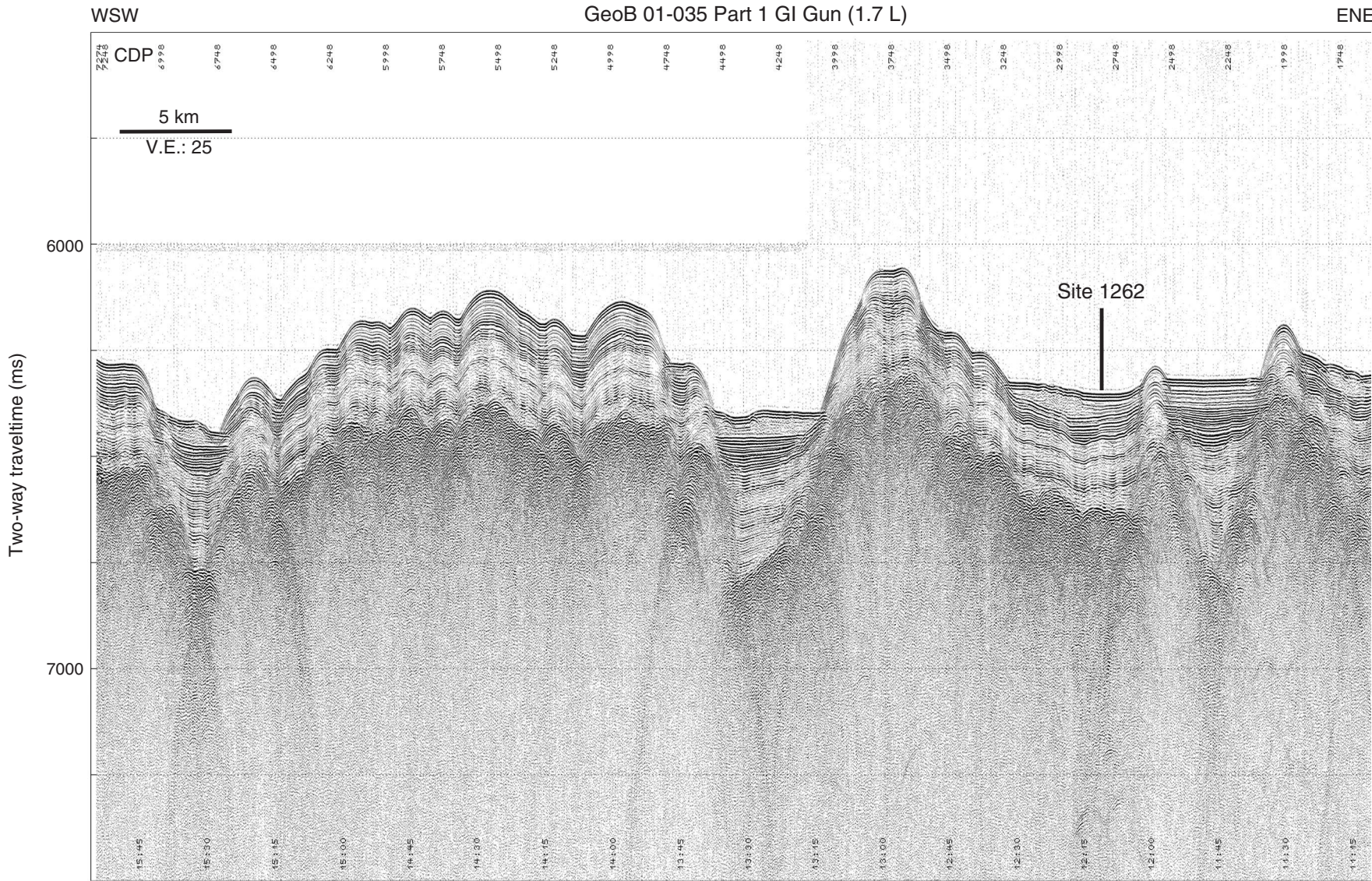


Figure F3. Line GeoB 01-035 and Site 1262 plotted along with age estimates of prominent reflectors. R_1 is a regional reflector that marks a local unconformity. Although time transgressive, sediments below the reflector tend to be Paleogene and sediments above the reflector are Neogene. The P/E boundary reflector ($R_{P/E}$) is estimated to be at 126 mbsf and the K/P boundary ($R_{K/P}$) at 198 mbsf. Both reflectors can be traced over most of the ridge. CDP = common depth point. V.E. = vertical exaggeration.

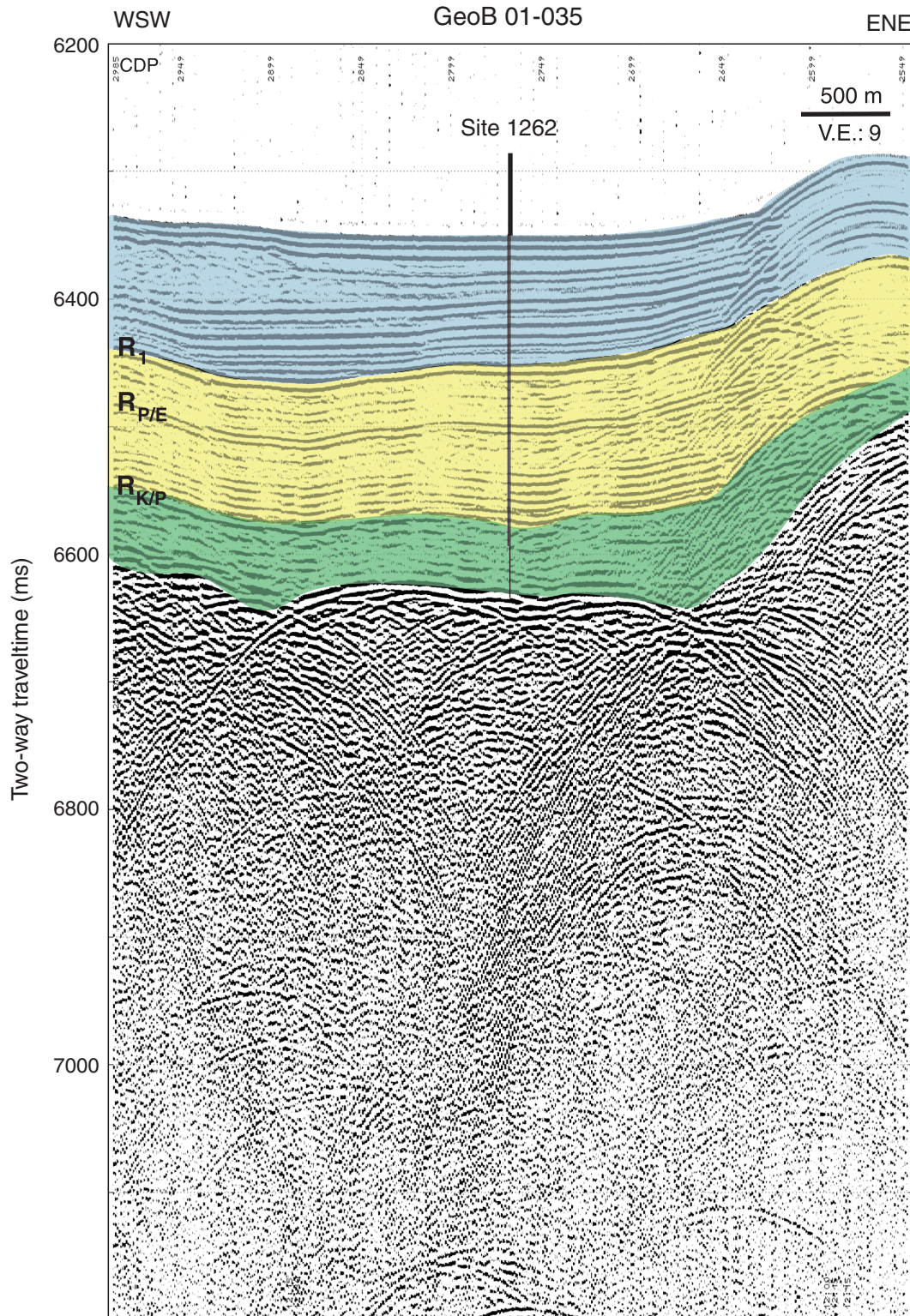


Figure F4. Magnetic susceptibility data for 0 to 236 mcd of Site 1262. Data from Holes 1262A, 1262B, and 1262C are offset from the spliced record by 10, 100, and 1000 times their values, respectively. Numbers near the tops of the individual core records are the core numbers. * = data from the top of the core is missing or removed because of coring disturbance.

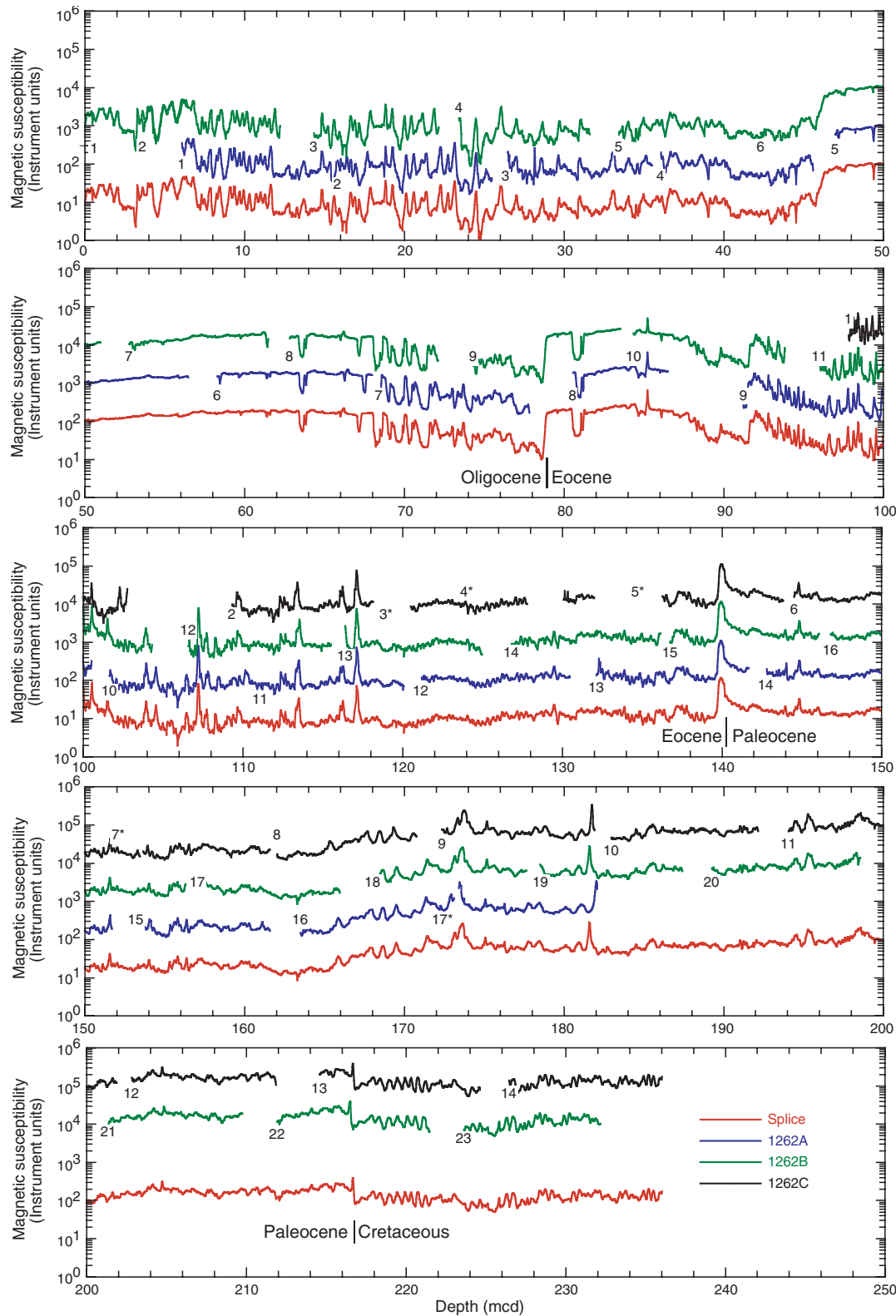


Figure F5. Mbsf vs. mcd growth rates for Holes 1262A, 1262B, and 1262C.

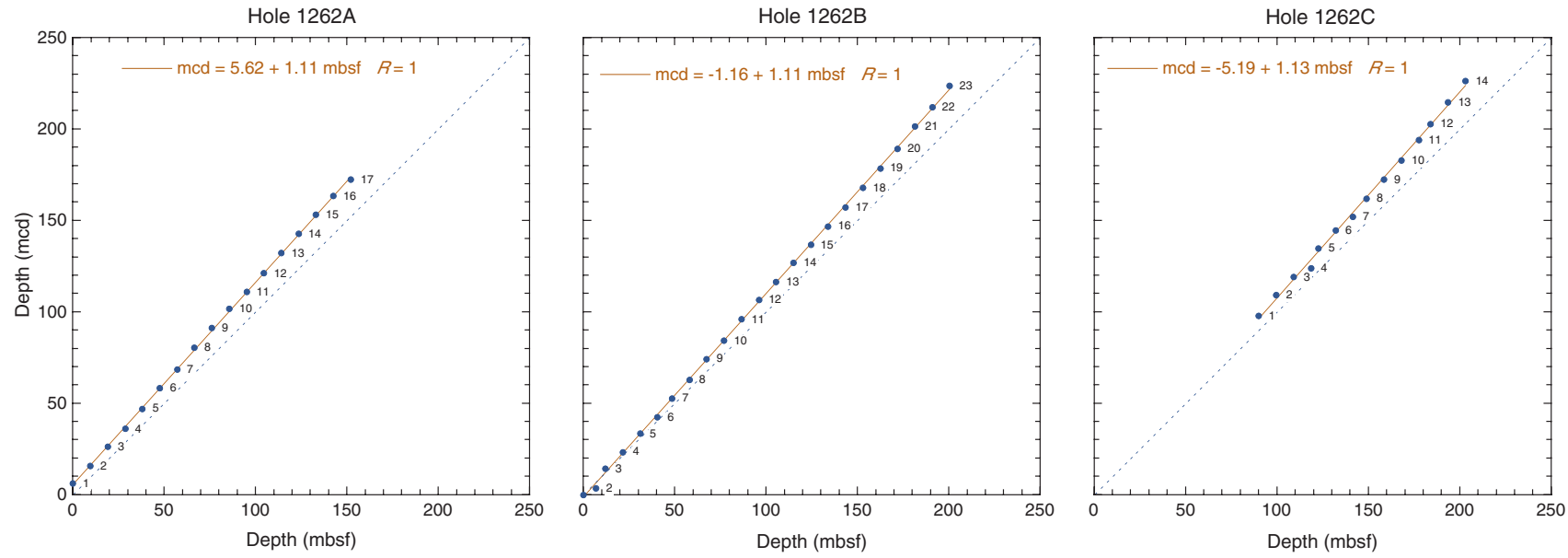


Figure F6. Site 1262 lithostratigraphic composite illustrating stratigraphic variation in predominant and accessory smear slide components. 3-pt MA = 3-point moving average.

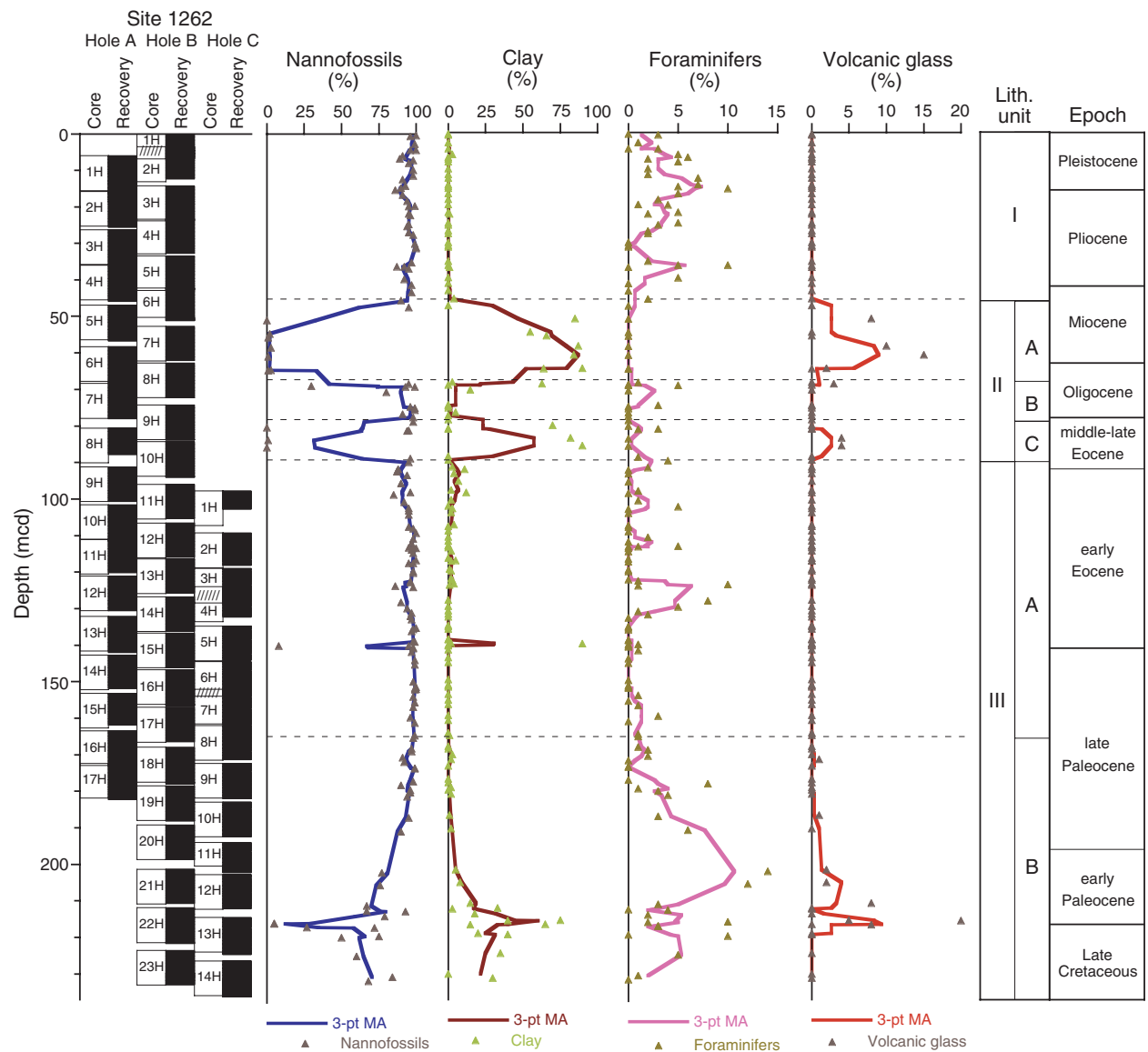


Figure F7. Site 1262 lithostratigraphic composite illustrating downhole variation in magnetic susceptibility (MS), natural gamma radiation (NGR), carbonate content, and sediment lightness (L^*). Major lithologic unit boundaries coincide with step changes in these parameters. MS and NGR variations largely correlate with clay and volcanioclastic content. The P/E and K/P boundaries are distinct from adjacent sediments in their MS and NGR values as they represent intervals of decreased carbonate deposition/preservation and increased clay and volcanic ash accumulation, both of which produce distinctive increases in MS and NGR. A single value reached 625 on the MS scale, as indicated in the figure.

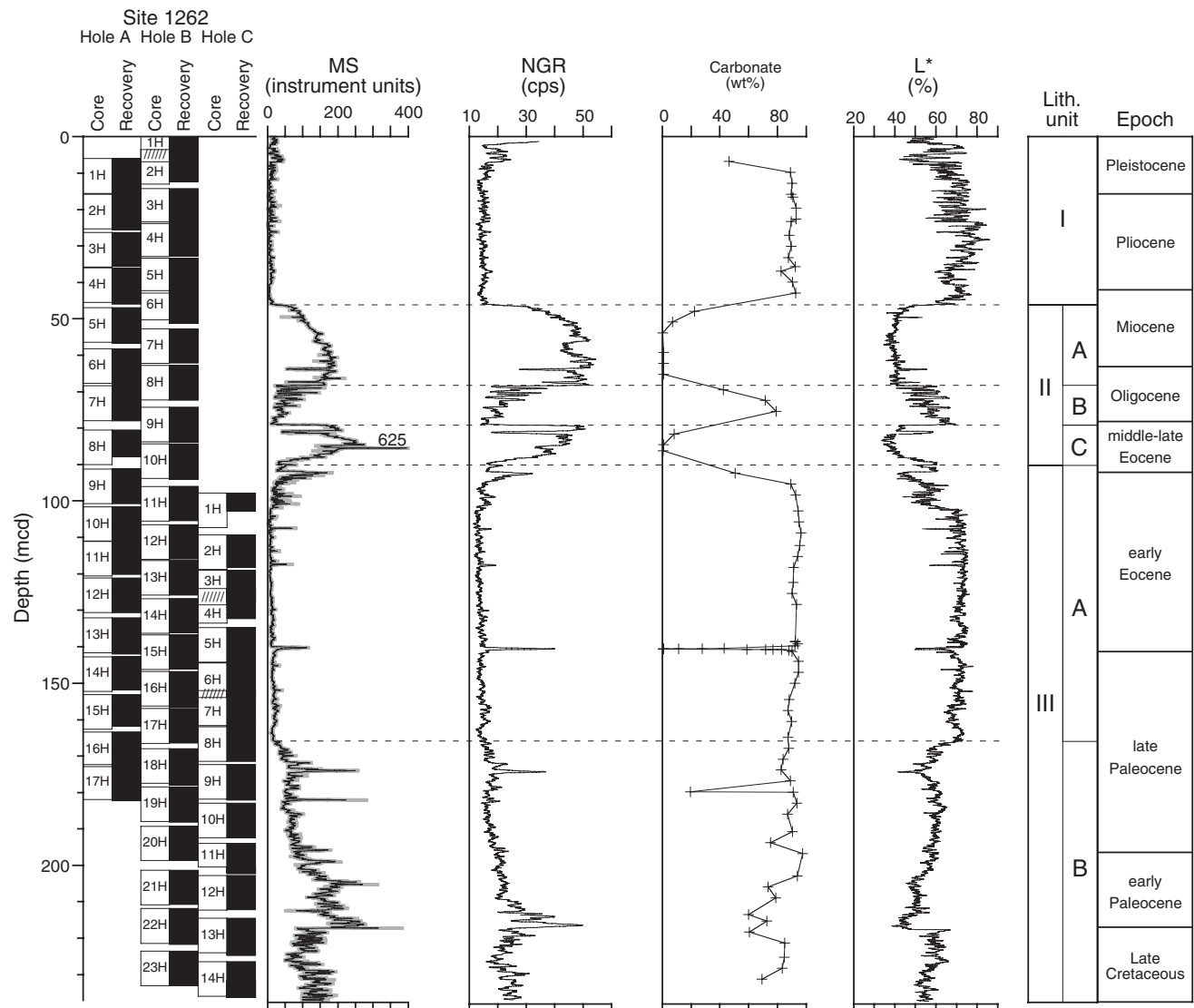


Figure F8. Site 1262 lithostratigraphic composite illustrating stratigraphic variation in whole-core multi-sensor track measurements of magnetic susceptibility (MS), natural gamma radiation (NGR), gamma ray attenuation (GRA) bulk density, and P -wave velocity. NGR data are smoothed with a 10-point moving average; all other data are smoothed with a 5-point moving average.

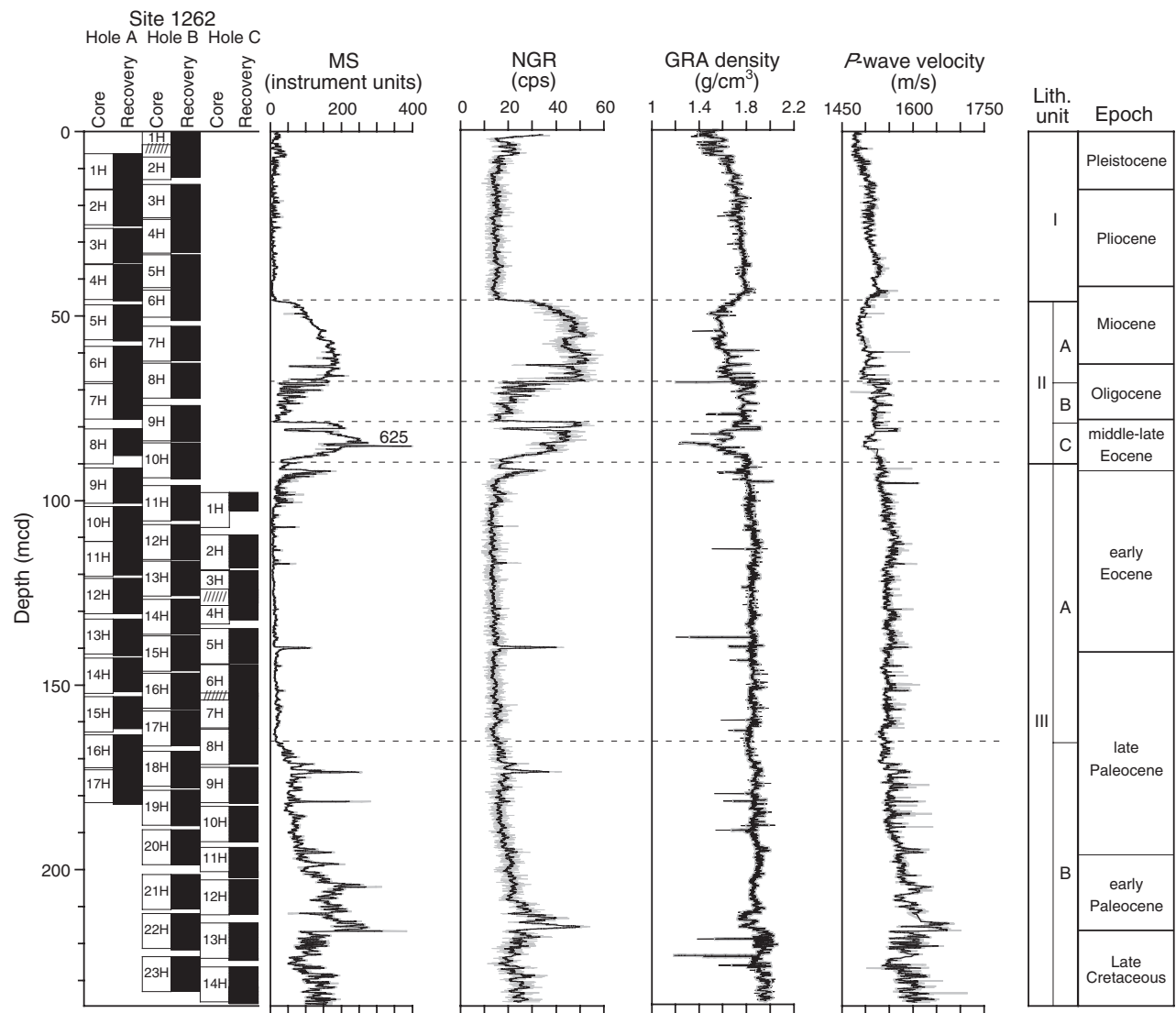


Figure F9. Site 1262 lithostratigraphic composite illustrating stratigraphic variation in lightness (L^*), carbonate content, and chromaticity (a^* and b^*).

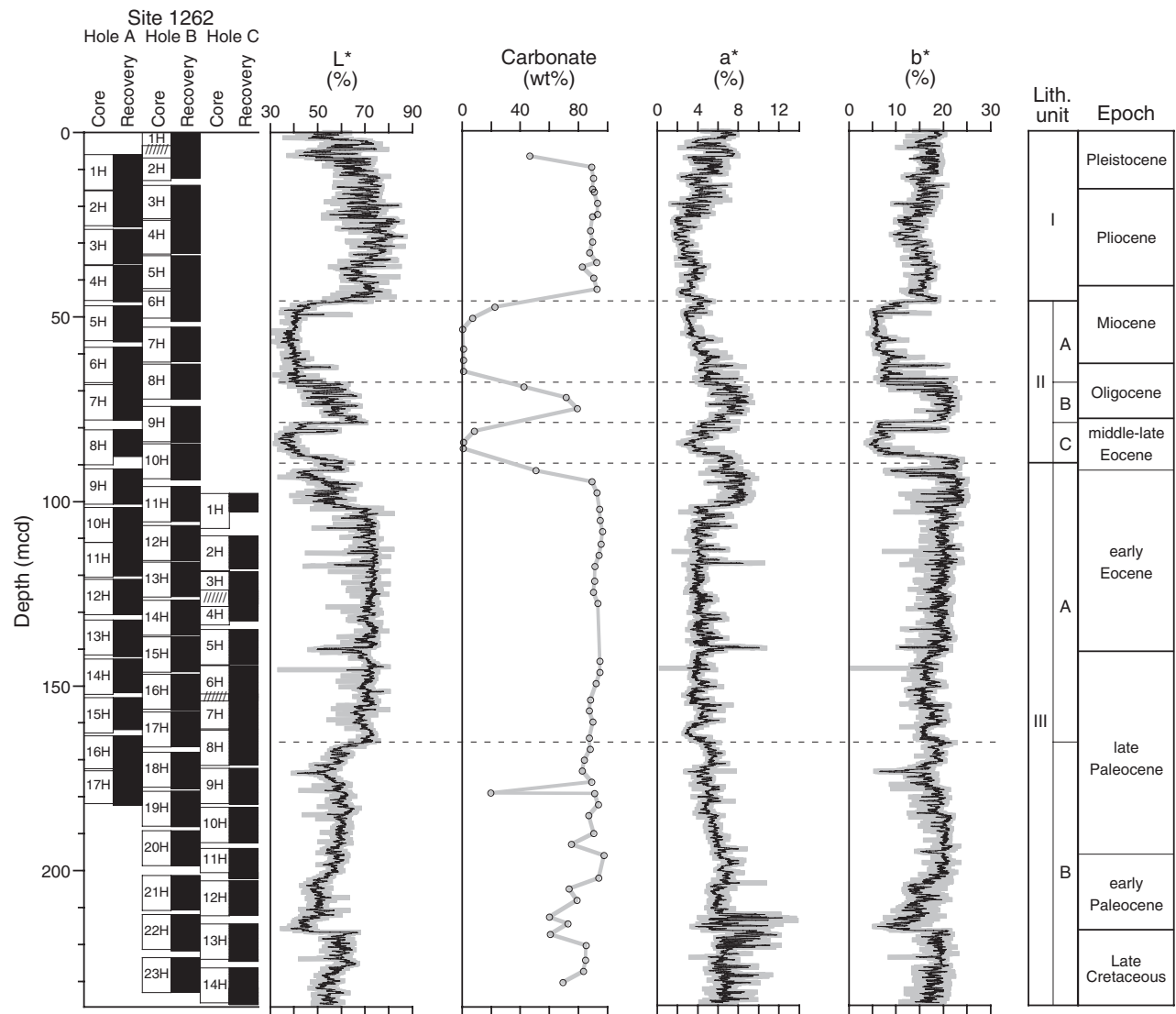
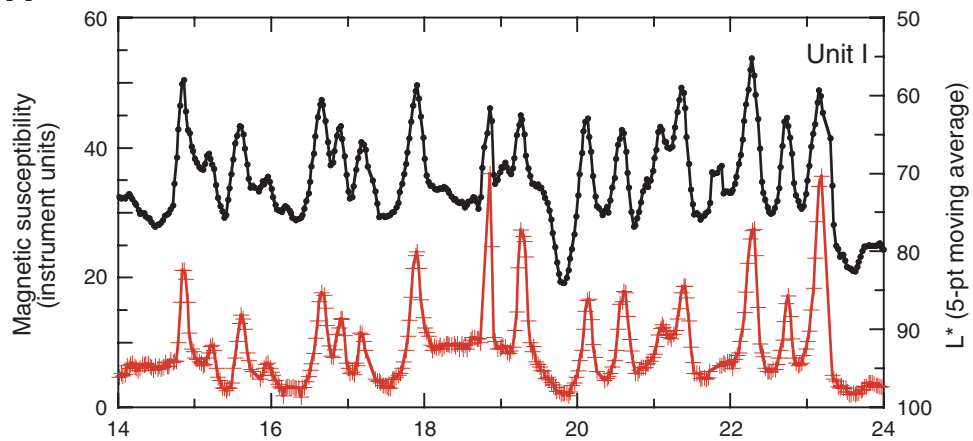
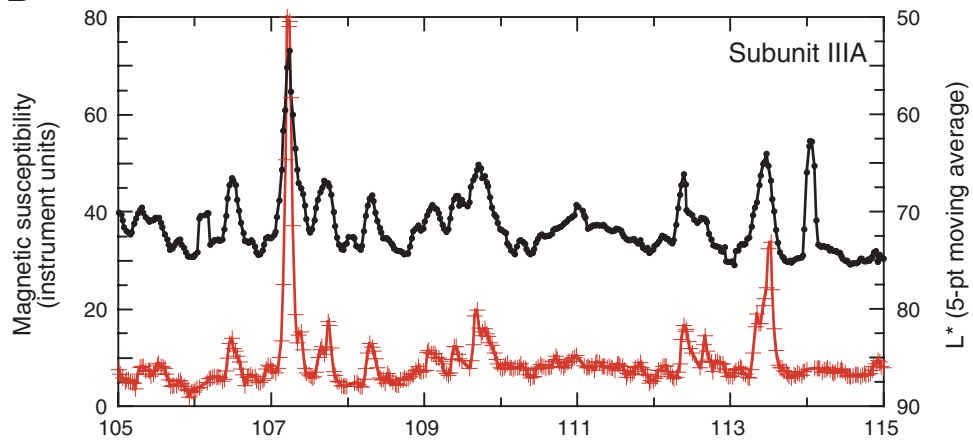


Figure F10. Example of cycles observed in signals of magnetic susceptibility (MS [black]) and sediment lightness (L^* [red]) in (A) Unit I, (B) Subunit IIIA, and (C) Subunit IIIB. L^* values were smoothed using a 5-point (5-pt) running average; MS measurements are unsmoothed.

A



B



C

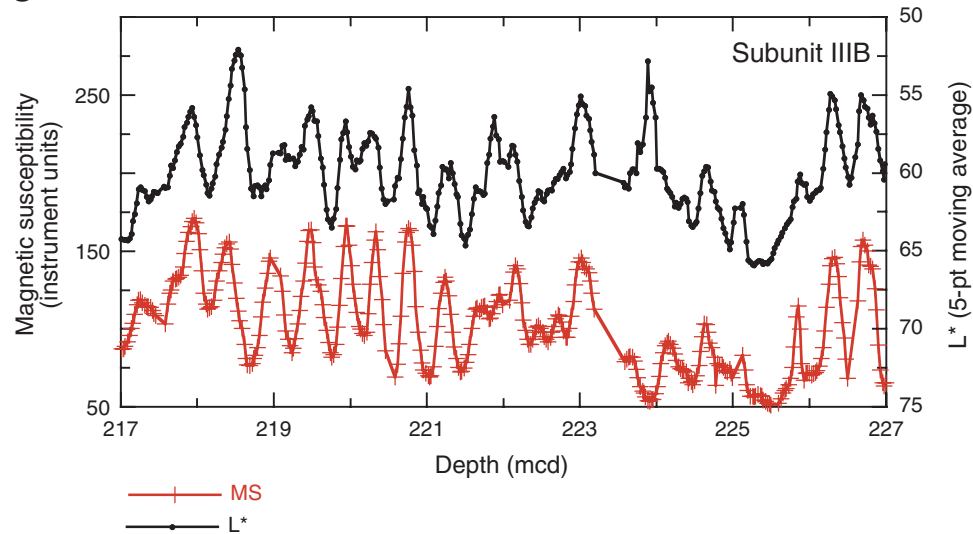


Figure F11. Stratigraphic variation in physical properties of grain density (GD), bulk density (BD; MAD method), porosity, and P -wave velocity for Holes 1262A and 1262B.

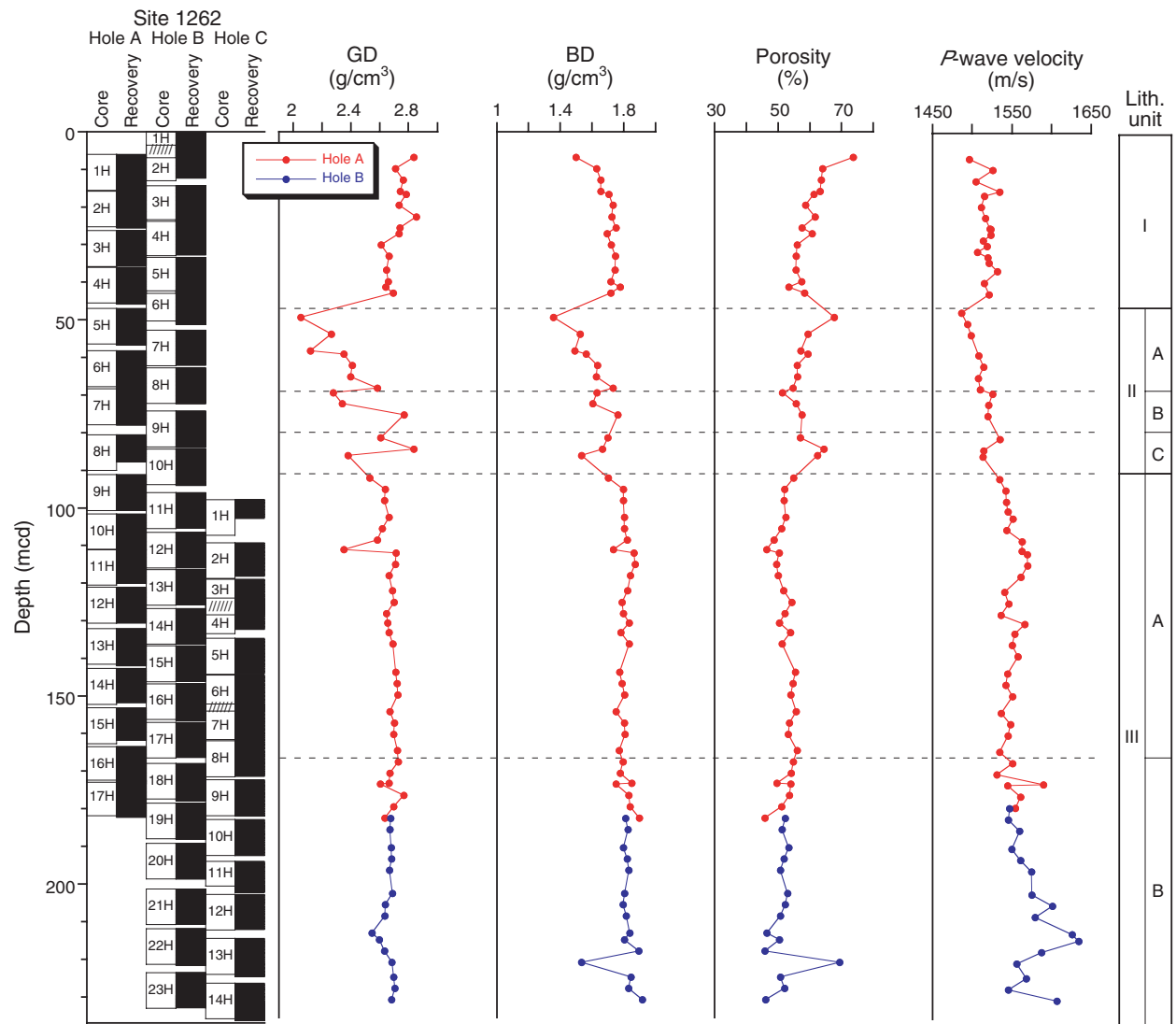


Figure F12. A, B. Comparison between bulk density measured by gamma ray attenuation (GRA) and the moisture and density (MAD) methods. C. Correlation of grain density (GD) with bulk density (BD; MAD method). D. Correlation of porosity with BD (MAD method). E. Correlation of P-wave velocity sensor (PWS3) measurements and BD (MAD method).

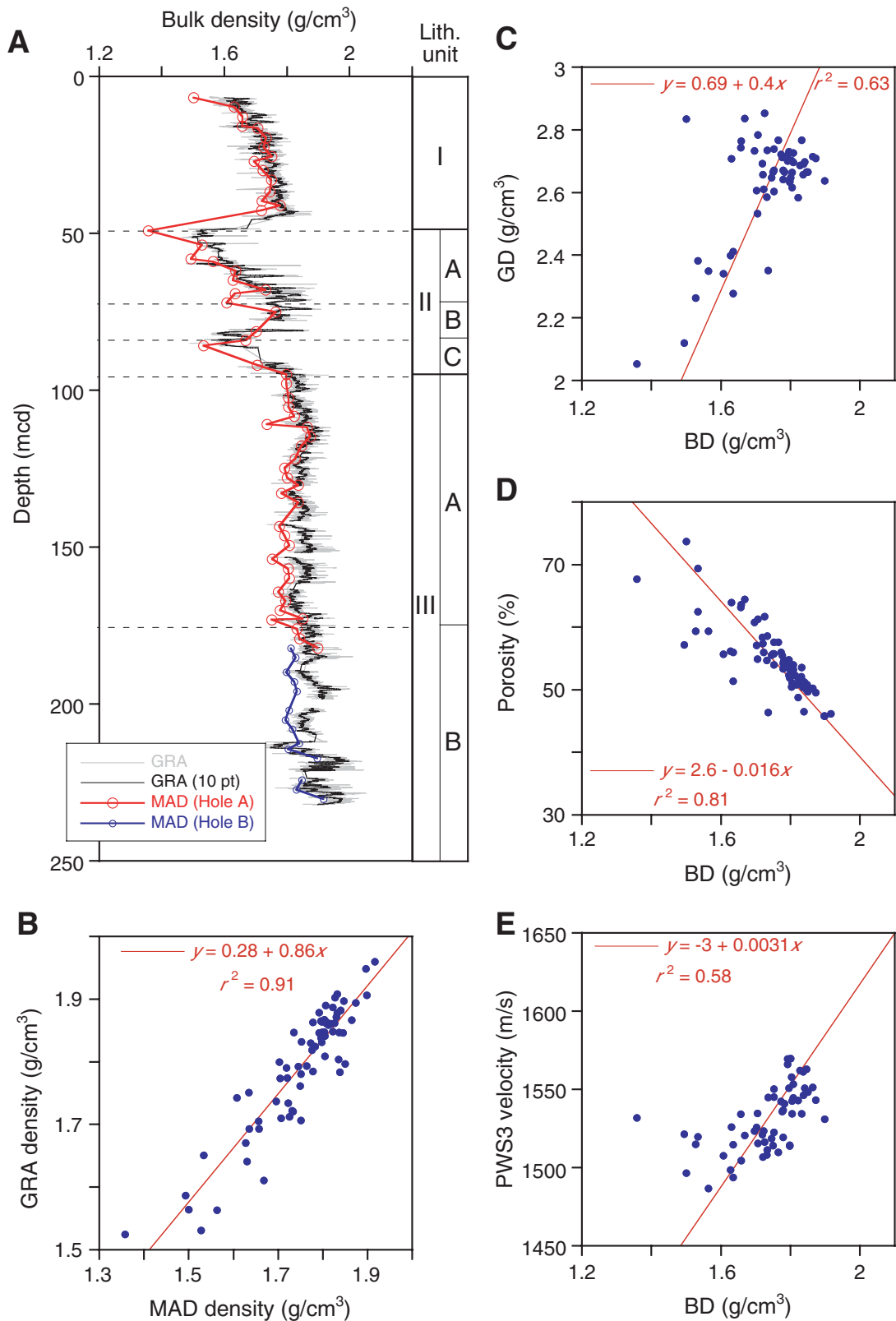


Figure F13. A. Comparison of *P*-wave velocities measured on the whole-core multisensor track *P*-wave logger (PWL) and the split-core *P*-wave velocity (PWS3) transducer. B. Scatterplot of *P*-wave velocities (PWL) vs. PWS3.

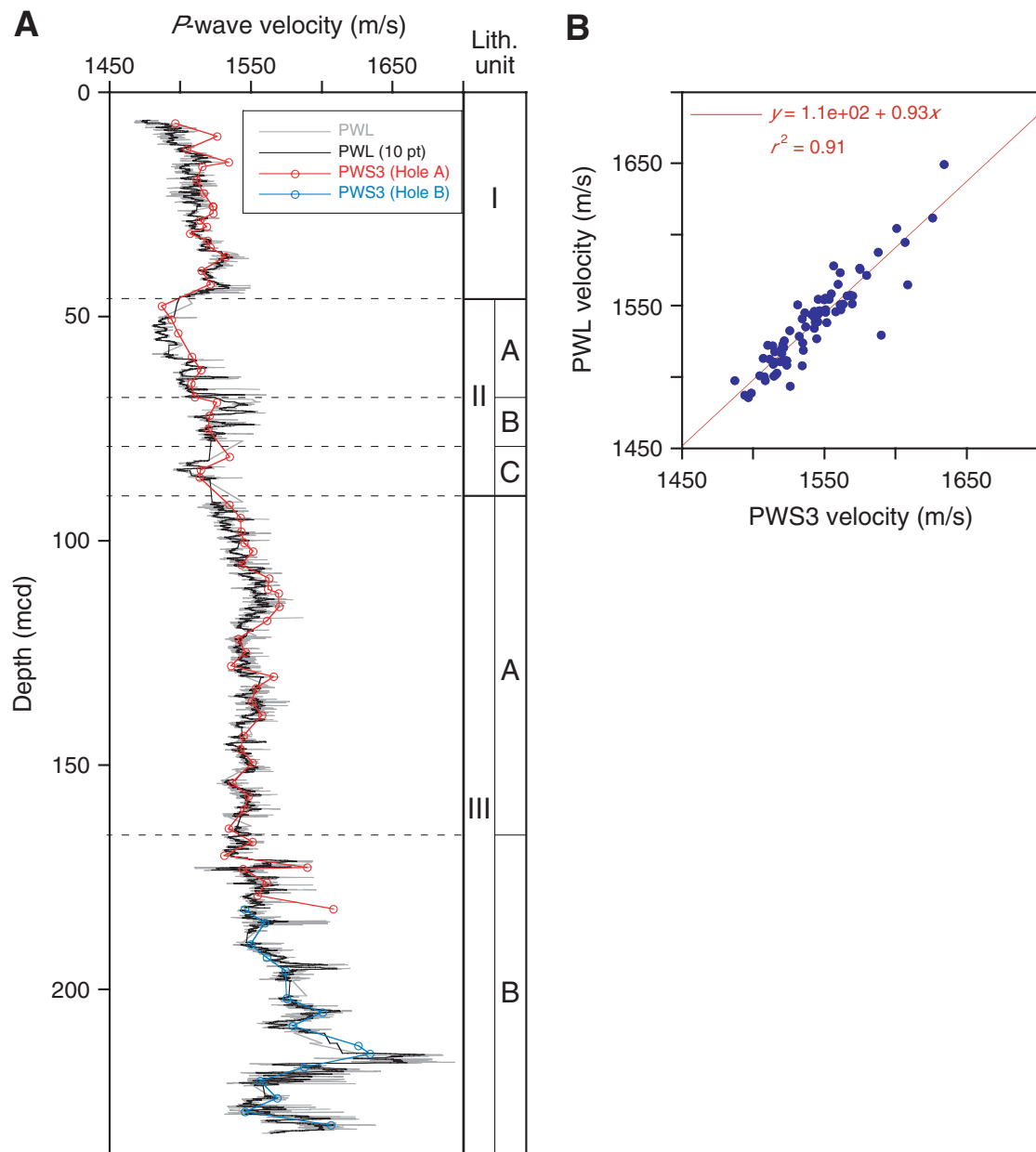


Figure F14. Color reflectance data. A. Sediment lightness (L^*) and calcium carbonate concentration. B. Chromaticity a^*/b^* . C. Scatterplot of L^* and calcium carbonate concentration. D. Scatterplot of L^* and a^*/b^* .

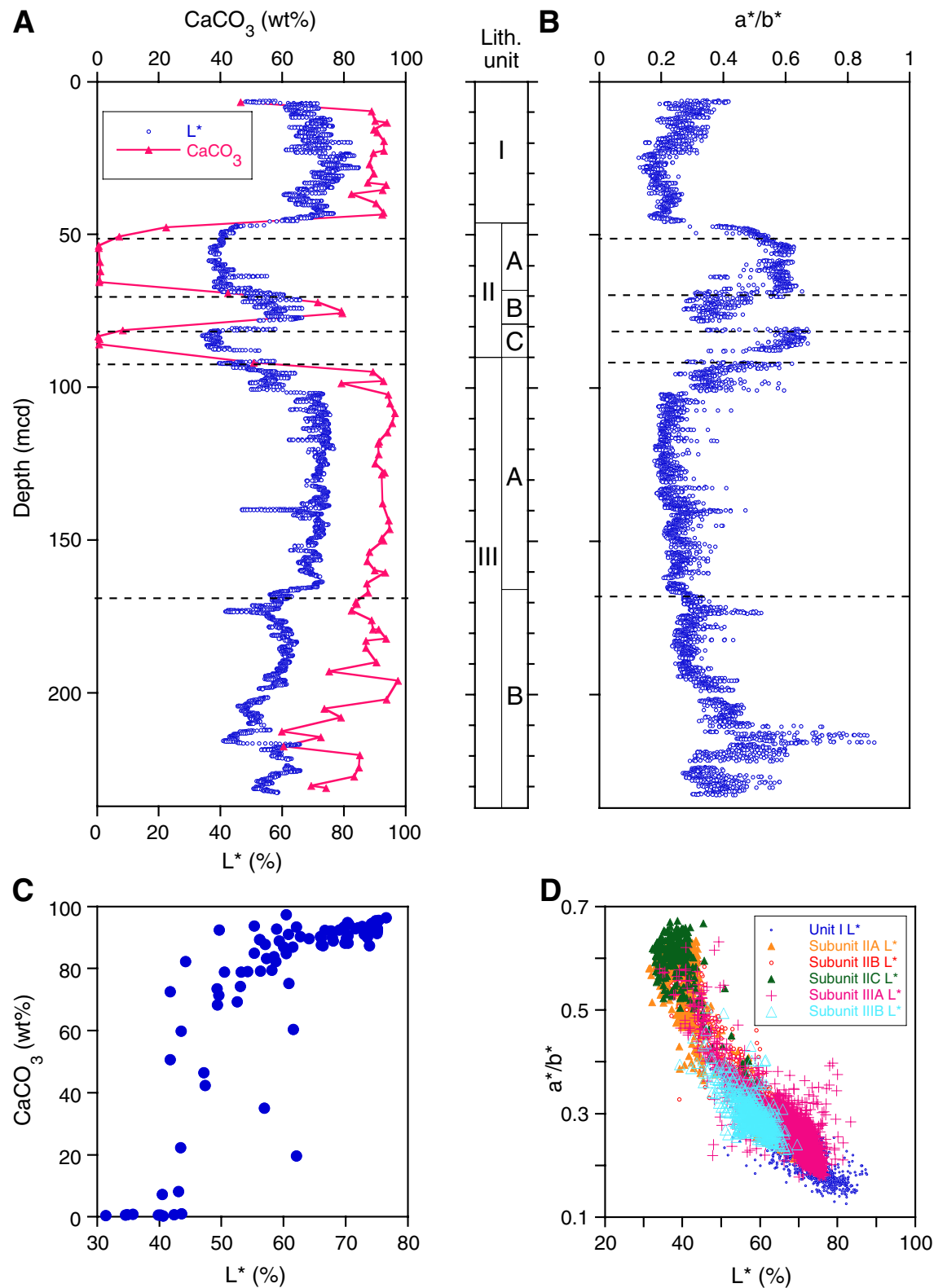


Figure F15. Close-up photograph of turbidites and gravity flows in Subunit IIB (interval 208-1262A-6H-4, 64–121 cm).

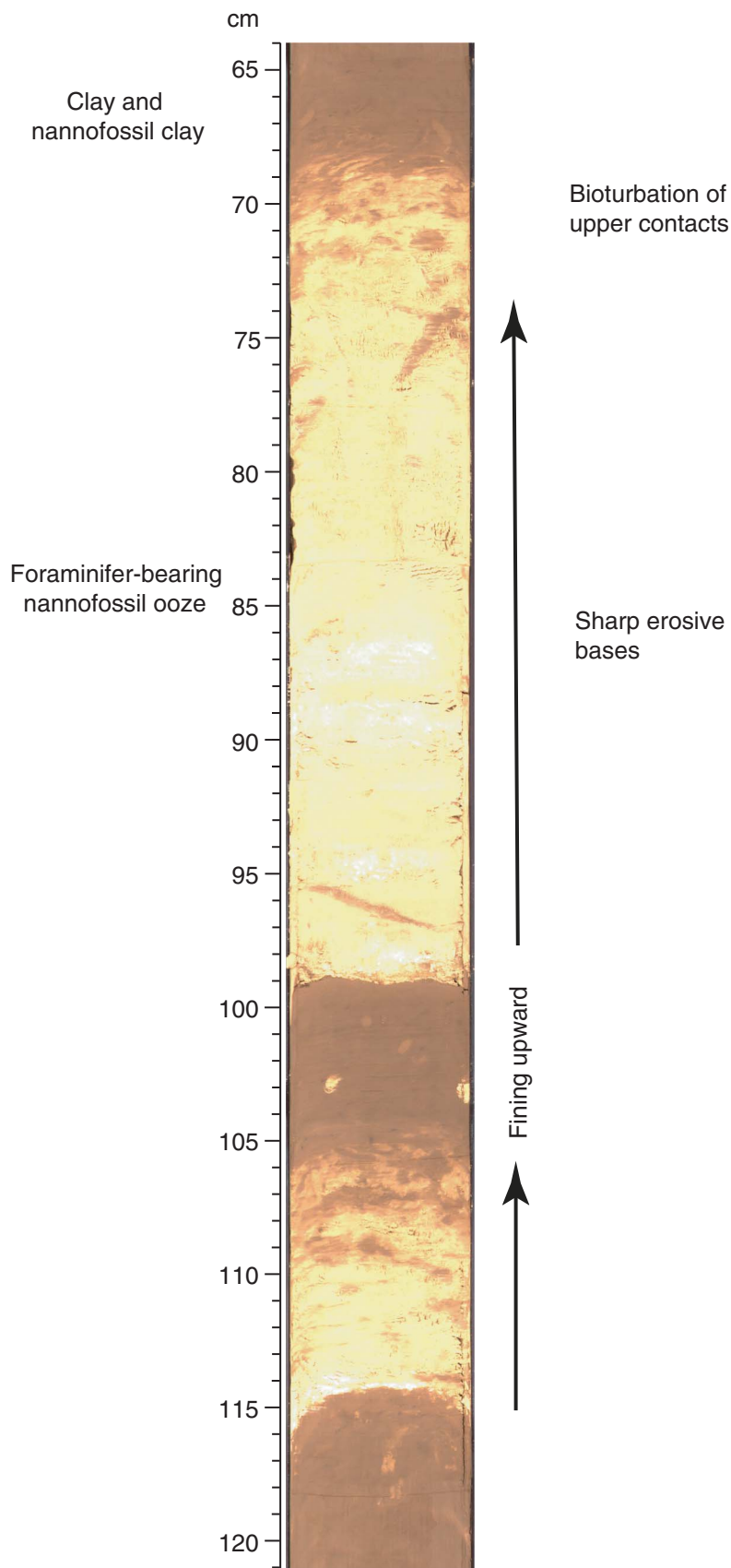


Figure F16. Composite digital images, sediment lightness (L^*), natural gamma radiation (NGR), magnetic susceptibility (MS), and red-green-blue color variations across the Eocene/Oligocene boundary interval (67.45–76.7 mbsf [74.32–83.57 mcd]). The boundary occurs in the lithologic transition from brown clay to light brown nannofossil ooze and is reflected in an increase in L^* and a decrease in MS and NGR.

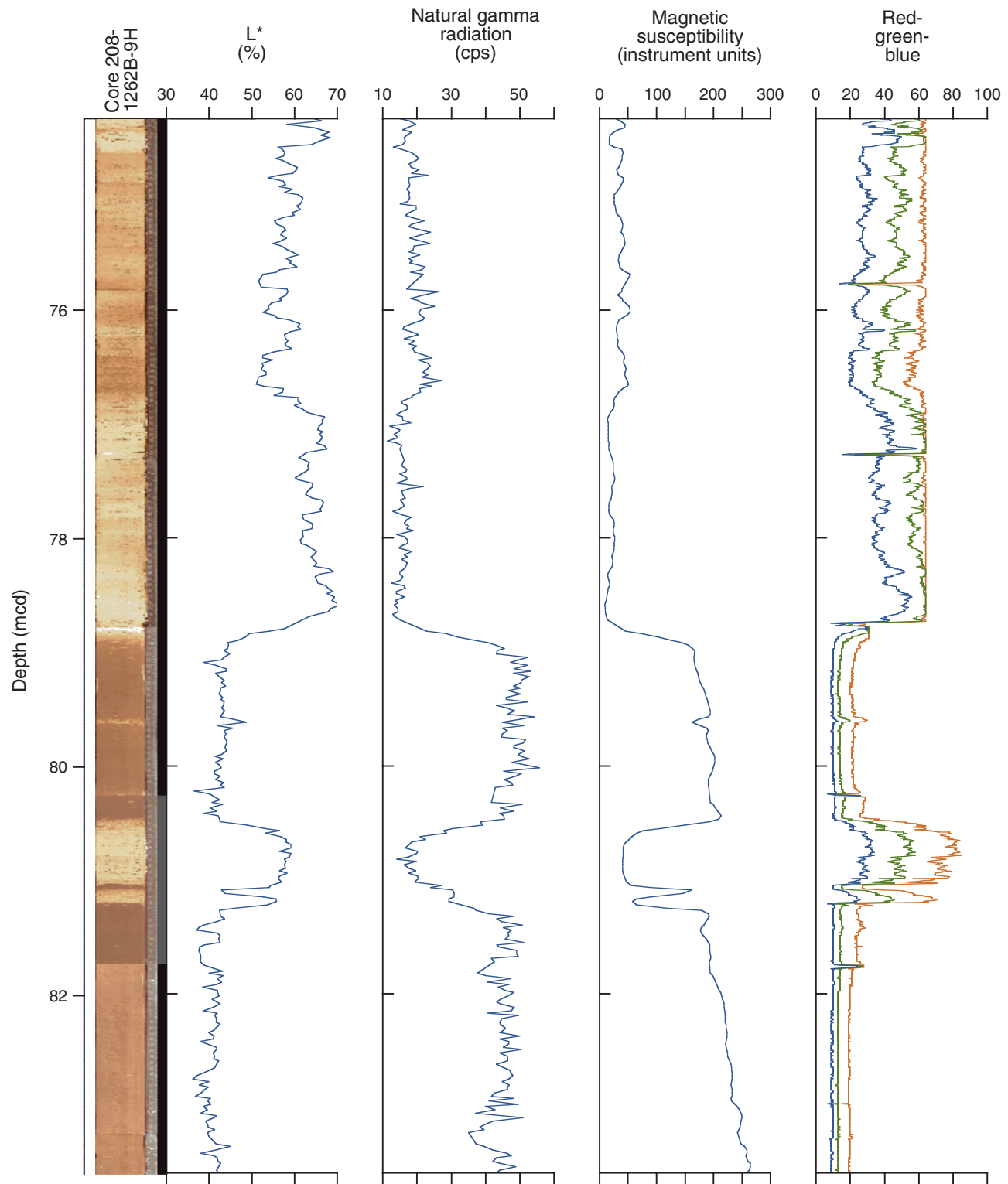


Figure F17. Composite digital images, chromaticity a^* (red), and magnetic susceptibility (black) of the clay horizon at 117.3 mcd, Site 1262.

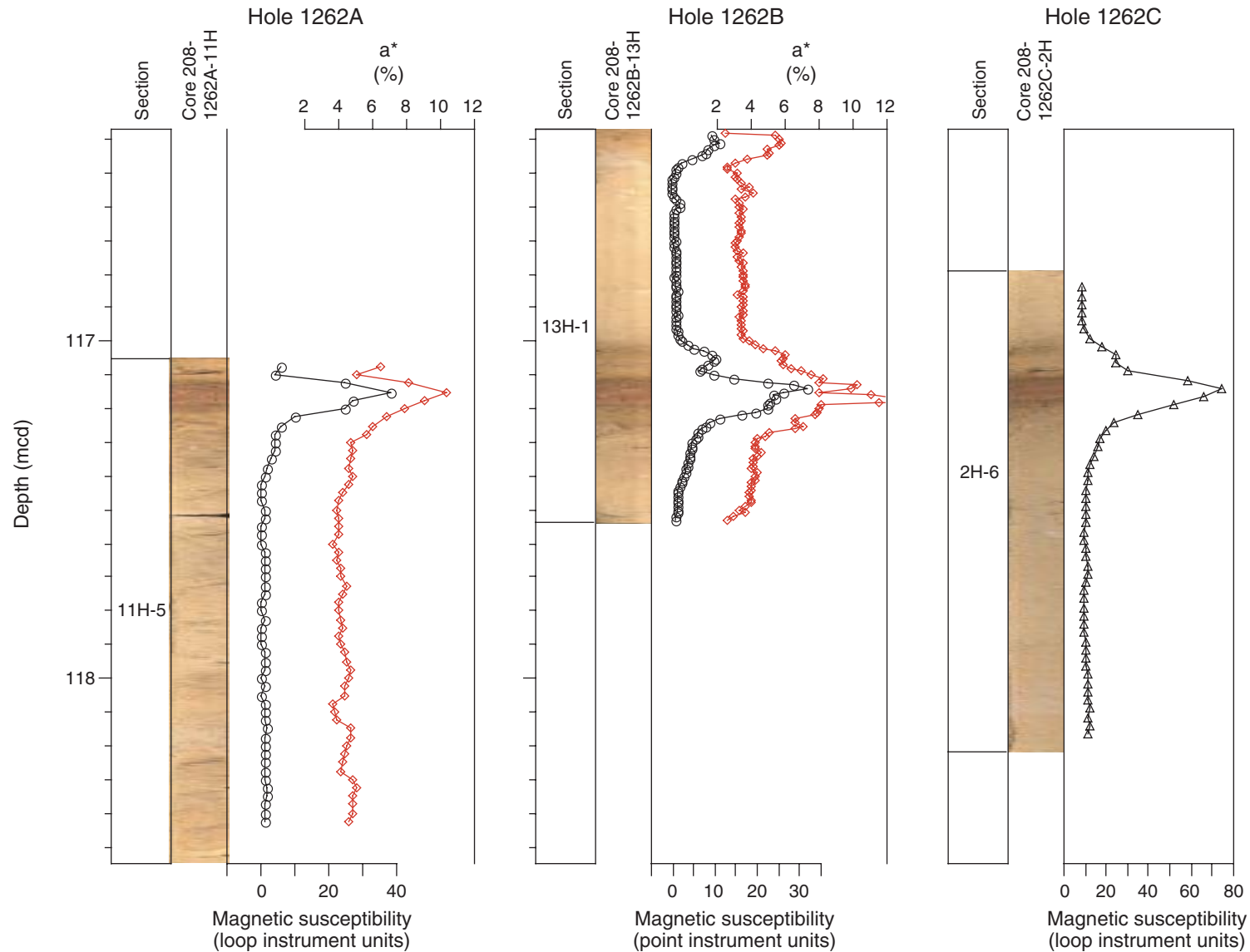


Figure F18. Composite digital images, carbonate content, magnetic susceptibility, and red-green chromaticity (a^*) across the P/E boundary recovered in Holes 1262A, 1262B, and 1262C. Circle = magnetic susceptibility, triangle = CaCO_3 , diamond = a^* .

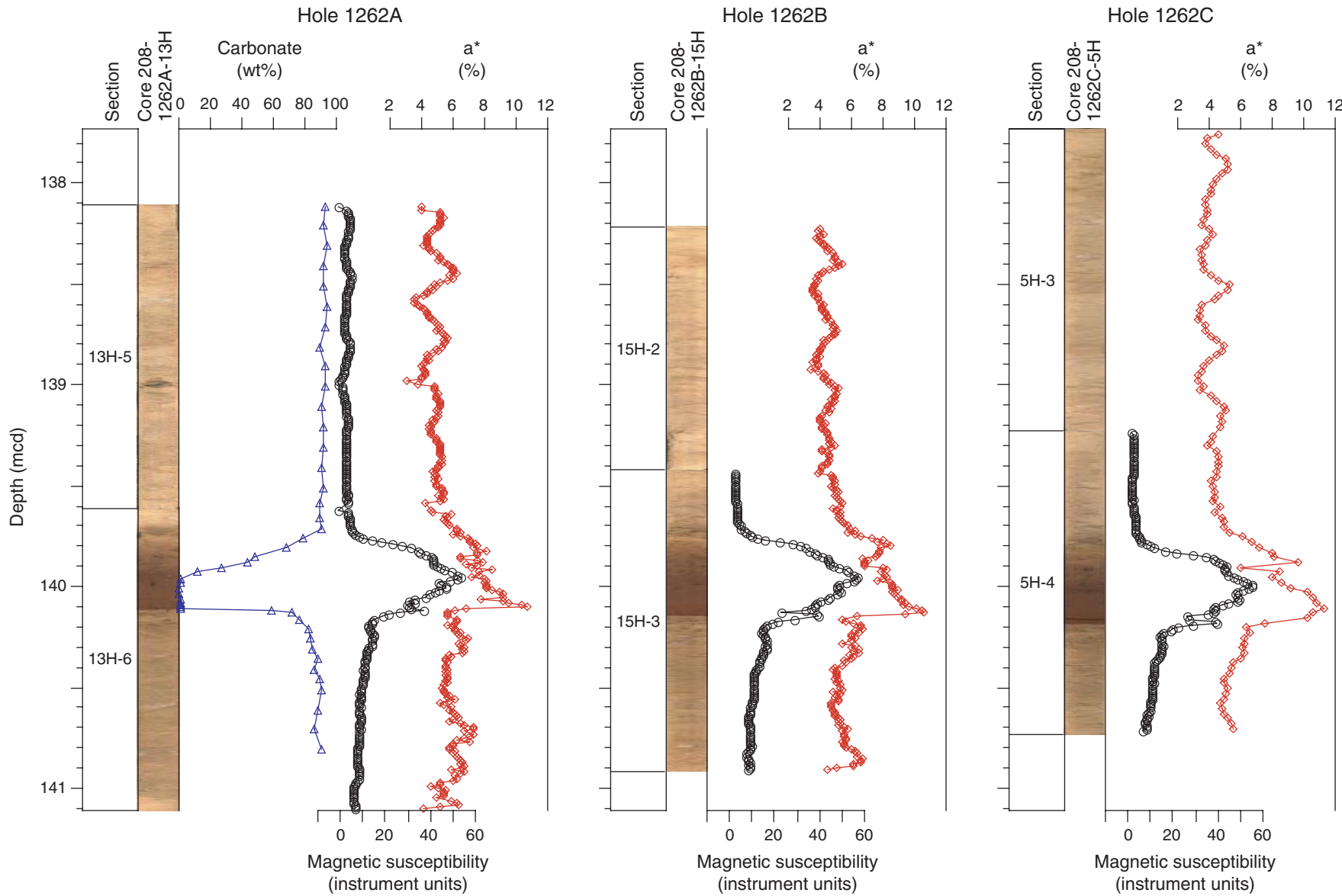


Figure F19. Close-up photograph, magnetic susceptibility, and color variations across the P/E boundary (interval 208-1262A-13H-6, 1–60 cm).

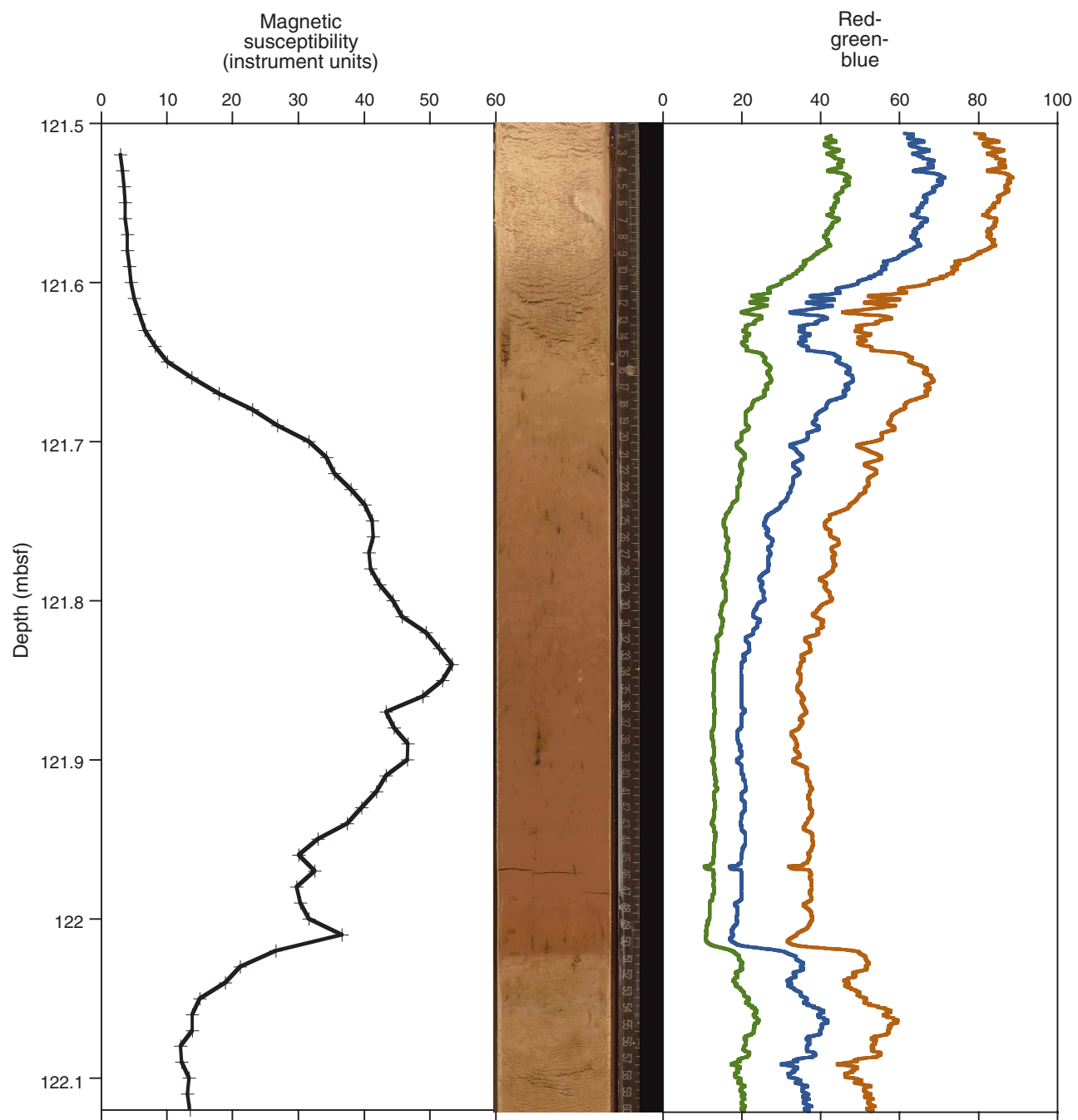


Figure F20. Magnetic susceptibility across the P/E boundary.

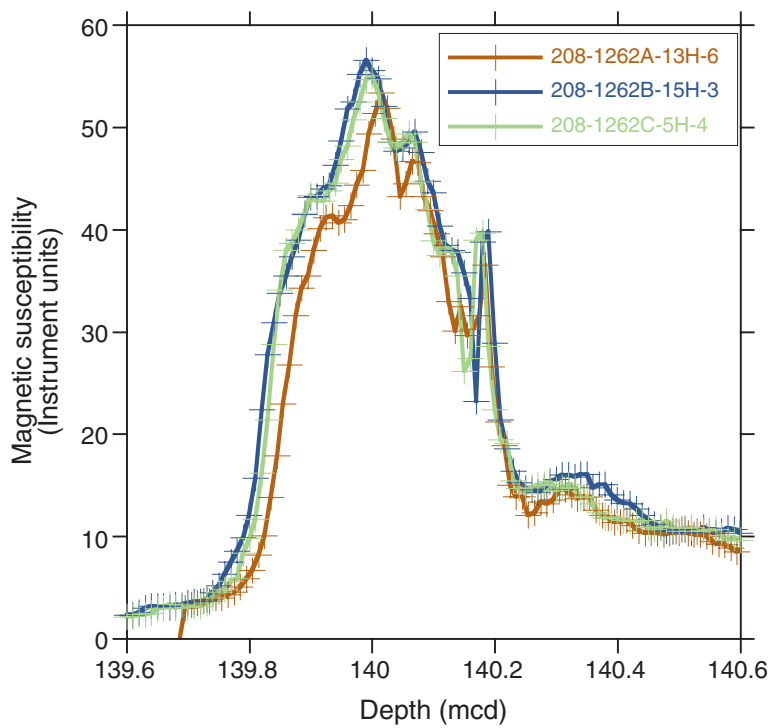


Figure F21. Close-up photograph of the Cretaceous/Paleogene (K/P) boundary in Holes 1262B and 1262C. Each transition (intervals 208-1262B-22H-4, 117–152 cm, and 208-1262C-13H-2, 52–81 cm) is marked by an irregular boundary between light gray-brown clay-bearing nannofossil ooze with foraminifers and an overlying red foraminifer-bearing nannofossil clay. This sequence grades upward into a brown nannofossil-bearing foraminifer-bearing clay that is moderately bioturbated. Microtectites are present in this reddish transition zone directly at the boundary.

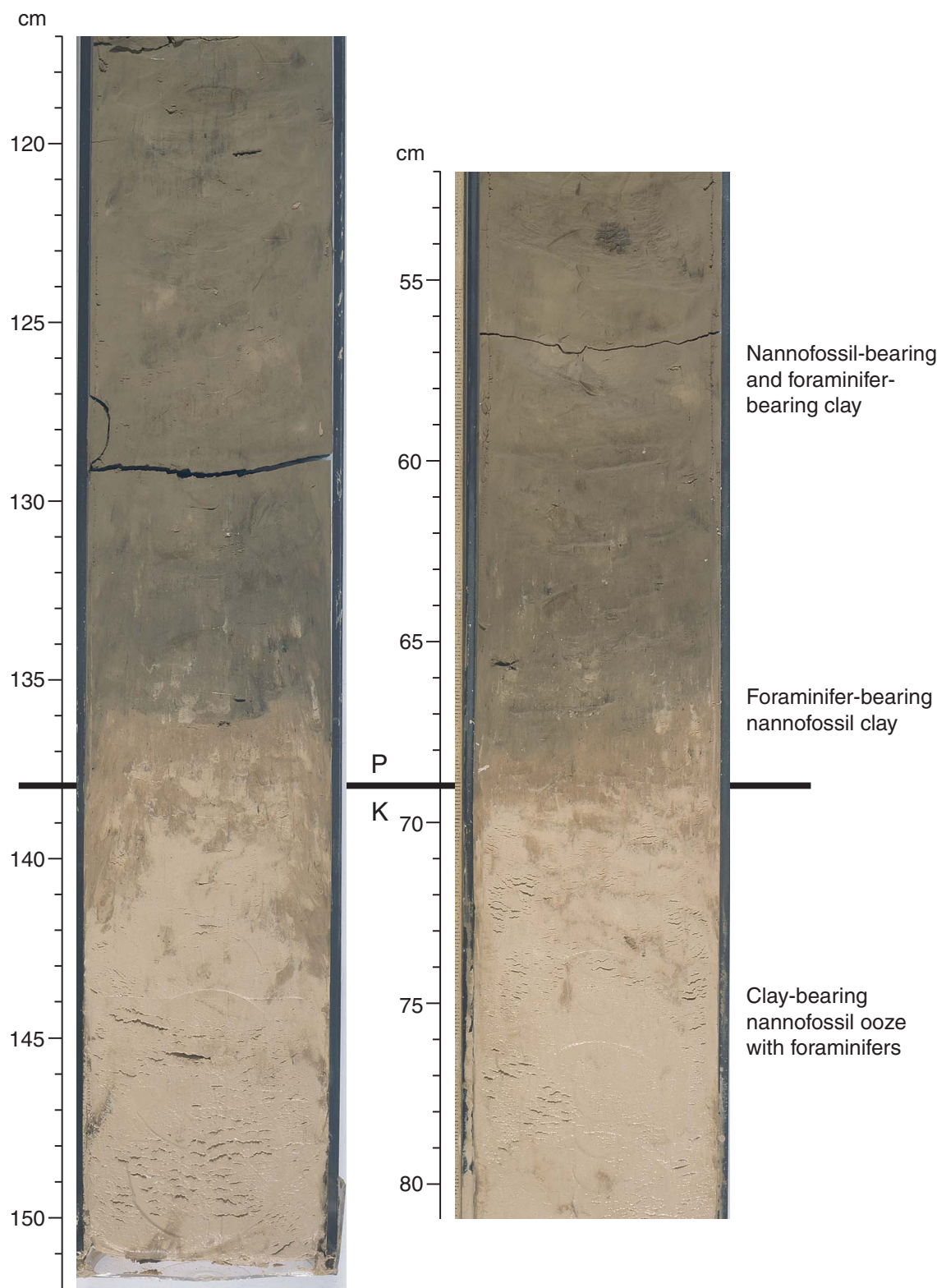


Figure F22. Summary of composite planktonic foraminiferal and calcareous nannofossil biozonations constructed for Site 1262. The paleobathymetric history of Site 1262 is inferred from benthic foraminifers shown on the right. Light shading = intervals of downslope transport and/or extensive reworking, dark shading = intervals of intense dissolution. P/E = Paleocene/Eocene, K/P = Cretaceous/Paleogene.

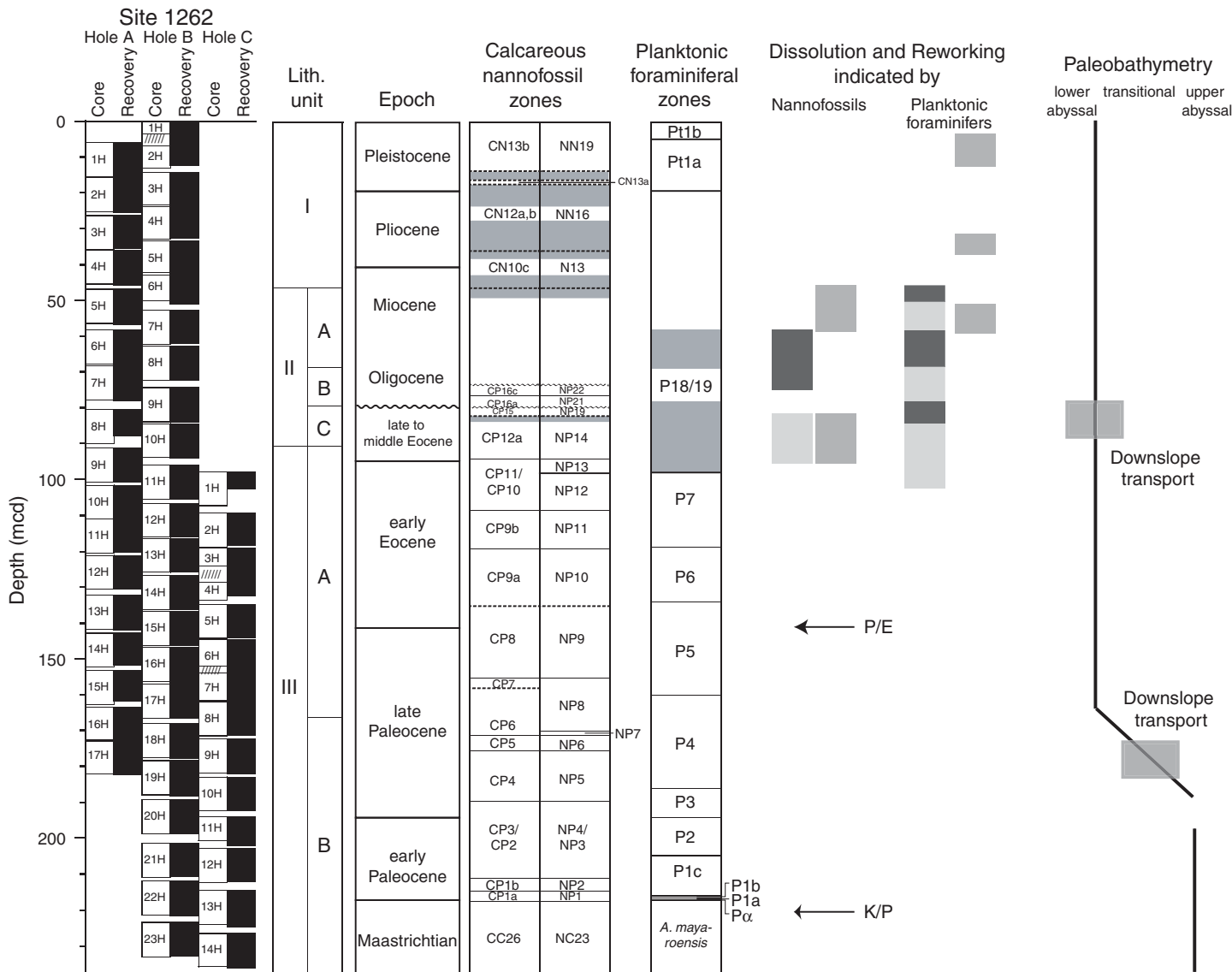


Figure F23. Summary of sedimentation rates at Site 1262 as delineated by a composite age/depth curve constructed using calcareous nannofossils and planktonic and benthic foraminifers.

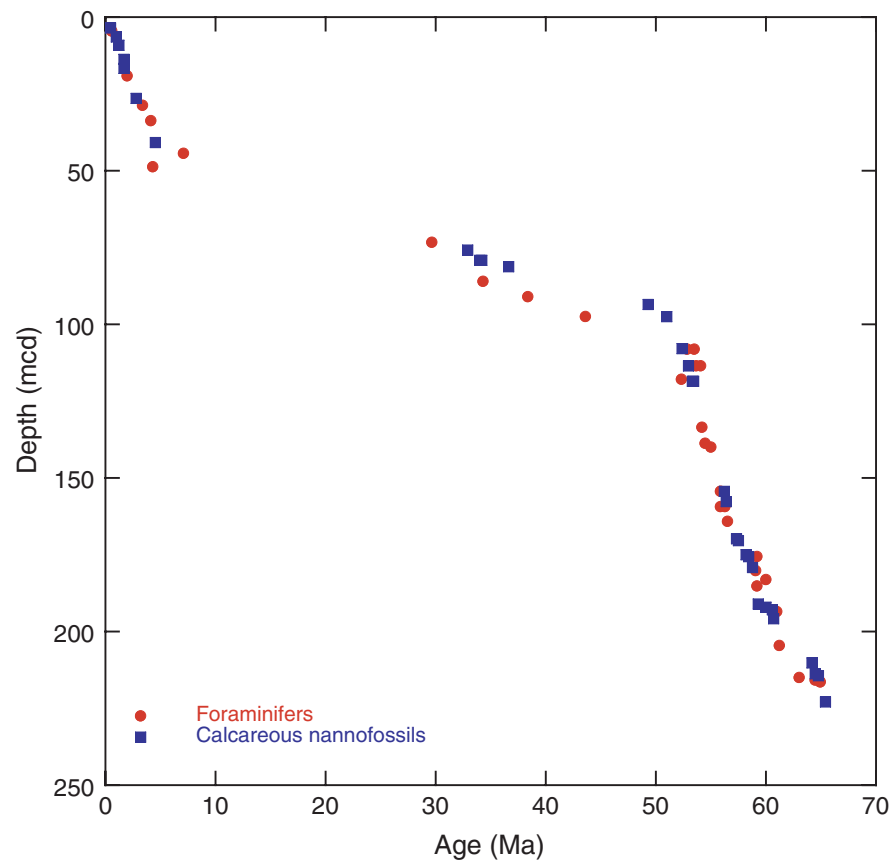


Figure F24. Inclination and intensity data, respectively, for Hole 1262B (145–172.5 mcd). Natural remanent magnetization (NRM) data show the presence of a strong drilling overprint in the downhole direction, resulting in very steep inclinations and high intensities. Demagnetization at 10 mT removes most of the overprint.

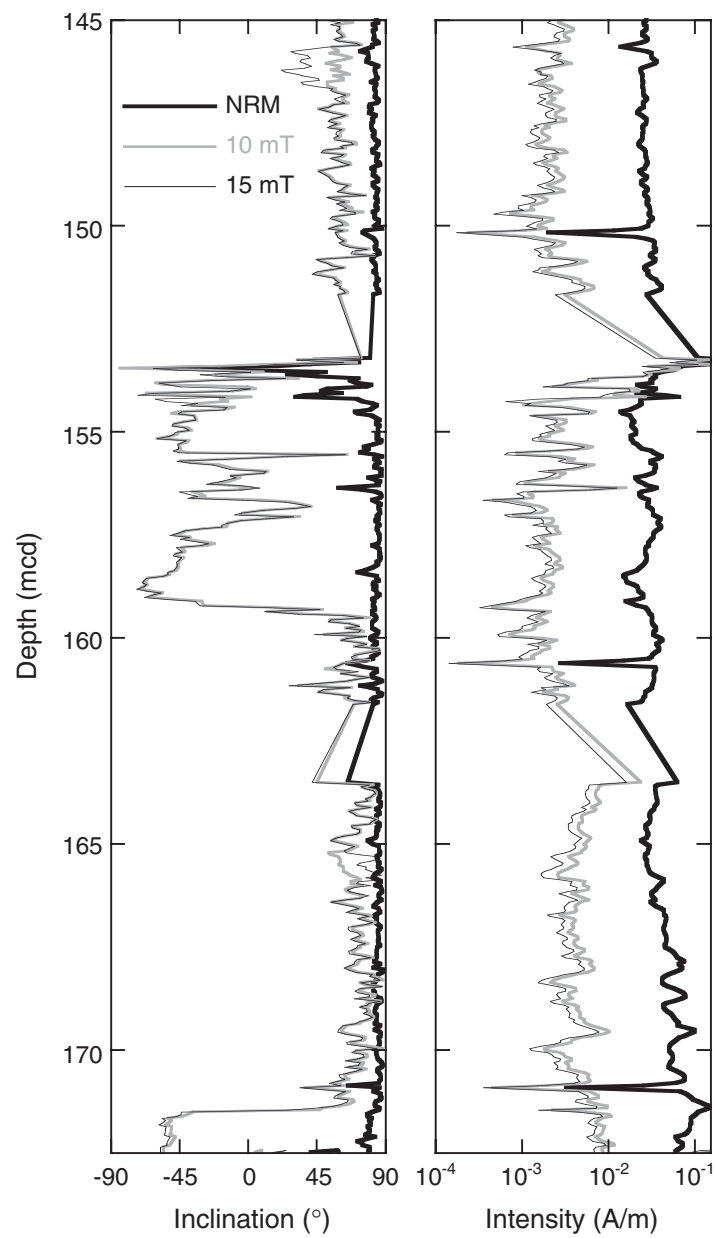


Figure F25. Downhole variation in intensities of remanent magnetization at 0 mT (gray) and 15 mT (black) for Holes 1262A, 1262B, and 1262C.

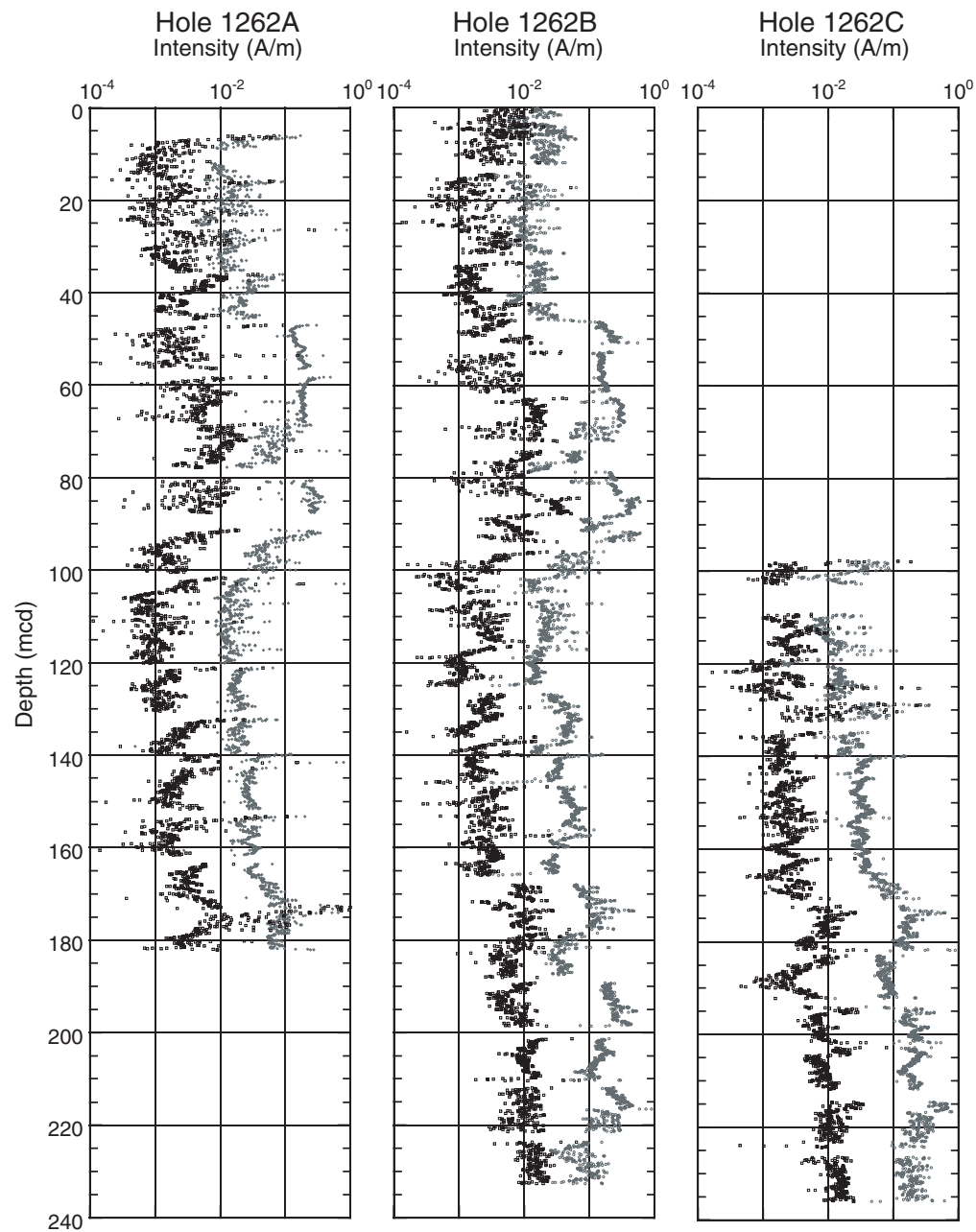


Figure F26. Hole 1262A. A. Downhole variations in depositional remanent magnetization (DRM) after 15-mT demagnetization. B. DRM after 15-mT demagnetization and normalized by susceptibility (nDRM). C. Normalized differential DRM (ndDRM) between 10- and 15-mT demagnetization. D. Magnetic susceptibility.

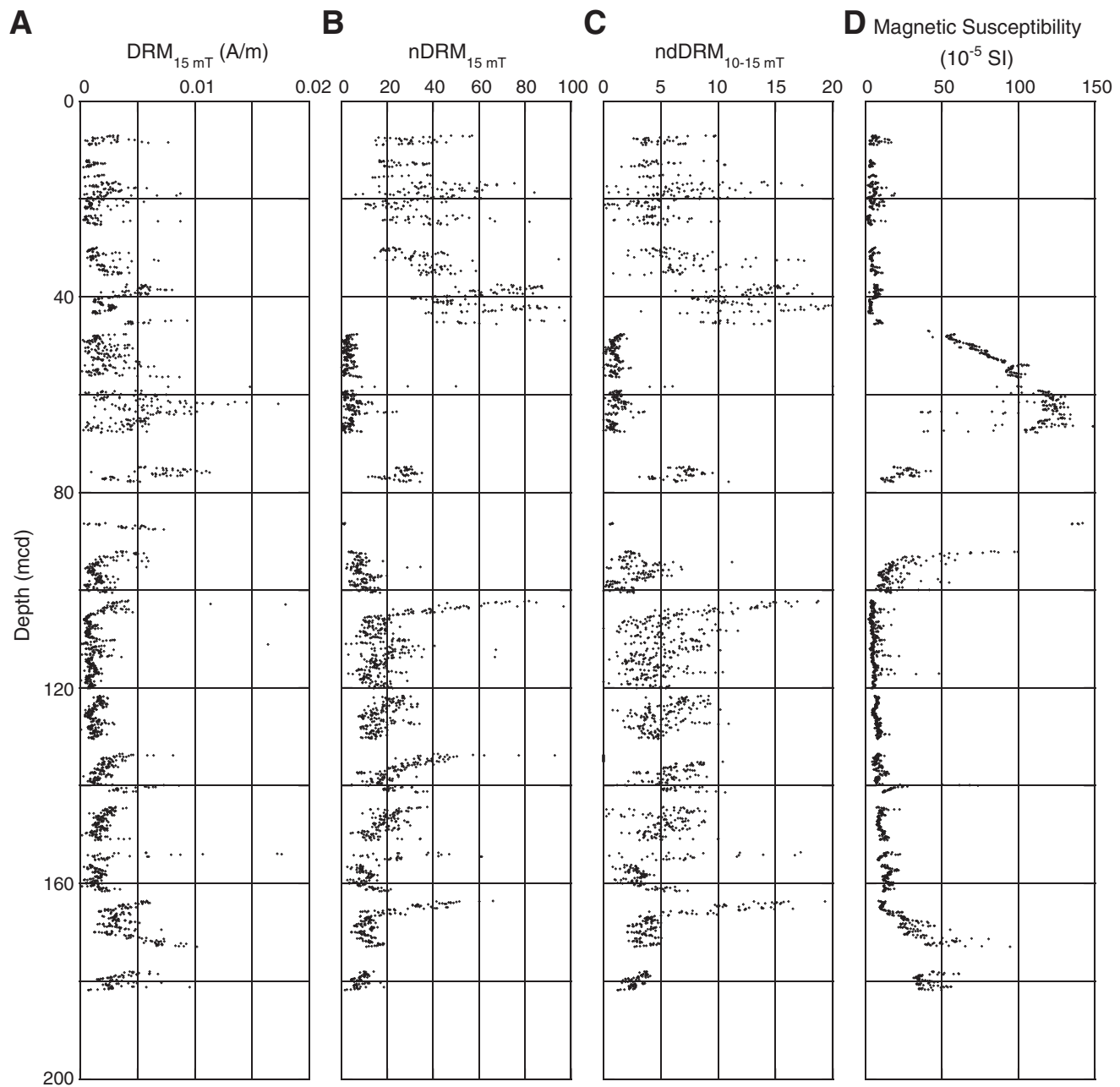


Figure F27. Preliminary magnetostratigraphic interpretation. Inclination data (at 15 mT) are shown for Holes 1262A, 1262B, and 1262C. Data within 50 cm of a core top and 5 cm of section ends are not shown. Green squares = core breaks. Black rectangles = normal polarity, white rectangles = reversed polarity, shaded rectangles = uncertain polarity. X = depths with no core recovery. Cobb Mtn. = Cobb Mountain event. A. 0–55 mcd. (Continued on next four pages.)

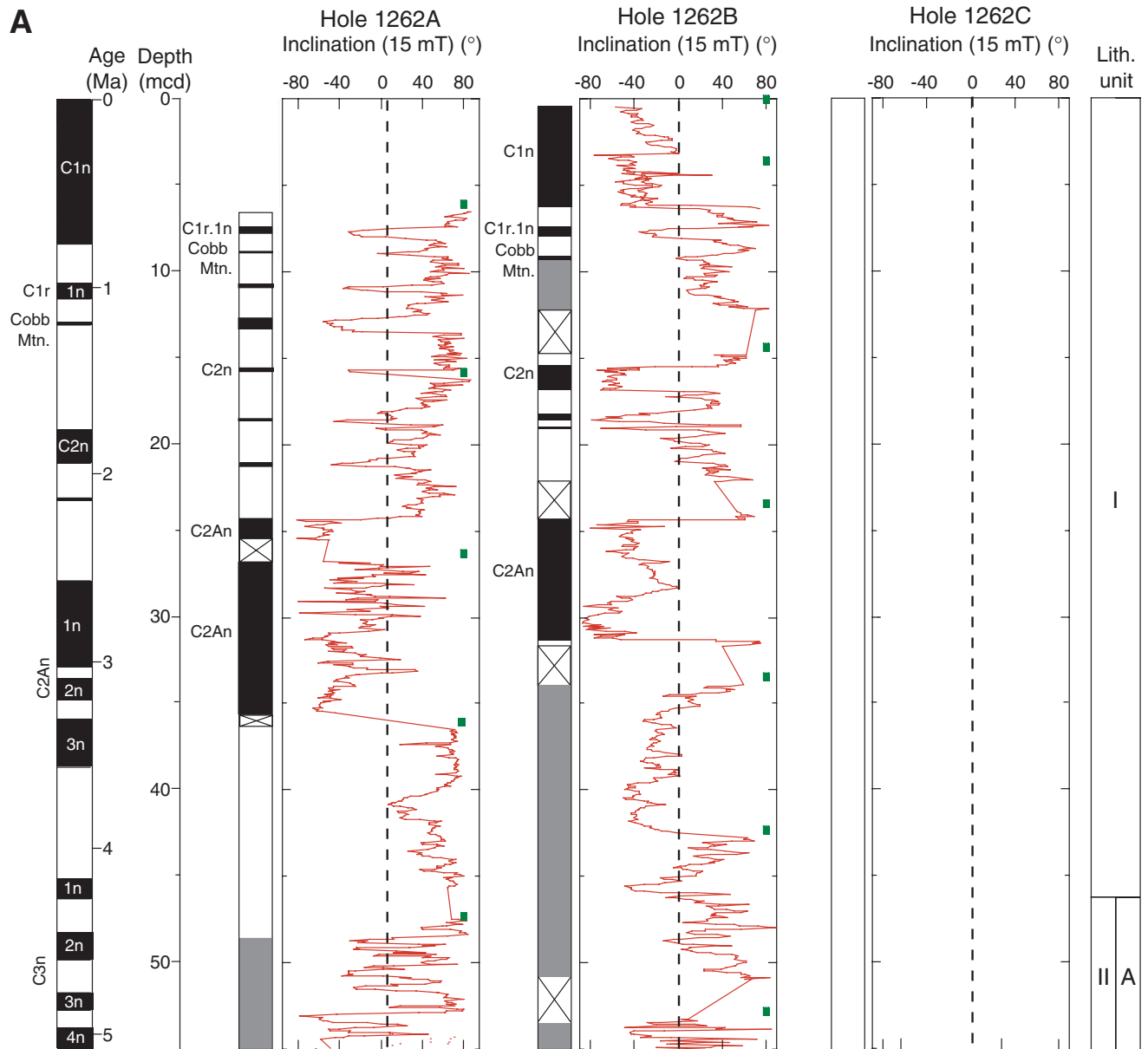


Figure F27 (continued). B. 45–105 mcd.

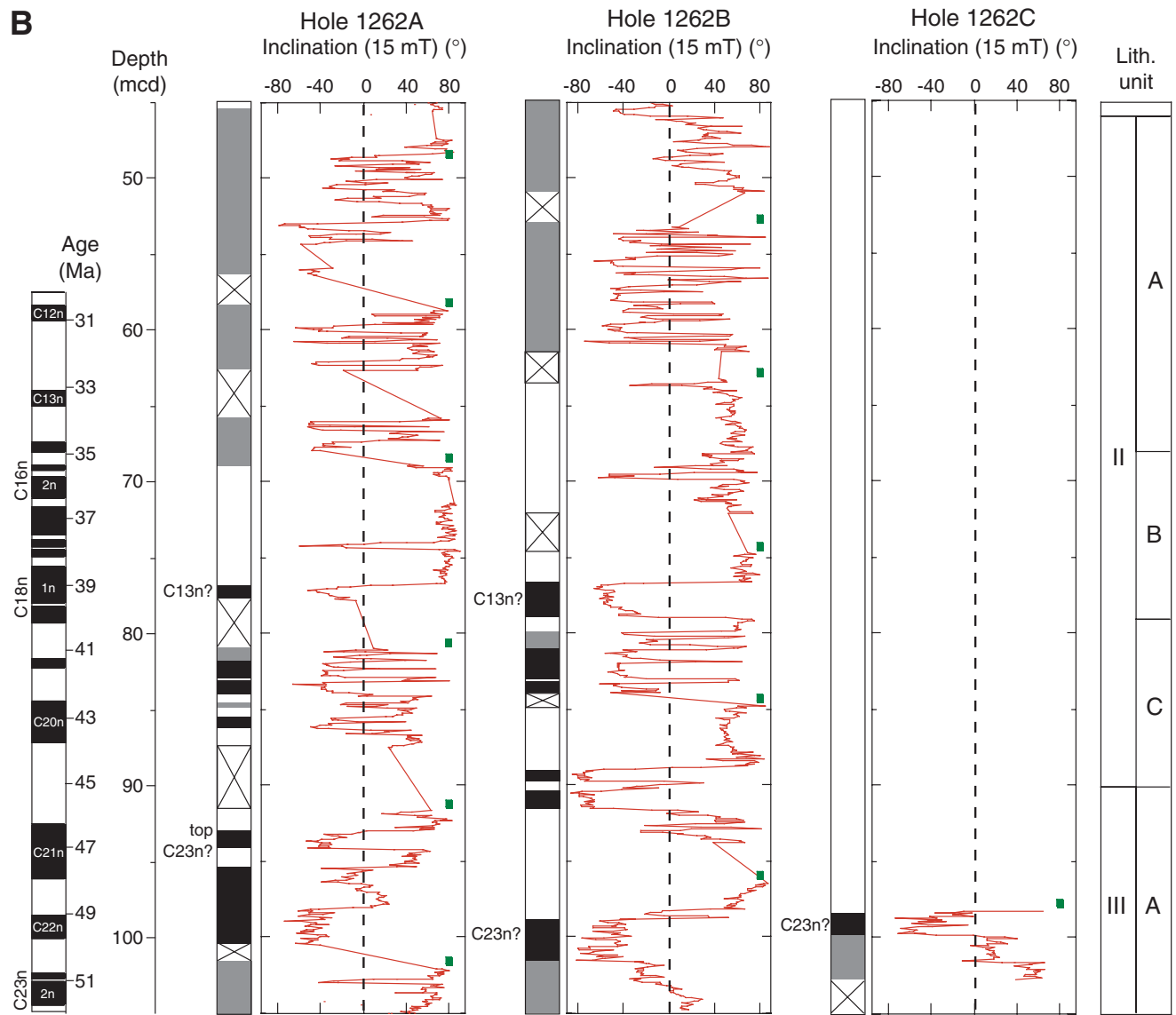


Figure F27 (continued). C. 95–155 mcd.

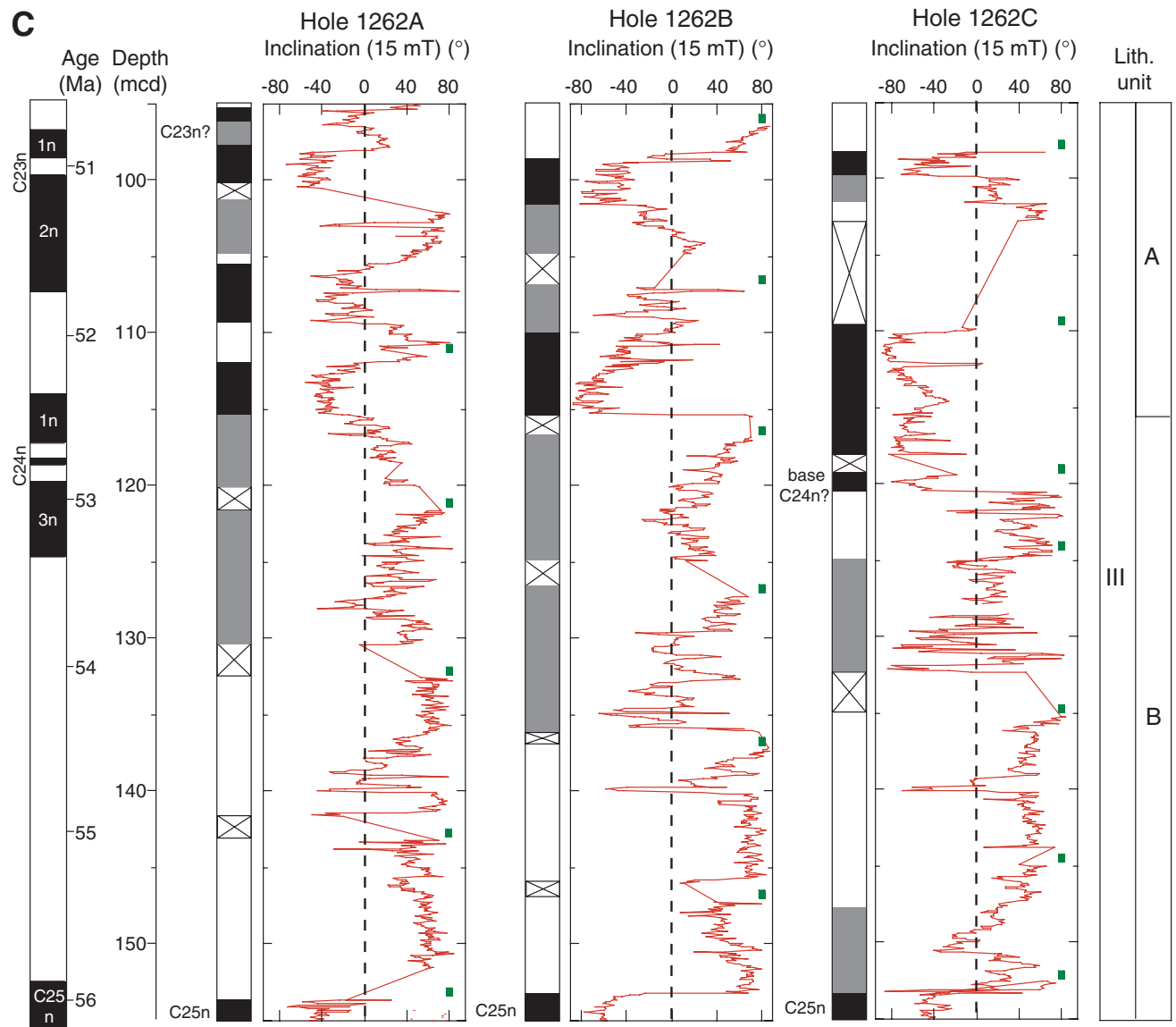


Figure F27 (continued). D. 145–205 mcd.

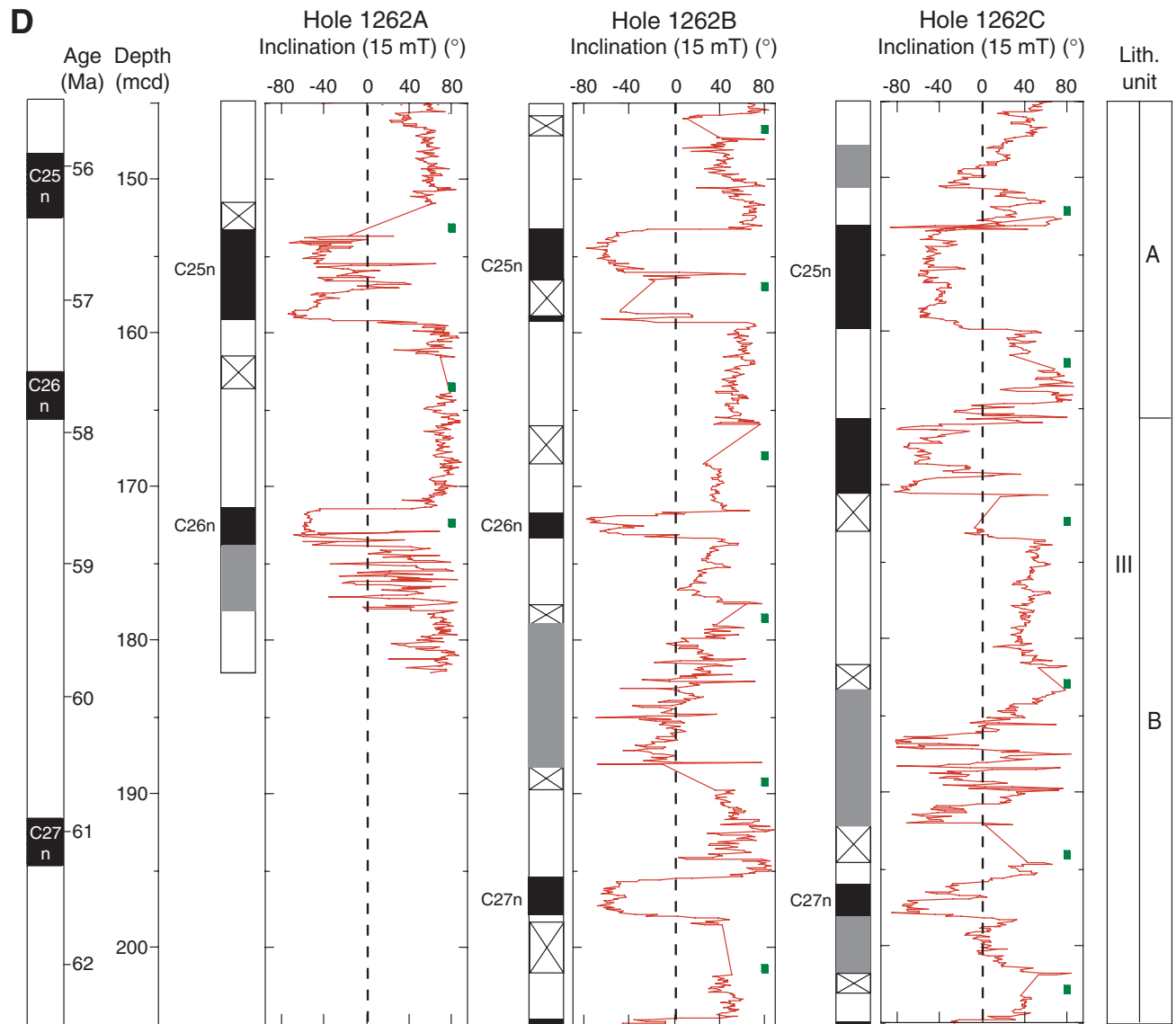


Figure F27 (continued). E. 195–235 mcd.

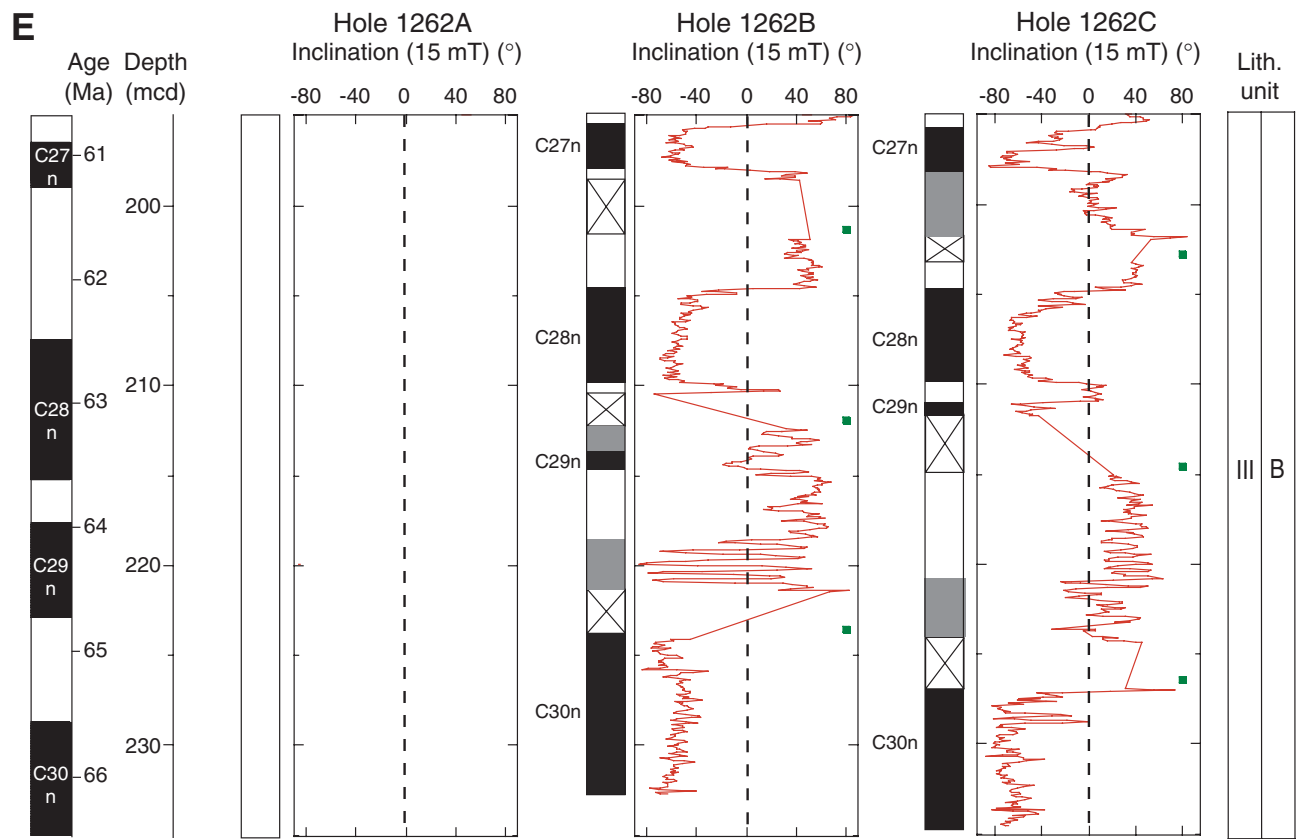


Figure F28. Discrete sample positions with respect to depositional remanent magnetization (DRM) after 15-mT AF demagnetization and magnetic susceptibility records.

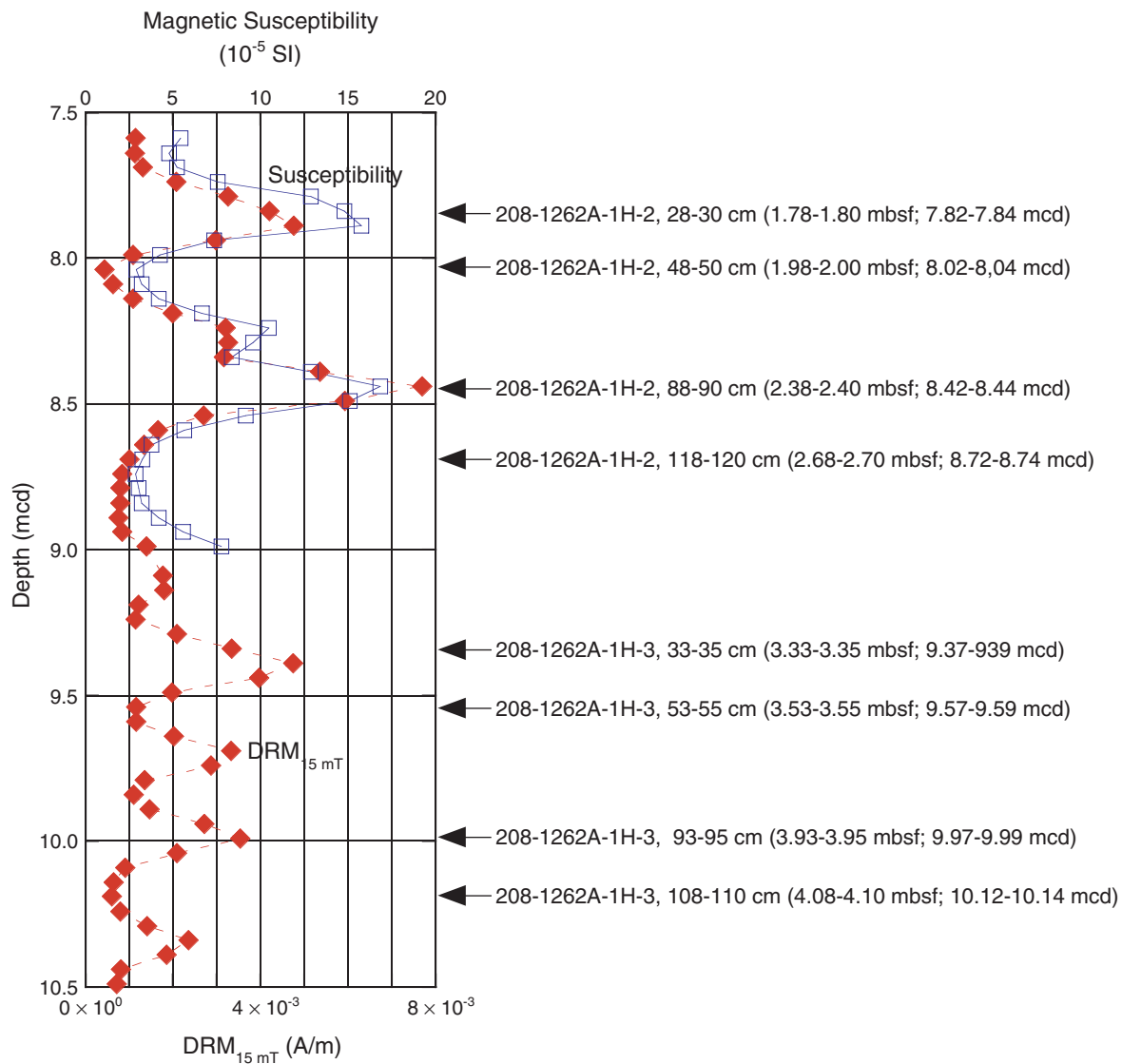


Figure F29. Profiles of chemical constituents in interstitial waters, Site 1262. A. Alkalinity. B. Chloride. C. Sodium. D. Potassium. E. Calcium. F. Magnesium. G. Strontium. H. Lithium. I. Boron. J. Barium. K. Sulfate. L. Manganese. M. Iron. N. Silicon. O. Zinc.

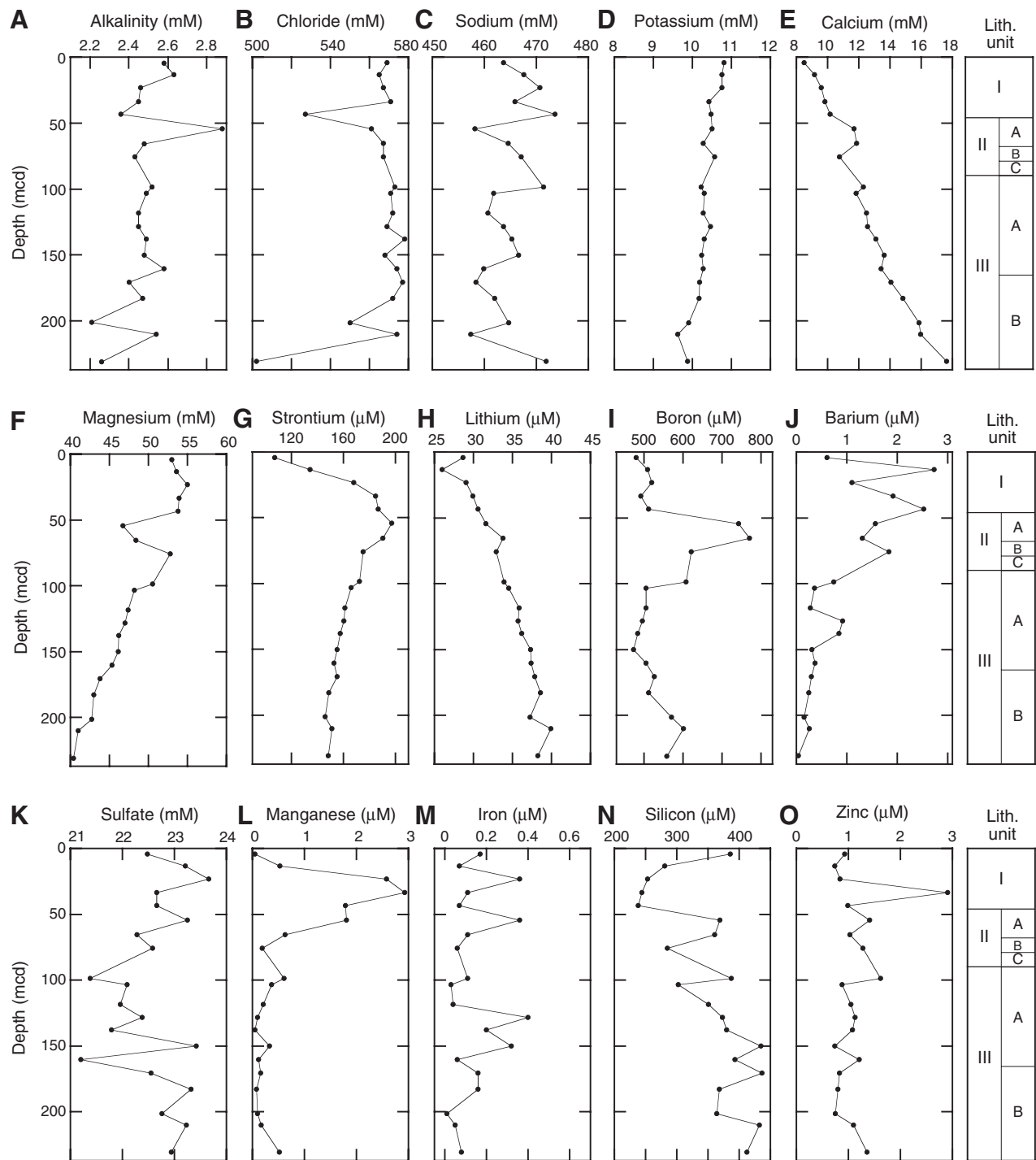


Figure F30. Sedimentary carbonate contents vs. composite depth for (A) the entire Site 1262 section with samples from Holes 1262A (dots), 1262B (open squares), and 1262C (crosses), and (B) the P/E boundary section at high resolution.

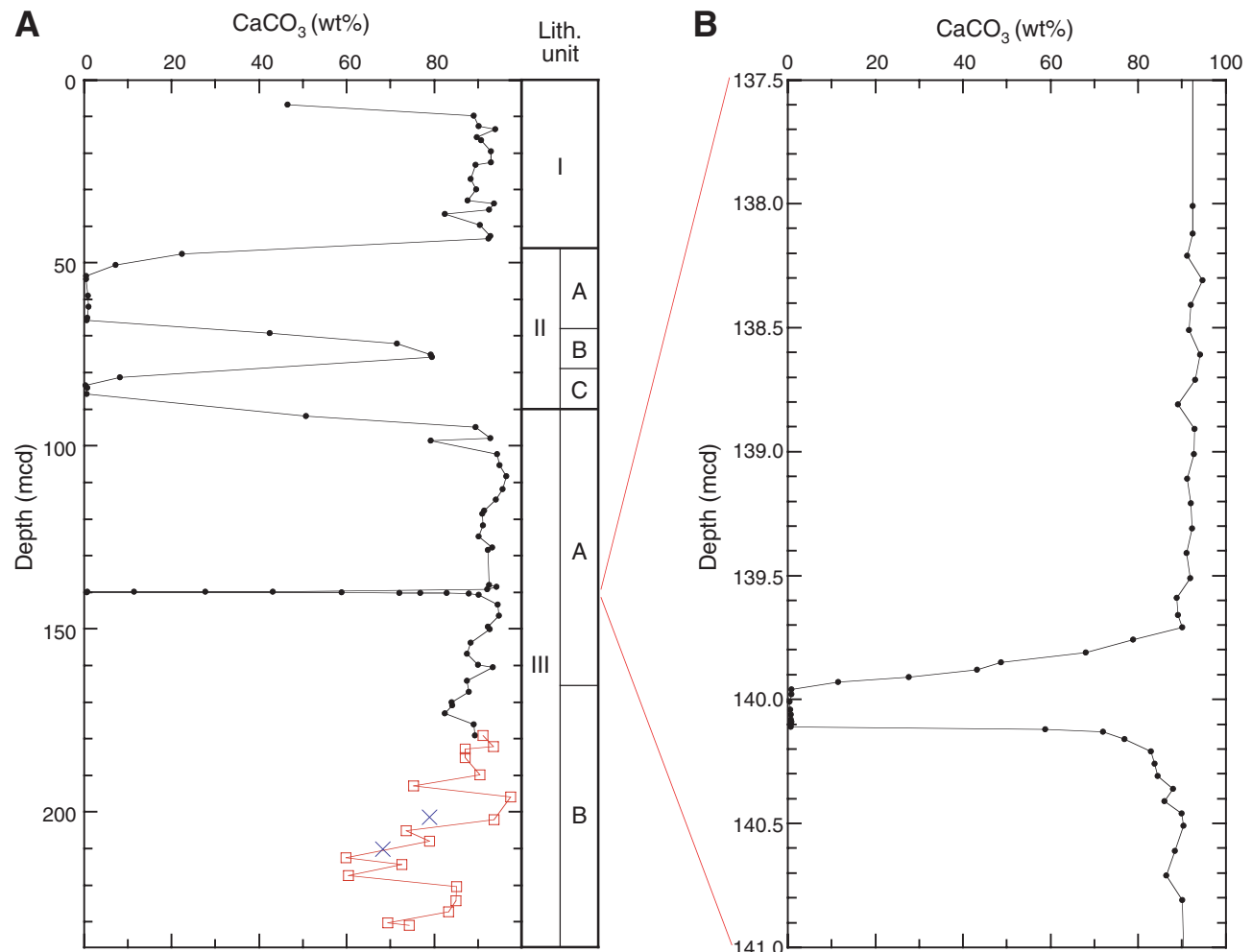


Figure F31. Gas chromatogram of Sample 208-1262A-8H-2, 140–150 cm, showing m/z 85 and 127.

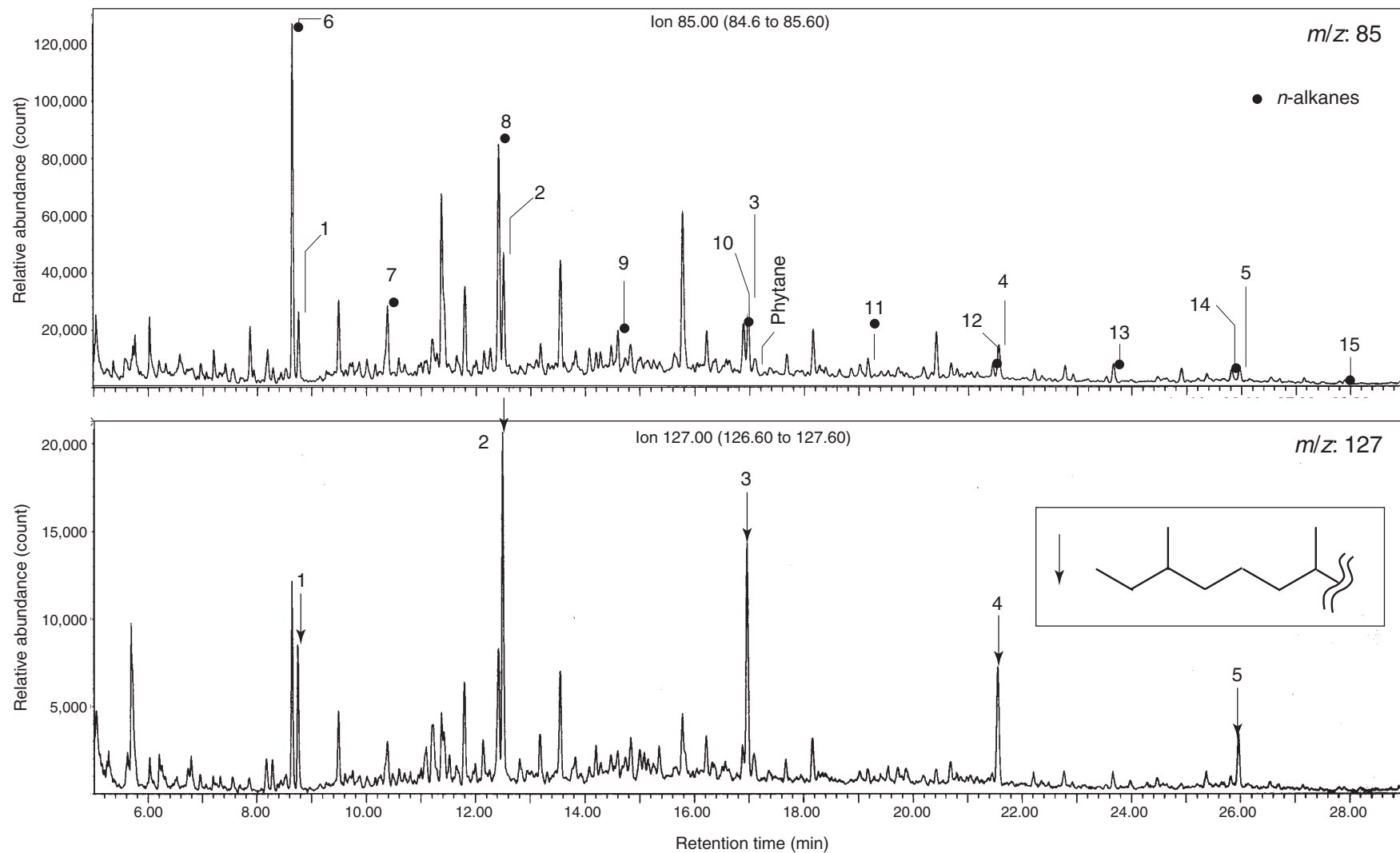


Figure F32. A. Core recovery plot. B. Shipboard biostratigraphic and magnetostratigraphic datums and the interpreted age-depth model. C. Corrected linear sedimentation rate (LSR), total, carbonate, and noncarbonate mass accumulation rates (MARs), calculated from the age model sampled at 1-m.y. intervals, and dry density and calcium carbonate concentrations averaged over the same 1-m.y. intervals. B = bottom, T = top.

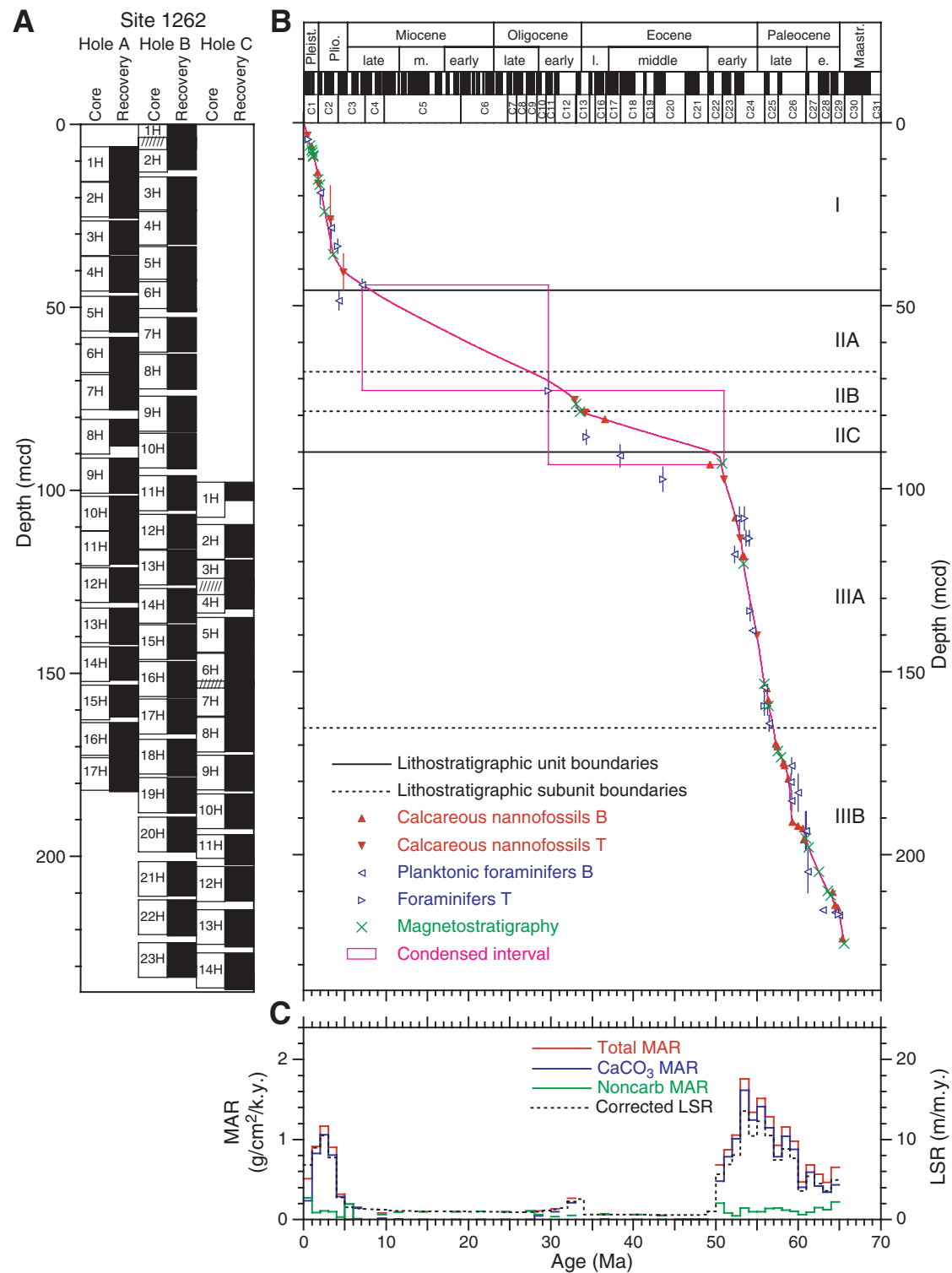


Table T1. Coring summary, Site 1262.

Core	Date (Mar 2003)	Local time (hr)	Depth (mbsf)		Length (m)		Recovery (%)	Tool deployment		
			Top	Bottom	Cored	Recovered				
208-1262A-										
1H	25	420	0.0	9.5	9.5	10.02	105.5	NMCB		
2H	25	555	9.5	19.0	9.5	9.97	105.0	NMCB		
3H	25	710	19.0	28.5	9.5	9.46	99.6	Tensor, NMCB		
4H	25	845	28.5	38.0	9.5	10.07	106.0	APCT, Tensor		
5H	25	1000	38.0	47.5	9.5	9.92	104.4	Tensor, NMCB		
6H	25	1125	47.5	57.0	9.5	10.16	107.0	Tensor, NMCB		
7H	25	1250	57.0	66.5	9.5	9.78	103.0	APCT, Tensor		
8H	25	1410	66.5	76.0	9.5	7.48	78.7	Tensor, NMCB		
9H	25	1520	76.0	85.5	9.5	9.68	101.9	Tensor, NMCB		
10H	25	1655	85.5	95.0	9.5	9.84	103.6	APCT, Tensor		
11H	25	1810	95.0	104.5	9.5	9.29	97.8	Tensor, NMCB		
12H	25	2010	104.5	114.0	9.5	9.61	101.2	Tensor, NMCB		
13H	25	2150	114.0	123.5	9.5	10.02	105.5	APCT, Tensor		
14H	26	15	123.5	133.0	9.5	9.26	97.5	Tensor, NMCB		
15H	26	630	133.0	142.5	9.5	8.84	93.1	DO, Tensor, NMCB		
16H	26	750	142.5	152.0	9.5	10.08	106.1	Tensor, NMCB		
17H	26	915	152.0	161.5	9.5	10.02	105.5	Tensor, NMCB		
			Cored totals:		161.5	163.5	101.2			
208-1262B-										
1H	26	1520	0.0	6.9	6.9	6.91	100.1	APCT		
2H	26	1655	6.9	11.9	5.0	8.98	179.6			
3H	26	1805	11.9	21.4	9.5	8.13	85.6	NMCB		
4H	26	1930	21.4	30.9	9.5	8.50	89.5	Tensor		
5H	26	2045	30.9	40.4	9.5	9.36	98.5	Tensor, NMCB		
6H	26	2205	40.4	48.4	8.0	9.05	113.1	Tensor		
7H	26	2320	48.4	57.9	9.5	9.12	96.0	Tensor, NMCB		
8H	27	45	57.9	67.4	9.5	9.69	102.0	Tensor		
9H	27	210	67.4	76.9	9.5	9.72	102.3	Tensor, NMCB		
10H	27	315	76.9	86.4	9.5	9.86	103.8	Tensor		
11H	27	430	86.4	95.9	9.5	9.04	95.2	Tensor, NMCB		
12H	27	535	95.9	105.4	9.5	9.20	96.8	Tensor		
13H	27	655	105.4	114.9	9.5	8.72	91.8	Tensor, NMCB		
14H	27	820	114.9	124.4	9.5	9.57	100.7	Tensor		
15H	27	940	124.4	133.9	9.5	9.57	100.7	Tensor, NMCB		
16H	27	1055	133.9	143.4	9.5	9.94	104.6	Tensor		
17H	27	1155	143.4	152.9	9.5	9.26	97.5	Tensor, NMCB		
18H	27	1310	152.9	162.4	9.5	10.04	105.7	Tensor		
19H	27	1420	162.4	171.9	9.5	9.77	102.8	Tensor		
20H	27	1525	171.9	181.4	9.5	9.61	101.2	Tensor		
21H	27	1645	181.4	190.9	9.5	9.25	97.4	Tensor		
22H	27	1810	190.9	200.4	9.5	9.94	104.6	Tensor		
23H	27	1940	200.4	209.9	9.5	9.30	97.9	Tensor		
			Cored totals:		209.9	212.53	101.3			
208-1262C-										
*****Drilled from 0.0 to 90.0 mbsf*****										
1H	28	110	90.0	99.5	9.5	5.16	54.3	Tensor, NMCB		
2H	28	245	99.5	109.0	9.5	9.03	95.1	Tensor		
3H	28	415	109.0	118.5	9.5	9.02	94.9	Tensor, NMCB		
4H	28	525	118.5	122.5	4.0	8.45	211.2	Tensor		
5H	28	640	122.5	132.0	9.5	9.38	98.7	Tensor, NMCB		
6H	28	750	132.0	141.5	9.5	9.18	96.6	Tensor		
7H	28	908	141.5	149.0	7.5	9.84	131.2	Tensor, NMCB		
8H	28	1013	149.0	158.5	9.5	8.92	93.9	Tensor		
9H	28	1120	158.5	168.0	9.5	9.90	104.2	Tensor		
10H	28	1230	168.0	177.5	9.5	9.70	102.1	Tensor		
11H	28	1345	177.5	184.0	6.5	8.34	128.3	Tensor		
12H	28	1455	184.0	193.5	9.5	9.30	97.9	Tensor		
13H	28	1610	193.5	203.0	9.5	10.24	107.8	Tensor		
14H	28	1730	203.0	212.5	9.5	10.01	105.4	Tensor		
			Cored totals:		122.5	126.5	103.2			
			Totals:		493.9	502.5	101.7			

Notes: NMCB = nonmagnetic core barrel, including cutting shoe (made from Monel). Tensor = brand name for core barrel orientation tool. APCT = Advanced Piston Corer Temperature tool (stainless steel housing is cutting shoe). DO = drillover. See Table T1, p. 106, in the "Leg 208 Summary" chapter.

SHIPBOARD SCIENTIFIC PARTY
CHAPTER 3, SITE 1262

62

Table T2. Composite depth scale, Site 1262.

Core	Offset (m)	Top (mbsf)	Top (mcd)
208-1262A-			
1H	6.04	0.00	6.04
2H	6.31	9.50	15.81
3H	7.31	19.00	26.31
4H	7.51	28.50	36.01
5H	8.96	38.00	46.96
6H	10.75	47.50	58.25
7H	11.39	57.00	68.39
8H	14.04	66.50	80.54
9H	15.21	76.00	91.21
10H	16.11	85.50	101.61
11H	16.05	95.00	111.05
12H	16.61	104.50	121.11
13H	18.11	114.00	132.11
14H	19.22	123.50	142.72
15H	20.16	133.00	153.16
16H	20.96	142.50	163.46
17H	20.39	152.00	172.39
208-1262B-			
1H	0.00	0.00	0.00
2H	-3.33	6.90	3.57
3H	2.41	11.90	14.31
4H	1.99	21.40	23.39
5H	2.51	30.90	33.41
6H	1.88	40.40	42.28
7H	4.33	48.40	52.73
8H	4.89	57.90	62.79
9H	6.87	67.40	74.27
10H	7.42	76.90	84.32
11H	9.58	86.40	95.98
12H	10.64	95.90	106.54
13H	10.97	105.40	116.37
14H	11.89	114.90	126.79
15H	12.32	124.40	136.72
16H	12.86	133.90	146.76
17H	13.62	143.40	157.02
18H	15.09	152.90	167.99
19H	16.09	162.40	178.49
20H	17.33	171.90	189.23
21H	19.94	181.40	201.34
22H	20.99	190.90	211.89
23H	23.18	200.40	223.58
208-1262C-			
1H	7.78	90.00	97.78
2H	9.79	99.50	109.29
3H	9.97	109.00	118.97
4H	5.51	118.50	124.01
5H	12.23	122.50	134.73
6H	12.49	132.00	144.49
7H	10.59	141.50	152.09
8H	13.00	149.00	162.00
9H	13.82	158.50	172.32
10H	14.92	168.00	182.92
11H	16.52	177.50	194.02
12H	18.78	184.00	202.78
13H	21.04	193.50	214.54
14H	23.42	203.00	226.42

Table T3. Splice tie points, Site 1262.

Hole, core, section, interval (cm)	Depth		Hole, core, section, interval (cm)	Depth		
	(mbsf)	(mcd)		(mbsf)	(mcd)	
208-						
1262B-1H-4, 100	5.50	5.50	Tie to	1262B-2H-2, 42	8.83	5.50
1262B-2H-3, 25	10.15	6.82	Tie to	1262A-1H-1, 77.5	0.78	6.82
1262A-1H-6, 132.5	8.82	14.86	Tie to	1262B-3H-1, 55	12.45	14.86
1262B-3H-4, 7.5	16.48	18.89	Tie to	1262A-2H-3, 7.5	12.58	18.89
1262A-2H-6, 127.5	18.24	24.55	Tie to	1262B-4H-1, 114.5	22.56	24.55
1262B-4H-5, 32.5	27.72	29.71	Tie to	1262A-3H-3, 40	22.40	29.71
1262A-3H-6, 25	26.75	34.06	Tie to	1262B-5H-1, 65	31.55	34.06
1262B-5H-3, 55	34.45	36.96	Tie to	1262A-4H-1, 95	29.45	36.96
1262A-4H-7, 15	37.65	45.16	Tie to	1262B-6H-2, 137.5	43.28	45.16
1262B-6H-5, 110	47.50	49.38	Tie to	1262A-5H-2, 92.5	40.42	49.38
1262A-5H-6, 135	46.85	55.81	Tie to	1262B-7H-3, 75	51.48	55.81
1262B-7H-7, 55	56.22	60.55	Tie to	1262A-6H-2, 80	49.80	60.55
1262A-6H-4, 100	53.00	63.75	Tie to	1262B-8H-1, 94.5	58.86	63.75
1262B-8H-5, 130	65.20	70.09	Tie to	1262A-7H-2, 20	58.70	70.09
1262A-7H-6, 77.5	65.28	76.67	Tie to	1262B-9H-2, 90	69.80	76.67
1262B-9H-5, 105	74.45	81.32	Tie to	1262A-8H-1, 77.5	67.28	81.32
1262A-8H-5, 17.5	71.30	85.34	Tie to	1262B-10H-1, 102.5	77.92	85.34
1262B-10H-6, 97.5	85.38	92.80	Tie to	1262A-9H-2, 8.5	77.59	92.80
1262A-9H-5, 125	83.25	98.46	Tie to	1262B-11H-2, 97.5	88.88	98.46
1262B-11H-6, 45	94.35	103.93	Tie to	1262A-10H-2, 82.5	87.82	103.93
1262A-10H-4, 112.5	91.12	107.23	Tie to	1262B-12H-1, 68.5	96.59	107.23
1262B-12H-4, 137.5	101.78	112.42	Tie to	1262A-11H-1, 136	96.37	112.42
1262A-11H-5, 45	101.45	117.50	Tie to	1262B-13H-1, 146	106.53	117.50
1262B-13H-6, 55	113.12	124.09	Tie to	1262A-12H-2, 148	107.48	124.09
1262A-12H-7, 5	113.05	129.66	Tie to	1262B-14H-2, 136	117.77	129.66
1262B-14H-5, 115	122.05	133.94	Tie to	1262A-13H-2, 32	115.83	133.94
1262A-13H-4, 62.5	119.12	137.23	Tie to	1262B-15H-1, 51	124.91	137.23
1262B-15H-6, 82.5	132.42	144.74	Tie to	1262A-14H-2, 52.5	125.52	144.74
1262A-14H-6, 85	131.85	151.07	Tie to	1262B-16H-3, 131	138.21	151.07
1262B-16H-6, 115	142.55	155.41	Tie to	1262A-15H-2, 75	135.25	155.41
1262A-15H-5, 77.5	139.78	159.94	Tie to	1262B-17H-2, 142.5	146.32	159.94
1262B-17H-5, 127.5	150.68	164.30	Tie to	1262A-16H-1, 83.5	143.34	164.30
1262A-16H-5, 97.5	149.48	170.44	Tie to	1262B-18H-2, 95	155.35	170.44
1262B-18H-5, 90	159.80	174.89	Tie to	1262A-17H-2, 100	154.50	174.89
1262A-17H-6, 20	159.70	180.09	Tie to	1262B-19H-2, 10	164.00	180.09
1262B-19H-5, 100	169.40	185.49	Tie to	1262C-10H-2, 106	170.57	185.49
1262C-10H-6, 72.5	176.22	191.14	Tie to	1262B-20H-2, 41	173.81	191.14
1262B-20H-5, 52.5	178.42	195.75	Tie to	1262C-11H-2, 22	179.23	195.75
1262C-11H-6, 20	185.20	201.72	Tie to	1262B-21H-1, 37.5	181.78	201.72
1262B-21H-2, 62.5	183.52	203.46	Tie to	1262C-12H-1, 67.5	184.68	203.46
1262C-12H-7, 67.5	193.18	211.96	Tie to	1262B-22H-1, 6	190.97	211.96
1262B-22H-4, 10	194.26	215.25	Tie to	1262C-13H-1, 71	194.21	215.25
1262C-13H-7, 87.5	203.38	224.42	Tie to	1262B-23H-1, 83.5	201.24	224.42
1262B-23H-3, 40	203.80	226.98	Tie to	1262C-14H-1, 54.5	203.56	226.98
1262C-14H-7, 62.5	212.62	236.04				

Note: This table is also available in [ASCII](#).

Table T4. Lithostratigraphic subdivisions, Site 1262.

Unit/ subunit	Unit boundary depth (mcd)	Hole 1262A						Hole 1262B						Hole 1262C					
		Core, section, interval (cm)		Depth (mbsf)		Depth (mcd)		Core, section, interval (cm)		Depth (mbsf)		Depth (mcd)		Core, section, interval (cm)		Depth (mbsf)		Depth (mcd)	
		Top	Base	Top	Base	Top	Base	Top	Base	Top	Base	Top	Base	Top	Base	Top	Base	Top	Base
I	45.8	1H-1	4H-CC	0.0	38.6	6.0	46.1	1H-1	6H-3, 52	0.0	43.9	0.0	45.8	—	—	—	—	—	—
IIA	68.1	5H-1	6H-CC	38.0	57.7	47.0	68.4	6H-3, 52	8H-4, 85	43.9	63.3	45.8	68.1	—	—	—	—	—	—
IIB	78.9	7H-1	7H-CC	57.0	66.8	68.4	78.2	8H-4, 85	9H-4, 10	63.3	72.0	68.1	78.9	—	—	—	—	—	—
IIC	90.0	8H-1	8H-CC	66.5	74.0	80.5	88.0	9H-4, 10	10H-4, 120	72.0	82.6	78.9	90.0	—	—	—	—	—	—
IIIA	165.4	9H-1	16H-2, 60	76.0	144.6	91.2	165.6	10H-4, 120	17H-CC	82.6	152.7	90.0	166.3	1H-1	8H-3, 13	90.0	152.1	97.8	165.1
IIIB	(236.4)*	16H-2, 60	17H-CC	144.6	162.0	165.6	182.4	18H-1	23H-CC	152.9	209.7	168.0	232.9	8H-3, 13	14H-CC	152.1	213.0	165.1	236.4

Notes: Bold intervals and depths define the unit boundaries; other intervals are recognized as part of units but do not contain the unit boundaries. — = lithostratigraphic unit not recovered. * = bottom of deepest hole.

Unit/ subunit	Unit boundary depth (mcd)	Description
I	45.8	Nannofossil ooze and foraminifer-bearing nannofossil ooze
IIA	68.1	Clay, ash-bearing clay, and nannofossil clay
IIB	78.9	Nannofossil ooze, foraminifer-bearing nannofossil ooze, and clayey nannofossil ooze
IIC	90.0	Clay, ash-bearing clay, and nannofossil clay
IIIA	165.4	Nannofossil ooze
IIIB	(236.4)*	Clayey nannofossil ooze

Table T5. Stratigraphic positions of selected calcareous nannofossil datums, Site 1262. (See table note. Continued on next page.)

Datum	Age (Ma)		Top of sample interval			Base of sample interval			Average (mcd)	
	Youngest	Oldest	Core, section, interval (cm)	Depth (mbsf)	Depth (mcd)	Core, section, interval (cm)	Depth (mbsf)	Depth (mcd)		
208-1262A-										
B	<i>Gephyrocapsa parallela</i>	0.98	1.03	1H-1, 1	0.01	6.05	1H-1, 100	1.00	7.04	6.55
T	<i>Large Gephyrocapsa</i>	1.22	1.26	1H-2, 120	2.70	8.74	1H-3, 48	3.48	9.52	9.13
B	Medium <i>Gephyrocapsa</i> spp.	1.69	1.71	1H-5, 145	7.45	13.49	1H-6, 30	7.80	13.84	13.67
	Zone CN13a assemblage	1.7	1.8	1H-CC	9.97	16.01	2H-1, 141	10.91	17.22	16.62
	Zone CN12aB assemblage	2.83	3.66	2H-1, 141	10.91	17.22	3H-CC	28.41	35.72	26.47
	Zone CN10c assemblage	4.56	5.05	3H-CC	28.41	35.72	4H-CC	38.52	46.03	40.88
T	<i>Ericsonia formosa</i>	32.9	32.9	7H-5, 90	63.90	75.29	7H-6, 127	65.77	77.16	76.23
T	<i>Discoaster saipanensis</i>	34.0	34.0	7H-CC	66.73	78.12	8H-1, 50	67.00	81.04	79.58
T	<i>Discoaster barbadiensis</i>	34.2	34.2	7H-CC	66.73	78.12	8H-1, 50	67.00	81.04	79.58
T	<i>Tribrachiatius orthostylus</i>	51.0	51.0	9H-4, 120	81.70	96.91	9H-5, 70	82.70	97.91	97.41
B	<i>Discoaster lodoensis</i>	52.4	52.4	10H-5, 6	91.56	107.67	10H-5, 50	92.00	108.11	107.89
T	<i>Discoaster multiradiatus</i>	53.0	53.0	11H-2, 70	97.20	113.25	11H-2, 140	97.90	113.95	113.60
B	<i>Tribrachiatius orthostylus</i>	53.4	53.4	11H-5, 120	102.20	118.25	11H-6, 90	103.40	119.45	118.85
	<i>Fasciculithus</i> spp.	54.1	54.1	13H-4, 43	118.93	137.04	13H-4, 60	119.10	137.21	137.13
	Increase <i>Zygrhablithus bijugatus</i>			13H-6, 10	121.60	139.71	13H-6, 25	121.75	139.86	139.79
B	<i>Rhomboaster</i> spp.			13H-6, 25	121.75	139.86	13H-6, 38	121.88	139.99	139.93
B	<i>Discoaster multiradiatus</i>	56.2	56.2	14H-CC	132.71	151.93	15H-1, 100	134.00	154.16	153.05
B	<i>Heliolithus riedelii</i>	57.3	57.3	16H-4, 87	147.87	168.83	16H-5, 24	148.74	169.70	169.27
B	<i>Discoaster mohleri</i>	57.5	57.5	16H-4, 87	147.87	168.83	16H-5, 24	148.74	169.70	169.27
B	<i>Heliolithus kleinpellii</i>	58.2	58.2	17H-2, 129	154.79	175.18	17H-3, 34	155.34	175.73	175.46
B	<i>Sphenolithus anarrhopus</i>	58.4	58.4	17H-2, 129	154.79	175.18	17H-3, 34	155.34	175.73	175.46
208-1262B-										
T	<i>Pseudoemiliania lacunosa</i>	0.46	0.46	1H-3, 7	3.07	3.07	1H-3, 90	3.90	3.90	3.49
T	<i>Ericsonia formosa</i>	32.9	32.9	9H-1, 143	68.83	75.70	9H-2, 10	69.00	75.87	75.79
T	<i>Discoaster saipanensis</i>	34.0	34.0	9H-4, 6	71.96	78.83	9H-4, 85	72.75	79.62	79.23
T	<i>Discoaster barbadiensis</i>	34.2	34.2	9H-4, 6	71.96	78.83	9H-4, 85	72.75	79.62	79.23
B	<i>Isthmolithus recurvus</i>	36.6	36.6	9H-5, 81	74.21	81.08	9H-5, 97	74.37	81.24	81.16
B	<i>Discoaster subloedoensis</i>	49.3	49.3	10H-6, 145	85.85	93.27	10H-7, 40	86.30	93.72	93.50
T	<i>Tribrachiatius orthostylus</i>	51.0	51.0	11H-1, 80	87.20	96.78	11H-2, 80	88.70	98.28	97.53
B	<i>Discoaster lodoensis</i>	52.4	52.4	12H-1, 130	97.20	107.84	12H-2, 40	97.80	108.44	108.14
T	<i>Discoaster multiradiatus</i>	53.0	53.0	13H-1, 100	106.40	117.37	13H-2, 50	107.07	118.04	117.71
B	<i>Sphenolithus radians</i>	53.3	53.3	13H-2, 50	107.07	118.04	13H-2, 140	107.97	118.94	118.49
B	<i>Tribrachiatius orthostylus</i>	53.4	53.4	13H-2, 50	107.07	118.04	13H-2, 140	107.97	118.94	118.49
T	<i>Fasciculithus</i> spp.			14H-CC	124.34	136.23	15H-CC	133.84	146.16	141.20
B	<i>Rhomboaster</i> spp.			14H-CC	124.34	136.23	15H-CC	133.84	146.16	141.20
B	<i>Discoaster multiradiatus</i>	56.2	56.2	16H-5, 100	140.90	153.76	16H-6, 100	142.40	155.26	154.51
B	<i>Discoaster okadai</i>	56.4	56.4	17H-1, 20	143.60	157.22	17H-1, 130	144.70	158.32	157.77
B	<i>Heliolithus riedelii</i>	57.3	57.3	18H-1, 140	154.30	169.39	18H-2, 54	154.94	170.03	169.71
B	<i>Discoaster mohleri</i>	57.5	57.5	18H-2, 54	154.94	170.03	18H-2, 140	155.80	170.89	170.46
B	<i>Heliolithus kleinpellii</i>	58.2	58.2	18H-5, 40	159.30	174.39	18H-5, 140	160.30	175.39	174.89
B	<i>Sphenolithus anarrhopus</i>	58.4	58.4	18H-5, 140	160.30	175.39	18H-6, 40	160.80	175.89	175.64
B	<i>Heliolithus cantabriae</i>	58.8	58.8	19H-1, 20	162.60	178.69	19H-1, 130	163.70	179.79	179.24
B	<i>Fasciculithus pileatus</i>	59.3	59.3	19H-CC	172.07	188.16	20H-1, 20	172.10	189.43	188.80
B	<i>Fasciculithus tympaniformis</i>	59.7	59.7	19H-CC	172.07	188.16	20H-1, 20	172.10	189.43	188.80
B	<i>Fasciculithus</i> spp.	60.0	60.0	20H-1, 20	172.10	189.43	20H-1, 135	173.25	190.58	190.01
B	<i>Sphenolithus primus</i>	60.6	60.6	20H-3, 20	175.10	192.43	20H-3, 110	176.00	193.33	192.88
B	<i>Chiasmolithus bidens</i>	60.7	60.7	20H-5, 20	178.10	195.43	20H-5, 110	179.00	196.33	195.88
B	<i>Chiasmolithus danicus</i>	64.2	64.2	21H-7, 10	190.00	209.94	21H-CC	190.55	210.49	210.22
B	<i>Cruciplacolithus tenuis</i> s.s.	64.5	64.5	22H-2, 72	192.62	213.61	22H-3, 33	192.99	213.98	213.80
B	<i>Cruciplacolithus primus</i>	64.8	64.8	22H-3, 33	192.99	213.98	22H-3, 130	193.96	214.95	214.47
B	<i>Micula prinsii</i>	65.4	65.4	22H-CC	200.76	221.75	23H-1, 40	200.80	223.98	222.87
208-1262C-										
B	<i>Discoaster lodoensis</i>	52.4	52.4	1H-CC	95.06	102.84	2H-CC	108.43	118.22	110.53
T	<i>Discoaster multiradiatus</i>	53.0	53.0	2H-CC	108.43	118.22	3H-CC	117.92	127.89	123.06
B	<i>Sphenolithus radians</i>	53.3	53.3	2H-CC	108.43	118.22	3H-CC	117.92	127.89	123.06
B	<i>Tribrachiatius orthostylus</i>	53.4	53.4	2H-CC	108.43	118.22	3H-CC	117.92	127.89	123.06
B	<i>Rhomboaster cuspis</i>	54.1	54.1	4H-CC	126.90	132.41	5H-CC	131.83	144.06	138.24
T	<i>Fasciculithus</i> spp.	54.1	54.1	4H-CC	126.90	132.41	5H-CC	131.83	144.06	138.24
B	<i>Discoaster multiradiatus</i>	56.2	56.2	6H-CC	141.05	153.54	7H-CC	151.29	161.88	157.71
B	<i>Discoaster mohleri</i>	57.5	57.5	7H-CC	151.29	161.88	8H-CC	157.82	170.82	166.35
B	<i>Heliolithus kleinpellii</i>	58.2	58.2	9H-1, 150	160.00	173.82	9H-CC	168.35	182.17	178.00
B	<i>Sphenolithus anarrhopus</i>	58.4	58.4	9H-1, 150	160.00	173.82	9H-CC	168.35	182.17	178.00
B	<i>Heliolithus cantabriae</i>	58.8	58.8	9H-1, 150	160.00	173.82	9H-CC	168.35	182.17	178.00
B	<i>Fasciculithus pileatus</i>	59.3	59.3	10H-6, 30	175.80	190.72	10H-6, 100	176.50	191.42	191.07

Table T5 (continued).

Datum	Age (Ma)		Top of sample interval			Base of sample interval			Average (mcd)
	Youngest	Oldest	Core, section, interval (cm)	Depth (mbsf)	Depth (mcd)	Core, section, interval (cm)	Depth (mbsf)	Depth (mcd)	
B <i>Fasciculithus</i> spp.	60.0	60.0	10H-7, 4	176.74	191.66	10H-CC	177.65	192.57	192.12
B <i>Chiasmolithus danicus</i>	64.2	64.2	11H-CC	185.79	202.31	12H-CC	193.25	212.03	207.17
B <i>Cruciplacolithus tenuis</i> s.s.	64.5	64.5	12H-CC	193.25	212.03	13H-CC	203.69	224.73	218.38
B <i>Cruciplacolithus primus</i>	64.8	64.8	12H-CC	193.25	212.03	13H-CC	203.69	224.73	218.38
B <i>Micula prinsii</i>	65.4	65.4	13H-CC	203.69	224.73	14H-CC	212.96	236.38	230.56

Note: T = top, B = bottom.

Table T6. Stratigraphic positions of selected planktonic foraminiferal datums, Site 1262.

Datum	Age (Ma)		Top of sample interval		Base of sample interval		Average (mcd)			
	Youngest	Oldest	Hole, core, section, interval (cm)	Depth (mbsf)	(mcd)	Hole, core, section, interval (cm)	Depth (mbsf)	(mcd)		
			208-		208-					
T	<i>Globorotalia tosaensis</i>	0.61	0.61	1262B-2H-1, 62–64	10.12	4.19	1262B-1H-4, 62–64	5.12	5.12	4.66
B	<i>Globorotalia truncatulinoides</i>	2.02	2.02	1262A-1H-CC	9.97	16.01	1262B-3H-CC	19.98	22.39	19.20
B	<i>Globorotalia tosaensis</i>	3.35	3.35	1262A-2H-CC	19.42	25.73	1262B-4H-CC	29.85	31.84	28.79
T	<i>Globorotalia plesiotumida</i>	4.15	4.15	1262B-4H-CC	29.85	31.84	1262A-3H-CC	28.41	35.72	33.78
B	<i>Globorotalia crassaformis</i> (s.l.)	4.31	4.31	1262A-4H-CC	38.52	46.03	1262B-6H-CC	49.40	51.28	48.66
T	<i>Globoturborotalita nepenthes</i>	4.37	4.37	1262A-5H-CC	47.87	56.83	1262B-7H-CC	57.47	61.80	59.32
B	<i>Globoconella conomiozea</i>	7.12	7.12	1262B-5H-CC	40.21	42.72	1262A-4H-CC	38.52	46.03	44.38
T	<i>Subbotina angiporoidea</i>	29.67	29.67	1262A-6H-CC	57.61	68.36	1262A-7H-CC	66.73	78.12	73.24
T	<i>Globigerinatheka index</i>	34.30	34.30	1262B-9H-CC	77.07	83.94	1262A-8H-CC	73.93	87.97	85.96
B	<i>Globigerinatheka semiinvoluta</i>	38.40	38.40	1262A-8H-CC	73.93	87.97	1262B-10H-CC	86.71	94.13	91.05
T	<i>Morozovella aragonensis</i>	43.60	43.60	1262B-10H-CC	86.71	94.13	1262A-9H-CC	85.63	100.84	97.49
B	<i>Morozovella aragonensis</i>	52.30	52.30	1262B-12H-CC	105.05	115.69	1262A-11H-CC	104.24	120.29	117.99
T	<i>Morozovella aequa</i>	52.89	52.89	1262B-11H-CC	95.39	104.97	1262A-10H-CC	95.29	111.40	108.19
T	<i>Subbotina velascoensis</i>	53.50	53.50	1262B-11H-CC	95.39	104.97	1262A-10H-CC	95.29	111.40	108.19
B	<i>Morozovella lensiformis</i>	53.68	53.68	1262A-10H-CC	95.29	111.40	1262B-12H-CC	105.05	115.69	113.55
T	<i>Subbotina triangularis</i>	54.07	54.07	1262A-10H-CC	95.29	111.40	1262B-12H-CC	105.05	115.69	113.55
T	<i>Morozovella velascoensis</i>	54.17	54.17	1262A-12H-CC	114.06	130.67	1262B-14H-CC	124.34	136.23	133.45
B	<i>Morozovella gracilis</i>	54.46	54.46	1262A-13H-4, 140–150	119.90	138.01	1262A-13H-5, 138–139	121.38	139.49	138.75
T	<i>Stensioeina beccariiformis</i> *	55.00	55.00	1262A-13H-6, 43–44	121.93	140.04	1262A-13H-6, 57–58	122.07	140.18	140.11
B	<i>Morozovella subbotinæ</i>	55.90	55.90	1262A-14H-CC	132.71	151.93	1262B-16H-CC	143.79	156.65	154.29
T	<i>Globanomalina pseudomenardii</i>	55.90	55.90	1262B-16H-CC	143.79	156.65	1262A-15H-CC	141.79	161.95	159.30
T	<i>Acarinina mckannai</i>	56.30	56.30	1262B-16H-CC	143.79	156.65	1262A-15H-CC	141.79	161.95	159.30
B	<i>Acarinina soldadoensis</i>	56.50	56.50	1262A-15H-CC	141.79	161.95	1262B-17H-CC	152.61	166.23	164.09
B	<i>Morozovella aequa</i>	56.50	56.50	1262A-15H-CC	141.79	161.95	1262B-17H-CC	152.61	166.23	164.09
B	<i>Acarinina mckannai</i>	59.10	59.10	1262B-18H-CC	162.89	177.98	1262A-17H-CC	161.97	182.36	180.17
B	<i>Acarinina subsphaerica</i>	59.20	59.20	1262A-16H-CC	152.53	173.49	1262B-18H-CC	162.89	177.98	175.74
B	<i>Globanomalina pseudomenardii</i>	59.20	59.20	1262A-17H-CC	161.97	182.36	1262B-19H-CC	172.07	188.16	185.26
B	<i>Morozovella velascoensis</i>	60.00	60.00	1262B-18H-CC	162.89	177.98	1262B-19H-CC	172.07	188.16	183.07
B	<i>Morozovella conicotruncata</i>	60.90	60.90	1262B-19H-CC	172.07	188.16	1262B-20H-CC	181.46	198.79	193.48
B	<i>Morozovella angulata</i>	61.00	61.00	1262B-19H-CC	172.07	188.16	1262B-20H-CC	181.46	198.79	193.48
B	<i>Praemurica uncinata</i>	61.20	61.20	1262B-20H-CC	181.46	198.79	1262B-21H-CC	190.55	210.49	204.64
B	<i>Praemurica inconstans</i>	63.00	63.00	1262B-22H-3, 97.0–98.5	193.63	214.62	1262B-22H-4, 37.5–39.0	194.54	215.52	215.07
B	<i>Subbotina triloculinoides</i>	64.50	64.50	1262B-22H-4, 37.5–39.0	194.54	215.52	1262B-22H-4, 85.0–86.5	195.01	216.00	215.76
T	<i>Parvularugoglobigerina eugubina</i>	64.90	64.90	1262B-22H-4, 114.0–115.5	195.30	216.29	1262B-22H-4, 133.0–134.5	195.49	216.48	216.39
B	<i>Parvularugoglobigerina eugubina</i>	64.97	64.97	1262B-22H-4, 133.0–134.5	195.49	216.48	1262B-22H-4, 143.0–144.5	195.59	216.58	216.53

Notes: T = top, B = bottom. * = benthic foraminiferal datum.

Table T7. Stratigraphic ranges and relative abundances of selected calcareous nannofossils, Site 1262. ([See table notes](#). Continued on next five pages.)

SHIPBOARD SCIENTIFIC PARTY
CHAPTER 3, SITE 1262

Table T7 (continued).

Core, section, interval (cm)	Depth (mbsf)	Depth (mcd)	Preparation	Total abundance	Preservation	Zones and comment	Fossils																											
							Benthic forams		Forams		Gastropods		Bivalves		Cephalopods		Moll.		Cnidarians		Others													
							P	F	C	C	P	F	C	R	R	F	F	C	A	R	F	F	R	F	F/C	C	RR	C	T	Discoaster spp.	Terebellids spp.	Fasciolaria spp.	Rhomboasteridae	
208-1262A-																																		
1H-5, 145–150	7.45	13.49	SS	A	G	NN19/CN13b																												
1H-CC	9.97	16.01	SS	A	G	NN19/CN13a																												
2H-CC	19.42	25.73	SS	A	G	NN16/CN12aB																												
3H-CC	28.41	35.72	SS	A	G	NN16/CN12aB																												
4H-CC	38.52	46.03	SS	A	M/P	NN13–NN15/CN10c																												
5H-CC	47.87	56.83	SS	B																														
6H-CC	57.61	68.36	SS	B																														
7H-CC	66.73	78.12	SS	A	M	NP21/CP16																												
8H-CC	73.93	87.97	SS	A	M	NP15/CP13b																												
9H-CC	85.63	100.84	SS	A	M	NP12/CP10																												
10H-CC	95.29	111.40	SS	A	M/P	NP11/CP9b																												
11H-CC	104.24	120.29	SS	A	M	NP10/CP9																												
12H-CC	114.06	130.67	SS	A	P	NP9/CP8																												
13H-CC	123.97	142.08	SS	A	M/G	NP9/CP8																												
14H-CC	132.71	151.93	SS	A	M/G	NP9/CP8																												
15H-CC	141.79	161.95	SS	A	G	NP8/CP7–CP6																												
16H-CC	152.53	173.49	SS	A	P/M	NP6/CP5																												
17H-CC	161.97	182.36	SS	A	M	NP5/CP4																												
208-1262B-																																		
1H-CC	6.86	6.86	SS	A	M	NN19/CN13b																												
2H-CC	15.83	12.50	SS	A	M/G	NN19/CN13a																												
3H-CC	19.98	22.39	SS	A	M	NN16/CN12aB																												
4H-CC	29.85	31.84	SS	A	M	NN16/CN12aB																												
5H-CC	40.21	42.72	SS	A	M	NN13–NN15/CN10c																												
6H-CC	49.40	51.28	SS	B																														
7H-CC	57.47	61.80	SS	B																														
8H-CC	67.32	72.21	SS	A	M	NP23/CP17																												
9H-CC	77.07	83.94	SS	B																														
10H-CC	86.71	94.13	SS	C	P/M	NP14/CP12																												
11H-CC	95.39	104.97	SS	A	M/P	NP12/CP11																												
12H-CC	105.05	115.69	SS	A	M/G	NP11/CP9b																												
13H-CC	114.07	125.04	SS	A	M/G	NP10/CP9a																												
14H-CC	124.34	136.23	SS	A	M/G	NP9/CP8																												
15H-CC	133.84	146.16	SS	A	M	NP9/CP8																												
16H-CC	143.79	156.65	SS	A	M/P	NP8/CP7–CP6																												
17H-CC	152.61	166.23	SS	A	M/G	NP7/CP6																												
18H-CC	162.89	177.98	SS	A	M	NP5/CP4																												

Table T7 (continued).

Core, section, interval (cm)	Depth (mbsf)	Depth (mcd)	Preparation	Total abundance	Preservation	Zones and comment	Fasciculithus tympaniniformis	Ellipsolithus distichus	Fasciculithus involutus	Fasciculithus alani	Fasciculithus schaubii	Heliolithus spp.	Campyllosphaera spp.	Ericsonia cf. E. robusta	Ellipsolithus macellus	Discoaster nobilis	Heliolithus riedelii	Discoaster mohleri	Bomolithus elegans	Chiasmolithus bidens	Heliolithus kleinpellii	Sphenolithus anarrhopus	Fasciculithus pileatus	Heliolithus cantabriae	Cruciplacolithus tenuis	Chiasmolithus bidens	Toweius eminens	Toweius tovae	Cruciplacolithus primus	Cruciplacolithus edwardsii	Chiasmolithus danicus	Placozygus sigmoides	Biantholithus sparsus	Cyclagelosphaera alta	Micula printsi	Micula mutus	Arkhangelskiella cymbiformis
208-1262A-																																					
1H-5, 145–150	7.45	13.49	SS	A	G	NN19/CN13b																															
1H-CC	9.97	16.01	SS	A	G	NN19/CN13a																															
2H-CC	19.42	25.73	SS	A	G	NN16/CN12aB																															
3H-CC	28.41	35.72	SS	A	G	NN16/CN12aB																															
4H-CC	38.52	46.03	SS	A	M/P	NN13–NN15/CN10c																															
5H-CC	47.87	56.83	SS	B																																	
6H-CC	57.61	68.36	SS	B																																	
7H-CC	66.73	78.12	SS	A	M	NP21/CP16																															
8H-CC	73.93	87.97	SS	A	M	NP15/CP13b																															
9H-CC	85.63	100.84	SS	A	M	NP12/CP10																															
10H-CC	95.29	111.40	SS	A	M/P	NP11/CP9b																															
11H-CC	104.24	120.29	SS	A	M	NP10/CP9																															
12H-CC	114.06	130.67	SS	A	P	NP9/CP8																															
13H-CC	123.97	142.08	SS	A	M/G	NP9/CP8	C		C		F																										
14H-CC	132.71	151.93	SS	A	M/G	NP9/CP8	C		C																												
15H-CC	141.79	161.95	SS	A	G	NP8/CP7–CP6	F																														
16H-CC	152.53	173.49	SS	A	P/M	NP6/CP5	F																														
17H-CC	161.97	182.36	SS	A	M	NP5/CP4	R																														
208-1262B-																																					
1H-CC	6.86	6.86	SS	A	M	NN19/CN13b																															
2H-CC	15.83	12.50	SS	A	M/G	NN19/CN13a																															
3H-CC	19.98	22.39	SS	A	M	NN16/CN12aB																															
4H-CC	29.85	31.84	SS	A	M	NN16/CN12aB																															
5H-CC	40.21	42.72	SS	A	M	NN13–NN15/CN10c																															
6H-CC	49.40	51.28	SS	B																																	
7H-CC	57.47	61.80	SS	B																																	
8H-CC	67.32	72.21	SS	A	M	NP23/CP17																															
9H-CC	77.07	83.94	SS	B																																	
10H-CC	86.71	94.13	SS	C	P/M	NP14/CP12																															
11H-CC	95.39	104.97	SS	A	M/P	NP12/CP11																															
12H-CC	105.05	115.69	SS	A	M/G	NP11/CP9b																															
13H-CC	114.07	125.04	SS	A	M/G	NP10/CP9a																															
14H-CC	124.34	136.23	SS	A	M/G	NP9/CP8																															
15H-CC	133.84	146.16	SS	A	M	NP9/CP8	A	F																													
16H-CC	143.79	156.65	SS	A	P/M	NP8/CP7–CP6	C		C/A																												
17H-CC	152.61	166.23	SS	A	M/G	NP7/CP6	C	F																													
18H-CC	162.89	177.98	SS	A	M	NP5/CP4	F/C																														

Table T7 (continued).

Core, section, interval (cm)	Depth (mbsf)	Depth (mcd)	Preparation	Total abundance		Preservation	Zones and comment											
				A	M/G													
19H-CC	172.07	188.16	SS	A	M/G	NP5/CP4	<i>Pseudodemania lacunosa</i>											
20H-CC	181.46	198.79	SS	A	M	NP4/CP3 Cretaceous Rew	Large <i>Gephyrocapsa</i>											
21H-CC	190.55	210.49	SS	A	M/G	NP2/CP1b Cretaceous Rew	Medium <i>Gephyrocapsa</i>											
22H-CC	200.76	221.75	SS	A	M/P	CC26/NC23	<i>Calcidiscus macintyrei</i>											
23H-CC	209.60	232.78	SS	A	M/P	CC26/NC23	Small placoliths											
208-1262C-																		
1H-CC	95.06	102.84	SS	A	M	NP12/CP11	<i>Small Gephyrocapsa</i> spp.											
2H-CC	108.43	118.22	SS	A	M/G	NP11/CP9b	<i>Discoaster brouweri</i>											
3H-CC	117.92	127.89	SS	A	M	NP10/CP9a	<i>Discoaster pentradiatus</i>											
4H-CC	126.90	132.41	SS	A	M/G	NP9/CP8	<i>Discoaster surculus</i>											
5H-CC	131.83	144.06	SS	C	M	NP9/CP8	<i>Discoaster tamalis</i>											
6H-CC	141.05	153.54	SS	A	G	NP9/CP8	<i>Discoaster asymmetricus</i>											
7H-CC	151.29	161.88	SS	A	M	NP8/CP6-CP7	<i>Helicosphaera sellii</i>											
8H-CC	157.82	170.82	SS	A	M	NP6/CP5	<i>Ceratolithus rugosus</i>											
9H-CC	168.35	182.17	SS	A	M	NP5/CP4	<i>Discoaster variabilis</i>											
10H-CC	177.65	192.57	SS	A	M/G	NP4/CP3 Cretaceous Rew	<i>Discoaster intercalans</i>											
11H-CC	185.79	202.31	SS	A	G	NP3/CP2 Cretaceous Rew	<i>Sphenolithus</i> spp.											
12H-CC	193.25	212.03	SS	A	M/G	NP2/CP1b Cretaceous Rew	<i>Reticulofenestra pseudumbilicus</i>											
13H-CC	203.69	224.73	SS	A	M/P	CC26/NC23	<i>Amuroliithus primus</i>											
14H-CC	212.96	236.38	SS	A	M/P	CC26/NC23	<i>Discoaster 5 rays</i>											
							<i>Sphenolithus predistentus</i>											
							<i>Cyclicargolithus floridanus</i>											
							<i>Coccolithus pelagicus</i>											
							<i>Thoracosphaera</i> spp.											
							<i>Dictyococcites bipectus</i>											
							<i>Zygolithus bijugatus</i>											
							<i>Reticulofenestra umbilicus</i> ≥ 14 μm											
							<i>Discoaster tanii</i> group											
							<i>Sphenolithus pseudotetradiums</i>											
							<i>Towadius crassus</i>											
							<i>Chiphramnolithus calathus</i>											

Notes: Preparation: SS = smear slide. Total abundance: A = abundant, C = common, B = barren. Preservation: G = good, M = moderate, P = poor. Taxon abundance: AA = very abundant (acme), A = abundant, C = common, P = present, F = few, R = rare, RR = single specimens. Rew = reworking.

Table T7 (continued).

Core, section, interval (cm)	Depth (mbst)	Depth (mcd)	Preparation			Zones and comment		Fossils											
			Total abundance		Preservation			Benthic forams					Radiolaria						
			A	M/G				M	G	M/G	M/P	M/P	M	M	M	M	M		
19H-CC	172.07	188.16	SS	A	M/G	NP5/CP4		<i>Reticulofenestra dictyoda</i>											
20H-CC	181.46	198.79	SS	A	M	NP4/CP3 Cretaceous Rew		<i>Ericsonia formosa</i>											
21H-CC	190.55	210.49	SS	A	M/G	NP2/CP1b Cretaceous Rew		<i>Discoaster solpanensis</i>											
22H-CC	200.76	221.75	SS	A	M/P	CC26/NC23		<i>Discoaster barbadiensis</i>											
23H-CC	209.60	232.78	SS	A	M/P	CC26/NC23		<i>Isthmolithus recurvus</i>											
208-1262C-1	95.06	102.84	SS	A	M	NP12/CP11		<i>Bramletteius seracoides</i>											
	108.43	118.22	SS	A	M/G	NP11/CP9b		<i>Dicyococtites bisectus</i>											
	117.92	127.89	SS	A	M	NP10/CP9a		<i>Calcidiscus protoannulus</i>											
	126.90	132.41	SS	A	M/G	NP9/CP8		<i>Cribrocentrum reticulatum</i>											
	131.83	144.06	SS	C	M	NP9/CP8		<i>Sphenolithus radians</i>											
	141.05	153.54	SS	A	G	NP9/CP8		<i>Chiastolithus sp.</i>											
	151.29	161.88	SS	A	M	NP8/CP6-CP7		<i>Nanotetina fulgens</i>											
	157.82	170.82	SS	A	M	NP6/CP5		<i>Chiastolithus gigas</i>											
	168.35	182.17	SS	A	M	NP5/CP4		<i>Nanotetina sp.</i>											
	177.65	192.57	SS	A	M/G	NP4/CP3 Cretaceous Rew		<i>Campylosphaera dela</i>											
	185.79	202.31	SS	A	G	NP3/CP2 Cretaceous Rew		<i>Chiastolithus consuetus</i>											
	193.25	212.03	SS	A	M/G	NP2/CP1b Cretaceous Rew		<i>Discoaster lodoensis</i>											
	203.69	224.73	SS	A	M/P	CC26/NC23		<i>Discoaster sublodensis</i>											
	212.96	236.38	SS	A	M/P	CC26/NC23		<i>Tribacchiatus orthostylus</i>											
								<i>Brarudosphaera sp.</i>											
								<i>Discoaster multitridatus</i>											
								<i>Rhombohedrons</i>											
								<i>Discoaster delicatus</i>											
								<i>Discoasters kuepferi</i>											
								<i>Discoaster dasypus</i>											
								<i>Tribacchiatus sp.</i>											
								<i>Discoaster spp.</i>											
								<i>Fasciularia spp.</i>											
								<i>Rhomboaster cuspidis</i>											

Table T7 (continued).

Table T8. Stratigraphic ranges and relative abundances for selected planktonic foraminifer taxa, Site 1262. (See table notes. Continued on next five pages.)

Table T8 (continued).

Table T8 (continued).

Hole, core, section, interval (cm)	Depth (mbsf)	Depth (mcd)	Preparation	Abundance	Preservation	Comment	Praemurica uncinata	Praemurica inconstans	Praemurica taurica	Globanomalina archeocompressa	Globocornus daubjergensis	Subbotina trilobulinoidea	Globanomalina planocompressa	Eoglobigerina edulisoides	Parasubbotina pseudobulloides	Biserial morphotypes	Parvularugoglobigerina rugulina	Guembelitria cretacea	Abathomphalus mayaroensis	Contractinaria contusa	Heterohelix spp.
208-																					
1262B-1H-1, 62–64	0.62	0.62	S A M																		
1262B-1H-3, 62–64	3.62	3.62	S A G																		
1262B-2H-1, 62–64	7.52	4.19	S A P																		
1262B-1H-4, 62–64	5.12	5.12	S A M																		
1262B-1H-5, 42–44	6.42	6.42	S A P																		
1262A-1H-1, 62–64	0.62	6.66	S A G																		
1262B-1H-CC	6.86	6.86	S A G																		
1262A-1H-2, 62–64	2.12	8.16	S A M																		
1262A-1H-3, 62–64	3.62	9.66	S A M																		
1262B-2H-CC	15.83	12.50	S A M																		
1262A-1H-5, 62–64	6.62	12.66	S A P																		
1262A-1H-CC	9.97	16.01	S A M																		
1262B-3H-CC	19.98	22.39	S A G																		
1262A-2H-CC	19.42	25.73	S A M																		
1262B-4H-CC	29.85	31.84	S A M																		
1262A-3H-CC	28.41	35.72	S A M																		
1262B-5H-CC	40.21	42.72	S A G																		
1262A-4H-CC	38.52	46.03	S A P																		
1262B-6H-CC	49.40	51.28	S B P																		
1262A-5H-CC	47.87	56.83	S R P																		
1262B-7H-CC	57.47	61.80	S B P																		
1262A-6H-CC	57.61	68.36	S B P																		
1262B-8H-CC	67.32	72.21	S A P																		
1262A-7H-CC	66.73	78.12	S A M																		
1262B-9H-CC	77.07	83.94	S B P																		
1262A-8H-CC	73.93	87.97	S A P																		
1262B-10H-CC	86.71	94.13	S R P																		
1262A-9H-CC	85.63	100.84	S A M																		
1262B-11H-CC	95.39	104.97	S A G																		
1262A-10H-CC	95.29	111.40	S A G																		
1262B-12H-CC	105.05	115.69	S A G																		
1262A-11H-CC	104.24	120.29	S A M																		
1262B-13H-CC	114.07	125.04	S A G																		
1262A-12H-CC	114.06	130.67	S A G																		
1262B-14H-CC	124.34	136.23	S A G																		
1262A-13H-4, 140–150	119.90	138.01	S A M																		
1262A-13H-5, 138–139	121.38	139.49	S A G																		
1262A-13H-6, 4–5	121.54	139.65	S A G–M																		

Table T8 (continued).

Hole, core, section, interval (cm)	Depth (mbsf)	Depth (mcd)	Preparation	Abundance	Preservation	Comment	Globorotalia truncatulinoides	Globocoenella inflata	Globorotalia crassaformis	Globorotalia tosaensis	Globocoenella puncticulata	Globocoenella conomicoza	Globocoenella sphericomioza	Globoturborotalita woodi	Globigerinoides obliquus	Dentoglobigerina altispira	Globiquadrina venezuelana	Sphaeroidinallopsis sp.	Sphaeroidinallopsis disjuncta	Globorotalia plesioturnida	Acarina spp.	Pulleniatina obliquiloculata	Acarina bullbrookii	Sphaeroidinallopsis seminulina	Sphaeroidinallopsis subdehisca	Globigerina nepenthes	Globigerina diuryi	Globocoenella micoza	Subbotina angaporides	Globorotaloides suteri	Acarina primitiva	Globigerinoides sanniovalua	Morozovella lensiformis	Morozovella aragonensis	Morozovella formosa
1262A-13H-6, 19–20	121.69	139.80	S R M																																
1262A-13H-6, 30–31	121.80	139.91	S R M																																
1262A-13H-6, 43–44	121.93	140.04	S R M																																
1262A-13H-6, 57–58	122.07	140.18	S R P																																
1262A-13H-6, 95–96	122.45	140.56	S A M																																
1262A-13H-CC	123.97	142.08	S A M																																
1262B-15H-CC	133.84	146.16	S A M																																
1262A-14H-CC	132.71	151.93	S A M																																
1262B-16H-CC	143.79	156.65	S A M																																
1262A-15H-CC	141.79	161.95	S A G																																
1262B-17H-CC	152.61	166.23	S A M																																
1262A-16H-CC	152.53	173.49	S R P																																
1262B-18H-CC	162.89	177.98	S A P																																
1262A-17H-CC	161.97	182.36	S R P																																
1262B-19H-CC	172.07	188.16	S A M-G																																
1262B-20H-CC	181.46	198.79	S A G																																
1262B-21H-CC	190.55	210.49	S A G																																
1262B-22H-1, 17.5–19.0	191.07	212.07	38 A G																																
1262B-22H-3, 47.0–48.5	193.13	214.12	38 A G																																
1262B-22H-3, 97.0–98.5	193.63	214.62	38 A G																																
1262B-22H-4, 37.5–39.0	194.54	215.52	38 A G																																
1262B-22H-4, 85.0–86.5	195.01	216.00	38 A G																																
1262B-22H-4, 114.0–115.5	195.30	216.29	38 A G																																
1262B-22H-4, 133.0–134.5	195.49	216.48	38 A G																																
1262B-22H-4, 143.0–144.5	195.59	216.58	38 A M-G																																
1262B-22H-CC	200.76	221.75	S A M																																
1262B-23H-CC	209.60	232.78	S A M-G																																

Notes: Preparation: S = >63-µm size fraction, 38 = >38-µm size fraction. Abundance: A = abundant, R = rare, B = barren. Preservation: G = good, M = moderate, P = poor. Occurrence: a = abundant, c = common, f = frequent, r = rare, b = barren.

Table T8 (continued).

Hole, core, section, interval (cm)	Depth (mbsf)	Depth (mcd)	Preparation	Abundance	Preservation	Comment	<i>Morozovella gracilis</i>	<i>Morozovella subbotinae</i>	<i>Chiloguembelina</i> spp.	<i>Morozovella marginodentata</i>	<i>Chiloguembelina midwayensis</i>	<i>Chiloguembelina wilcoxensis</i>	<i>Morozovella aequa</i>	<i>Acarinina soldadoensis</i>	<i>Subbotina patagonica</i>	<i>Morozovella acuta</i>	<i>Morozovella velascoensis</i>	<i>Subbotina velascoensis</i>	<i>Acarinina coalingensis</i>	<i>Acarinina wilcoxensis</i>	<i>Morozovella angulata</i>	<i>Globanomalina imitata</i>	<i>Globanomalina australiformis</i>	<i>Globanomalina chapmani</i>	<i>Morozovella occulta</i>	<i>Globanomalina pseudomenardii</i>	<i>Acarinina subsphaerica</i>	<i>Subbotina triangularis</i>	<i>Acarinina mckannai</i>	<i>Morozovella conicotruncata</i>	<i>Igorina brodermannii</i>	<i>Igorina tadjikistanensis</i>	<i>Subbotina cancellata</i>	<i>Igorina albeari</i>	<i>Globanomalina ehrenbergi</i>	<i>Globanomalina compressa</i>
1262A-13H-6, 19–20	121.69	139.80	S R M			Diminutive forms	f						r f r r																							
1262A-13H-6, 30–31	121.80	139.91	S R M			Diminutive forms	r						r r r r																							
1262A-13H-6, 43–44	121.93	140.04	S R M			Diminutive forms	r						r c r f																							
1262A-13H-6, 57–58	122.07	140.18	S R P			Micronodules	r f f						c c																							
1262A-13H-6, 95–96	122.45	140.56	S A M				r						f c																							
1262A-13H-CC	123.97	142.08	S A M				c						r f f																							
1262B-15H-CC	133.84	146.16	S A M				r						r f f																							
1262A-14H-CC	132.71	151.93	S A M										f c																							
1262B-16H-CC	143.79	156.65	S A M										r f f																							
1262A-15H-CC	141.79	161.95	S A G										r r r r																							
1262B-17H-CC	152.61	166.23	S A M										r r r r																							
1262A-16H-CC	152.53	173.49	S R P										r r r r																							
1262B-18H-CC	162.89	177.98	S A P										r r r r																							
1262A-17H-CC	161.97	182.36	S R P										r r r r																							
1262B-19H-CC	172.07	188.16	S A M–G										r r r r																							
1262B-20H-CC	181.46	198.79	S A G										r r r r																							
1262B-21H-CC	190.55	210.49	S A G										r r r r																							
1262B-22H-1, 17.5–19.0	191.07	212.07	38 A G										r r r r																							
1262B-22H-3, 47.0–48.5	193.13	214.12	38 A G										r r r r																							
1262B-22H-3, 97.0–98.5	193.63	214.62	38 A G										r r r r																							
1262B-22H-4, 37.5–39.0	194.54	215.52	38 A G										r r r r																							
1262B-22H-4, 85.0–86.5	195.01	216.00	38 A G										r r r r																							
1262B-22H-4, 114.0–115.5	195.30	216.29	38 A G										r r r r																							
1262B-22H-4, 133.0–134.5	195.49	216.48	38 A G										r r r r																							
1262B-22H-4, 143.0–144.5	195.59	216.58	38 A M–G										r r r r																							
1262B-22H-CC	200.76	221.75	S A M										r r r r																							
1262B-23H-CC	209.60	232.78	S A M–G										r r r r																							
						Reworking																														
						Reworking																														

Table T8 (continued).

Hole, core, section, interval (cm)	Depth (mbsf)	Depth (mcd)	Preparation	Abundance	Preservation	Comment	<i>Praemurica uncinata</i>	<i>Praemurica inconstans</i>	<i>Praemurica taurica</i>	<i>Globanomalia archeocompressa</i>	<i>Globoconus daubjergensis</i>	<i>Subbotina trilobulinoidea</i>	<i>Globanomalia planocompressa</i>	<i>Eoglobigerina edulisoides</i>	<i>Parasubbotina pseudobulloides</i>	<i>Biserial morphotypes</i>	<i>Parvularugoglobigerina rugulina</i>	<i>Guembelitria cretacea</i>	<i>Abathomphalus mayaroensis</i>	<i>Conchotrotina contusa</i>	Heterogeneity spp.
1262A-13H-6, 19–20	121.69	139.80	S R M			Diminutive forms															
1262A-13H-6, 30–31	121.80	139.91	S R M			Diminutive forms															
1262A-13H-6, 43–44	121.93	140.04	S R M			Diminutive forms															
1262A-13H-6, 57–58	122.07	140.18	S R P			Micronodules															
1262A-13H-6, 95–96	122.45	140.56	S A M																		
1262A-13H-CC	123.97	142.08	S A M																		
1262B-15H-CC	133.84	146.16	S A M																		
1262A-14H-CC	132.71	151.93	S A M																		
1262B-16H-CC	143.79	156.65	S A M																		
1262A-15H-CC	141.79	161.95	S A G																		
1262B-17H-CC	152.61	166.23	S A M																		
1262A-16H-CC	152.53	173.49	S R P																		
1262B-18H-CC	162.89	177.98	S A P																		
1262A-17H-CC	161.97	182.36	S R P																		
1262B-19H-CC	172.07	188.16	S A M–G																		
1262B-20H-CC	181.46	198.79	S A G																		
1262B-21H-CC	190.55	210.49	S A G																		
1262B-22H-1, 17.5–19.0	191.07	212.07	38 A G																		
1262B-22H-3, 47.0–48.5	193.13	214.12	38 A G																		
1262B-22H-3, 97.0–98.5	193.63	214.62	38 A G																		
1262B-22H-4, 37.5–39.0	194.54	215.52	38 A G																		
1262B-22H-4, 85.0–86.5	195.01	216.00	38 A G																		
1262B-22H-4, 114.0–115.5	195.30	216.29	38 A G	Reworking																	
1262B-22H-4, 133.0–134.5	195.49	216.48	38 A G																		
1262B-22H-4, 143.0–144.5	195.59	216.58	38 A M–G																		
1262B-22H-CC	200.76	221.75	S A M																		
1262B-23H-CC	209.60	232.78	S A M–G																		

Table T9. Occurrences of selected benthic foraminifer taxa, Site 1262. (Continued on next three pages.)

Hole, core, section, interval (cm)	Depth (mbsf)	Depth (mcd)	Abundance	Preservation	Paleodepth	<i>Abyssammina poagi</i>	<i>Abyssammina quadrata</i>	<i>Alabamina dissonata</i>	<i>Alabamina weddellensis</i>	<i>Ammodiscus</i> sp.	<i>Angulogerina szajinochae</i>	<i>Anomalinoides acutus</i>	<i>Anomalinoides praecutus</i> group	<i>Anomalinoides spissiformis</i>	<i>Aragonia aragonensis</i>	<i>Aragonia velascoensis</i>	<i>Bathyiphon</i> sp.	<i>Bolivinoides</i> sp. (small)	<i>Bulimina kugleri</i>	<i>Bulimina semicostata</i>	<i>Bulimina simplex</i>	<i>Bulimina thanetensis</i>	<i>Bulimina trinitatis</i>	<i>Bulimina velascoensis</i>	<i>Buliminella</i> spp.	
208-																										
1262B-1H-1, 0–2	0.00	0.00	F E	LA					x																	
1262B-1H-CC	6.86	6.86	F G	LA					x																	
1262A-1H-CC	9.97	16.01	F G	LA					x																	
1262A-2H-CC	19.42	25.73	F G	LA					x																	
1262A-3H-CC	28.41	35.72	F G	LA					x																	
1262A-4H-CC	38.52	46.03	C M	LA					x																	
1262A-5H-CC	47.87	56.83	B	?																						
1262A-6H-CC	57.61	68.36	B	?																						
1262A-7H-CC	66.73	78.12	C P	DT												x										
1262B-9H-CC	77.07	83.94	B	?																					x	
1262A-8H-CC	73.93	87.97	C M	DT	x x x						x x							x	x	x						
1262B-10H-CC	86.71	94.13	F G	LA	x x x						x x x							x	x	x	x					
1262A-9H-CC	85.63	100.84	F M	LA	x x						x x x															
1262B-11H-CC	95.39	104.97	R G	LA	x x x						x x x															
1262A-10H-CC	95.29	111.40	R G	LA	x x				x		x x							x	x	x				x*		
1262B-12H-CC	105.05	115.69	R G	LA	x x						x x							x	x	x	x					
1262C-2H-6, 35–36	107.35	117.14	C G	LA	xx x						x x											x	x			
1262A-11H-CC	104.24	120.29	R G	LA	x x						x x															
1262B-13H-CC	114.07	125.04	R G	LA	x x						x x															
1262A-12H-CC	114.06	130.67	R G	LA	x x						x x															
1262C-4H-CC	126.90	132.41	F G	LA	x x						x x							x x	x x	x x	x x					
1262B-14H-CC	124.34	136.23	R G	LA	x x						x x							x x	x x	x x	x x					
1262A-13H-4, 140–150	119.90	138.01	R G	LA	x xx						x x							x x	x x	x x	x x					
1262A-13H-6, 46–47	120.46	138.57	R G	LA	x x						x x							x x	x x	x x	x x					
1262A-13H-5, 94–95	120.94	139.05	R G	LA	x x						x x							x x	x x	x x	x x					
1262A-13H-5, 138–139	121.38	139.49	R G	LA	x x						x x							x x	x x	x x	x x					
1262A-13H-6, 4–5	121.54	139.65	R G	LA	x x						x x							x x	x x	x x	x x					
1262A-13H-6, 19–20	121.69	139.80	C G	LA	xx xx						x x							x x	x x	x x	x x					
1262A-13H-6, 30–31	121.80	139.91	R G	LA	x x						x x							x x	x x	x x	x*					
1262A-13H-6, 43–44	121.93	140.04	B	?																						
1262A-13H-6, 57–58	122.07	140.18	F G	LA	x x						x x							x x	x x	x x	x x				x	
1262A-13H-6, 95–96	122.45	140.56	F G	LA	x x						x x							x x	x x	x x	x x				x	
1262A-13H-CC	123.97	142.08	F M	LA	x x				x		x x							x x	x x	x x	x x				x	
1262C-5H-CC	131.83	144.06	C G	LA	x x				x		x x							x x	x x	x x	x x				x x	
1262B-15H-CC	133.84	146.16	R G	LA	x x				x		x x							x x	x x	x x	x x				x x	
1262A-14H-CC	132.71	151.93	F G	LA	x x				x		x x							x x	x x	x x	x x				x x	
1262B-16H-CC	143.79	156.65	F G	LA	x x				x		x x							x x	x x	x x	x x				x x	
1262A-15H-CC	141.79	161.95	F G	LA	x x				x		x x							x x	x x	x x	x x				x x	
1262B-17H-CC	152.61	166.23	F G	LA/UA														x x	x x	x x	x x				x x	
1262A-16H-CC	152.53	173.49	A P	DT					x								x x	x x	x x	x x				x x		
1262C-9H-1, 147–149	159.97	173.79	C M	DT	x												x x	x x	x x	x x				x x		
1262B-18H-CC	162.89	177.98	F G	LA/UA	x x												x x	x x	x x	x x				x x		
1262A-17H-CC	161.97	182.36	A P	DT					x								x x	x x	x x	x x				x x		
1262B-19H-CC	172.07	188.16	R G	LA/UA													x x	x x	x x	x x				x x		
1262B-20H-CC	181.46	198.79	F G	UA													x x	x x	x x	x x				x x		
1262B-21H-CC	190.55	210.49	F G	UA													x x	x x	x x	x x				x x		
1262C-12H-CC	193.25	212.03	F G	UA					x								x x	x x	x x	x x						
1262B-22H-4, 134–135	195.51	216.50	F G	UA												x x	x x	x x	x x							
1262B-22H-CC	200.76	221.75	F G	UA					x							x x	x x	x x	x x				x x			
1262C-13H-CC	203.69	224.73	R G	UA					x							x x	x x	x x	x x				x x			
1262B-23H-CC	209.60	232.78	F G	UA					x							x x	x x	x x	x x				x x			
1262C-14H-CC	212.96	236.38	R G	UA					x							x x	x x	x x	x x				x x			

Notes: Abundance: A = abundant, C = common, F = few, R = rare, B = barren. Preservation: E = excellent, G = good, M = moderate, P = poor. Paleodepth: LA = lower abyssal, DT = downslope transport, UA = upper abyssal, ? = unknown. x = present, xx = dominant species, * = reworked.

Table T9 (continued).

Hole, core, section, interval (cm)	Depth (mbsf)	Depth (mcd)	Abundance	Preservation	Paleodepth	<i>Cibicidoides dayi</i>	<i>Cibicidoides mundulus</i>	<i>Cibicidoides eocanensis</i>	<i>Cibicidoides hyphalus</i>	<i>Cibicidoides praemundulus</i>	<i>Cibicidoides velascoensis</i>	<i>Cibicidoides wuellestorfi</i>	<i>Clavulinoides amorpha</i>	<i>Clavulinoides trilatera</i>	<i>Clinapertina complanata</i>	<i>Clinapertina inflata</i>	<i>Clinapertina subplanispira</i>	<i>Eggerella bradyi</i>	<i>Epistomina exigua</i>	<i>Furcina sp.</i>	<i>Globocaudilina subglobosa</i>	<i>Gaudryina pyramidata</i>	<i>Glomospira spp.</i>	<i>Gyroidinoides acutus</i>	<i>Gyroidinoides beisseli</i>
1262B-1H-1, 0–2	0.00	0.00	F	E	LA		x					x						x			x		x		x
1262B-1H-CC	6.86	6.86	F	G	LA		x					x						x			x		x		x
1262A-1H-CC	9.97	16.01	F	G	LA		x					x						x			x		x		x
1262A-2H-CC	19.42	25.73	F	G	LA		x					x						x			x		x		x
1262A-3H-CC	28.41	35.72	F	G	LA		x					x						x			x		x		x
1262A-4H-CC	38.52	46.03	C	M	LA		x											x			x		x		x
1262A-5H-CC	47.87	56.83	B		?																				
1262A-6H-CC	57.61	68.36	B		?																				
1262A-7H-CC	66.73	78.12	C	P	DT		x											x			x		x		x
1262B-9H-CC	77.07	83.94	B		?													x			x		x		x
1262A-8H-CC	73.93	87.97	C	M	DT		x					x						x			x		x		x
1262B-10H-CC	86.71	94.13	F	G	LA		x					x						x			x		x		x
1262A-9H-CC	85.63	100.84	F	M	LA							x						x			x		x		x
1262B-11H-CC	95.39	104.97	R	G	LA							x						x			x		x		x
1262A-10H-CC	95.29	111.40	R	G	LA							x						x			x		x		x
1262B-12H-CC	105.05	115.69	R	G	LA							x						x			x		x		x
1262C-2H-6, 35–36	107.35	117.14	C	G	LA							x					x	x		x		x		x	
1262A-11H-CC	104.24	120.29	R	G	LA							x					x	x		x		x		x	
1262B-13H-CC	114.07	125.04	R	G	LA							x					x	x		x		x		x	
1262A-12H-CC	114.06	130.67	R	G	LA							x					x	x		x		x		x	
1262C-4H-CC	126.90	132.41	F	G	LA							x					x	x		x		x		x	
1262B-14H-CC	124.34	136.23	R	G	LA							x					x	x		x		x		x	
1262A-13H-4, 140–150	119.90	138.01	R	G	LA							x					x	x		x		x		x	
1262A-13H-5, 46–47	120.46	138.57	R	G	LA							x					x	x		x		x		x	
1262A-13H-5, 94–95	120.94	139.05	R	G	LA							x					x	x		x		x		x	
1262A-13H-5, 138–139	121.38	139.49	R	G	LA							x			x*		x	x		x		x		x	
1262A-13H-6, 4–5	121.54	139.65	R	G	LA							x			x*		x	x		x		x		x	
1262A-13H-6, 19–20	121.69	139.80	C	G	LA							x			x*		x	x		x		x		x	
1262A-13H-6, 30–31	121.80	139.91	R	G	LA							x			x*		x	x		x		x		x	
1262A-13H-6, 43–44	121.93	140.04	B		?																				
1262A-13H-6, 57–58	122.07	140.18	F	G	LA							x			x		x	x		x		x		x	
1262A-13H-6, 95–96	122.45	140.56	F	G	LA							x			x		x	x		x		x		x	
1262A-13H-CC	123.97	142.08	F	M	LA							x	x		x		x	x		x		x		x	
1262C-5H-CC	131.83	144.06	C	G	LA							x	x		x		x	x		x		x		x	
1262B-15H-CC	133.84	146.16	R	G	LA							x	x		x		x	x		x		x		x	
1262A-14H-CC	132.71	151.93	F	G	LA	x						x	x		x		x	x		x		x		x	
1262B-16H-CC	143.79	156.65	F	G	LA	x						x	x		x		xx					x		x	
1262A-15H-CC	141.79	161.95	F	G	LA	x						x	x		x		x	x		x		x		x	
1262B-17H-CC	152.61	166.23	F	G	LA/UA	x						x	x		xx		xx					x		x	
1262A-16H-CC	152.53	173.49	A	P	DT	x						x	x		x		x	x		x		x		x	
1262C-9H-1, 147–149	159.97	173.79	C	M	DT	x						x	x		x		x	x		x		x		x	
1262B-18H-CC	162.89	177.98	F	G	LA/UA	x						x	x		x		x	x		x		x		x	
1262A-17H-CC	161.97	182.36	A	P	DT	x						x	x		x		x	x		x		x		x	
1262B-19H-CC	172.07	188.16	R	G	LA/UA							x			x		x	x		x		x		x	
1262B-20H-CC	181.46	198.79	F	G	UA															x					
1262B-21H-CC	190.55	210.49	F	G	UA															x					
1262C-12H-CC	193.25	212.03	F	G	UA							x			x		x	x		x		x		x	
1262B-22H-4, 134–135	195.51	216.50	F	G	UA							x			x		x	x		x		x		x	
1262B-22H-CC	200.76	221.75	F	G	UA							x			x		x	x		x		x		x	
1262C-13H-CC	203.69	224.73	R	G	UA							x	x		x		x	x		x		x		x	
1262B-23H-CC	209.60	232.78	F	G	UA							x			x		x	x		x		x		x	
1262C-14H-CC	212.96	236.38	R	G	UA							x	x		x		x	x		x		x		x	

Table T9 (continued).

Table T9 (continued).

Hole, core, section, interval (cm)	Depth (mbsf)	Depth (mcd)	Abundance	Preservation	Paleodepth	<i>Præbuliminia reussi</i>	<i>Pullenia coryelli</i>	<i>Pullenia cretacea</i>	<i>Pullenia</i> spp.	<i>Quadratobuliminella</i> sp.	<i>Rectobuliminia carpentierae</i>	<i>Rhizammina</i> spp.	<i>Siphogenerinoides brevispinosa</i>	<i>Siphotextularia catenulata</i>	<i>Spiriplecammina dentata</i>	<i>Spiriplecammina spectabilis</i>	<i>Stainforthia complanata</i>	<i>Stensioeina beccariiformis</i>	<i>Stilostomellid</i> taxa	<i>Tappanina selmensis</i>	<i>Tritaxia havanensis</i>	<i>Trochammina globigeriniformis</i>	Unilocular taxa	<i>Uvigerina</i> spp.	<i>Vulvulina spinosa</i>
1262B-1H-1, 0–2	0.00	0.00	F	E	LA				x												x	x			
1262B-1H-CC	6.86	6.86	F	G	LA				x											x	x	x	x		
1262A-1H-CC	9.97	16.01	F	G	LA				x											x		x	x		
1262A-2H-CC	19.42	25.73	F	G	LA				x											x		x	x		
1262A-3H-CC	28.41	35.72	F	G	LA				x											x		x	x		
1262A-4H-CC	38.52	46.03	C	M	LA				x											x	x	x	x	x	
1262A-5H-CC	47.87	56.83	B		?																				
1262A-6H-CC	57.61	68.36	B		?																				
1262A-7H-CC	66.73	78.12	C	P	DT				x											x	x	x	x	x	
1262B-9H-CC	77.07	83.94	B		?															x		x	x	x	
1262A-8H-CC	73.93	87.97	C	M	DT															x		x	x	x	
1262B-10H-CC	86.71	94.13	F	G	LA															x	x	x	x	x	
1262A-9H-CC	85.63	100.84	F	M	LA															x	x	x	x	x	
1262B-11H-CC	95.39	104.97	R	G	LA															x	x	x	x	x	
1262A-10H-CC	95.29	111.40	R	G	LA															x	x	x	x	x	
1262B-12H-CC	105.05	115.69	R	G	LA															x	x	x	x	x	
1262C-2H-6, 35–36	107.35	117.14	C	G	LA																				
1262A-11H-CC	104.24	120.29	R	G	LA															x	x	x	x	x	
1262B-13H-CC	114.07	125.04	R	G	LA															x	x	x	x	x	
1262A-12H-CC	114.06	130.67	R	G	LA															x	x	x	x	x	
1262C-4H-CC	126.90	132.41	F	G	LA															x	x	x	x	x	
1262B-14H-CC	124.34	136.23	R	G	LA															x	x	x	x	x	
1262A-13H-4, 140–150	119.90	138.01	R	G	LA															x	x	x	x	x	
1262A-13H-5, 46–47	120.46	138.57	R	G	LA															x	x	x	x	x	
1262A-13H-5, 94–95	120.94	139.05	R	G	LA															x	x	x	x	x	
1262A-13H-5, 138–139	121.38	139.49	R	G	LA															x	x	x	x	x	
1262A-13H-6, 4–5	121.54	139.65	R	G	LA															x	x	x	x	x	
1262A-13H-6, 19–20	121.69	139.80	C	G	LA															x	x	x	x	x	
1262A-13H-6, 30–31	121.80	139.91	R	G	LA															x	x	x	x	x	
1262A-13H-6, 43–44	121.93	140.04	B		?																				
1262A-13H-6, 57–58	122.07	140.18	F	G	LA				x											x	x	x	x	x	
1262A-13H-6, 95–96	122.45	140.56	F	G	LA				x										x	x	x	x	x		
1262A-13H-CC	123.97	142.08	F	M	LA				x										x	x	x	x	x		
1262C-5H-CC	131.83	144.06	C	G	LA				x										x	x	x	x	x		
1262B-15H-CC	133.84	146.16	R	G	LA				x										x	x	x	x	x		
1262A-14H-CC	132.71	151.93	F	G	LA				x										x	x	x	x	x		
1262B-16H-CC	143.79	156.65	F	G	LA				x										x	x	x	x	x		
1262A-15H-CC	141.79	161.95	F	G	LA														x	x	x	x	x		
1262B-17H-CC	152.61	166.23	F	G	LA/UA				x										x	x	x	x	x		
1262A-16H-CC	152.53	173.49	A	P	DT				x										x	x	x	x	x		
1262C-9H-1, 147–149	159.97	173.79	C	M	DT				x										x	x	x	x	x		
1262B-18H-CC	162.89	177.98	F	G	LA/UA				x										x	x	x	x	x		
1262A-17H-CC	161.97	182.36	A	P	DT				x										x	x	x	x	x		
1262B-19H-CC	172.07	188.16	R	G	LA/UA				x										x	x	x	x	x		
1262B-20H-CC	181.46	198.79	F	G	UA														x	x	x	x	x		
1262B-21H-CC	190.55	210.49	F	G	UA														x	x	x	x	x		
1262C-12H-CC	193.25	212.03	F	G	UA				x										x	x	x	x	x		
1262B-22H-4, 134–135	195.51	216.50	F	G	UA				x										x	x	x	x	x		
1262B-22H-CC	200.76	221.75	F	G	UA				x										x	x	x	x	x		
1262C-13H-CC	203.69	224.73	R	G	UA				x	x	x								x	x	x	x	x		
1262B-23H-CC	209.60	232.78	F	G	UA				x	x	x								x	x	x	x	x		
1262C-14H-CC	212.96	236.38	R	G	UA				x	x	x								x	x	x	x	x		

Table T10. Magnetostratigraphic age-depth tie points, Site 1262.

Chron	Age (Ma)		Top		Bottom	
	1	2	Hole, core, section, interval (cm)	Depth (mbsf) (mcd)	Hole, core, section, interval (cm)	Depth (mbsf) (mcd)
208-						
C1n (o)	0.781	0.780	1262B-1H-5, 15	6.15	6.15	1262B-2H-2, 140
C1r.1n (y)	0.988	0.990	1262B-2H-2, 140	9.80	6.47	1262A-1H-2, 5
C1r.1n (o)	1.072	1.070	1262A-1H-2, 45	1.95	7.99	1262B-2H-4, 10
Cobb Mountain (y)	1.173	1.201	1262A-1H-2, 135	2.85	8.89	1262B-2H-4, 100
Cobb Mountain (o)	1.185	1.211	1262A-1H-3, 5	3.05	9.09	1262B-2H-4, 135
C2n (y)	1.785	1.770	1262B-3H-1, 115	13.05	15.46	1262B-3H-1, 125
C2n (o)	1.942	1.950	1262B-3H-2, 105	14.45	16.86	1262B-3H-2, 115
C2An.1n (y)	2.582	2.581	1262A-2H-6, 90	17.87	24.18	1262B-4H-1, 100
C2An.3n (o)	3.596	3.580	1262A-3H-7, 60	28.10	35.41	1262A-4H-1, 60
C13n (y)	33.058	33.058	1262B-9H-2, 90	69.80	76.67	1262A-7H-6, 125
C13n (o)	33.545	33.545	1262B-9H-4, 15	72.05	78.92	1262B-9H-4, 30
C23n (y)	50.778	50.778	1262A-9H-2, 30	77.80	93.01	1262A-9H-2, 60
C24n (o)	53.347	53.347	1262C-3H-1, 145	110.45	120.42	1262C-3H-2, 5
C25n (y)	55.904	55.904	1262B-16H-5, 45	140.35	153.21	1262B-16H-5, 55
C25n (o)	56.391	56.391	1262A-15H-5, 5	139.05	159.21	1262A-15H-5, 30
C26n (y)	57.554	57.554	1262A-16H-6, 45	150.45	171.41	1262B-18H-3, 95
C26n (o)	57.911	57.911	1262B-18H-4, 65	158.05	173.14	1262C-9H-1, 125
C27n (y)	60.920	60.920	1262B-20H-5, 20	178.10	195.43	1262B-20H-5, 40
C27n (o)	61.276	61.276	1262B-20H-6, 110	180.50	197.83	1262C-11H-3, 115
C28n (y)	62.499	62.499	1262B-21H-3, 25	184.65	204.59	1262B-21H-3, 40
C28n (o)	63.634	63.634	1262C-12H-5, 105	191.05	209.83	1262C-12H-5, 125
C29n (y)	63.976	63.976	1262C-12H-6, 70	192.20	210.98	1262C-12H-6, 80
C30n (y)	65.578	65.578	1262C-13H-7, 75	203.25	224.29	1262B-23H-1, 70
						201.10 224.28

Notes: o = old end of chron, y = young end of chron. 1 = ages as in Lourens et al. (in press), 2 = ages as in Cande and Kent (1995).

Table T11. Composition of headspace gases, Site 1262.

Hole, core, section, interval (cm)	Depth (mcd)	C ₁ /C ₂	C ₁ (ppm)	C ₂ (ppm)	C ₂₌ (ppm)	C ₃ (ppm)	C ₃₌ (ppm)
208-							
1262B-1H-4, 0-5	4.5	7.521	54.9	7.3	6.6	8.3	7.3
1262A-1H-6, 0-5	13.5		2.0	0.0	0.0	0.0	0.0
1262A-2H-6, 0-5	23.3		1.8	0.0	0.0	0.0	0.0
1262A-3H-6, 0-5	33.8		1.8	0.0	0.0	0.0	0.0
1262A-4H-6, 0-5	43.5		1.9	0.0	0.0	0.0	0.0
1262A-5H-6, 0-5	54.5		1.7	0.0	0.0	0.0	0.0
1262A-6H-6, 0-5	65.8		1.8	0.0	0.0	0.0	0.0
1262A-7H-6, 0-5	75.9		1.8	0.0	0.0	0.0	0.0
1262A-8H-3, 0-5	83.5		1.8	0.0	0.0	0.0	0.0
1262A-9H-6, 0-5	98.7		2.0	0.0	0.0	0.0	0.0
1262A-11H-6, 0-5	118.6		1.9	0.0	0.0	0.0	0.0
1262A-12H-6, 0-5	128.6		2.0	0.0	0.0	0.0	0.0
1262A-13H-5, 0-5	138.1		1.8	0.0	0.0	0.0	0.0
1262A-14H-6, 0-5	150.2		2.0	0.0	0.0	0.0	0.0
1262A-15H-6, 0-5	160.7		1.9	0.0	0.0	0.0	0.0
1262A-16H-6, 0-5	171.0	10.722	38.6	3.6	3.4	0.0	0.0
1262A-17H-6, 0-5	179.9	11.990	124.7	10.4	10.0	9.0	8.4
1262B-19H-4, 0-5	183.0		2.2	0.0	0.0	0.0	0.0
1262B-20H-6, 0-5	196.7		2.0	0.0	0.0	0.0	0.0
1262C-11H-6, 0-5	201.5		2.1	0.0	0.0	0.0	0.0
1262C-12H-6, 0-5	210.3		2.0	0.0	0.0	0.0	0.0
1262B-23H-6, 0-5	231.1		2.1	0.0	0.0	0.0	0.0
1262C-14H-6, 0-5	233.9		1.9	0.0	0.0	0.0	0.0

Table T12. Interstitial water analyses, Site 1262.

Hole, core, section, interval (cm)	Depth (mcd)	pH	Alkalinity (mM)	Salinity	Cl (mM)	SO ₄ (mM)	Na (mM)	K (mM)	Ca (mM)	Mg (mM)	B (µM)	Fe (µM)	Mn (µM)	Li (µM)	Ba (µM)	Sr (µM)	Si (µM)	Zn (µM)
208-																		
1262B-1H-3, 145–150	4.5	7.53	2.58	35.0	569	22.5	463.7	10.8	8.5	53.0	468.6	0.2	0.1	28.7	0.6	107.0	385.4	0.9
1262A-1H-5, 145–150	13.5	7.60	2.63	35.0	565	23.2	467.6	10.8	9.2	53.6	462.8	0.1	0.5	26.0	2.7	134.2	280.3	0.7
1262A-2H-5, 142–147	23.2	7.52	2.46	35.0	567	23.7	470.7	10.8	9.6	55.0	527.5	0.4	2.6	29.1	1.1	167.9	253.0	0.8
1262A-3H-5, 145–150	33.8	7.48	2.45	35.0	571	22.7	465.8	10.4	9.8	53.9	513.8	0.1	2.8	29.9	1.9	184.7	243.7	2.9
1262A-4H-5, 145–150	43.5	7.58	2.36	35.0	527	22.7	473.6	10.5	10.1	53.8	523.9	0.1	1.7	30.6	2.5	186.6	238.5	1.0
1262A-5H-5, 145–150	54.4	7.53	2.88	35.0	561	23.2	458.1	10.5	11.7	46.7	742.4	0.4	1.7	31.6	1.6	197.1	368.6	1.4
1262A-6H-5, 140–150	65.7	7.53	2.48	35.0	567	22.3	464.6	10.3	11.9	48.4	757.1	0.1	0.7	33.8	1.3	190.2	361.0	1.0
1262A-7H-5, 140–150	75.8	7.52	2.43	35.0	567	22.6	467.0	10.6	10.8	52.8	627.0	0.1	0.2	32.9	1.8	175.0	284.4	1.3
1262A-9H-5, 145–150	98.7	7.55	2.52	35.0	573	21.4	471.4	10.2	12.3	50.5	582.0	0.1	0.6	33.9	0.7	172.4	386.9	1.6
1262B-11H-5, 145–150	103.4	7.46	2.49	35.5	571	22.1	461.7	10.3	11.8	48.2	499.2	0.0	0.4	34.5	0.4	165.8	302.5	0.9
1262A-11H-5, 140–150	118.5	7.47	2.45	35.0	572	22.0	460.7	10.3	12.5	47.4	495.9	0.0	0.3	35.9	0.3	161.3	350.8	1.1
1262A-12H-5, 140–150	128.5	7.49	2.45	37.0	569	22.4	463.7	10.5	12.6	47.0	509.9	0.4	0.2	35.7	0.9	160.4	372.8	1.1
1262A-13H-4, 140–150	138.0	7.57	2.49	34.0	578	21.8	465.3	10.3	13.1	46.2	499.3	0.2	0.1	36.2	0.8	157.6	379.8	1.1
1262A-14H-5, 140–150	150.1	7.48	2.48	34.0	568	23.4	466.6	10.2	13.6	46.1	485.4	0.3	0.3	37.3	0.3	155.3	435.0	0.7
1262A-15H-5, 140–150	160.6	7.46	2.58	34.0	574	21.2	459.8	10.3	13.4	45.3	507.4	0.1	0.2	37.4	0.4	152.5	393.0	1.2
1262A-16H-5, 140–150	170.9	7.46	2.40	34.0	577	22.5	458.4	10.2	14.0	43.8	517.3	0.2	0.2	37.9	0.3	155.3	436.8	0.8
1262B-19H-3, 140–150	182.9	7.41	2.47	35.0	572	23.3	461.9	10.2	14.8	43.0	497.9	0.2	0.2	38.6	0.3	148.6	368.0	0.8
1262C-11H-5, 140–150	201.4	7.45	2.21	35.0	550	22.8	464.7	9.9	15.9	42.7	543.6	0.0	0.1	37.2	0.2	145.8	364.1	0.8
1262C-12H-5, 140–150	210.2	7.43	2.54	35.0	574	23.2	457.4	9.6	16.0	41.0	613.0	0.1	0.2	39.9	0.3	151.3	432.0	1.1
1262B-23H-5, 140–150	231.0	7.39	2.26	34.0	502	22.9	471.8	9.9	17.6	40.4	530.9	0.1	0.5	38.2	0.0	148.1	411.8	1.4

Table T13. Sedimentary calcium carbonate, total carbon, and organic carbon concentrations, Site 1262. ([See table notes](#). Continued on next page.)

Hole, core, section, interval (cm)	Depth (mcd)	Inorganic carbon (wt%)*	CaCO ₃ (wt%)*	Total carbon (wt%) [†]	Organic carbon (wt%) [‡]
208-					
1262A-1H-1, 72-74	6.76	5.6	46.5	5.5	0.0
1262A-1H-3, 72-74	9.76	10.7	89.0	10.5	0.0
1262A-1H-5, 72-74	12.76	10.8	90.1	10.6	0.0
1262A-1H-5, 145-150	13.49	11.3	93.9	11.2	0.0
1262A-1H-7, 72-74	15.76	10.8	89.7	10.6	0.0
1262A-2H-1, 72-74	16.53	10.9	90.7	10.7	0.0
1262A-2H-3, 72-74	19.53	11.2	92.9	11.0	0.0
1262A-2H-5, 72-74	22.53	11.2	92.9	11.2	0.0
1262A-2H-5, 142-147	23.23	10.7	89.5	11.0	0.3
1262A-3H-1, 72-74	27.03	10.6	88.3	10.3	0.0
1262A-3H-3, 72-74	30.03	10.8	89.6	10.7	0.0
1262A-3H-5, 72-74	33.03	10.5	87.6	10.7	0.2
1262A-3H-5, 145-150	33.76	11.2	93.6	10.3	0.0
1262A-3H-7, 72-73	35.53	11.1	92.5	10.8	0.0
1262A-4H-1, 72-73	36.73	9.9	82.4	9.4	0.0
1262A-4H-3, 72-73	39.73	10.9	90.4	10.6	0.0
1262A-4H-5, 72-73	42.73	11.1	92.8	10.9	0.0
1262A-4H-5, 145-150	43.46	11.1	92.4	10.8	0.0
1262A-5H-1, 72-74	47.68	2.7	22.3	2.8	0.1
1262A-5H-3, 72-74	50.68	0.9	7.3	0.9	0.0
1262A-5H-5, 72-74	53.68	0.1	0.6	0.1	0.0
1262A-5H-5, 145-150	54.41	0.1	0.5	0.0	0.0
1262A-6H-1, 72-74	58.97	0.1	0.9	0.1	0.0
1262A-6H-3, 72-74	61.97	0.1	1.1	0.1	0.0
1262A-6H-5, 72-74	64.97	0.1	0.8	0.0	0.0
1262A-6H-5, 140-150	65.65	0.1	0.7	0.0	0.0
1262A-7H-1, 78-79	69.17	5.1	42.4	5.1	0.0
1262A-7H-3, 72-74	72.11	8.6	71.5	8.6	0.0
1262A-7H-5, 72-74	75.11	9.5	79.2	9.2	0.0
1262A-7H-5, 140-150	75.79	9.5	79.5	9.8	0.2
1262A-8H-1, 72-74	81.26	1.0	8.3	0.8	0.0
1262A-8H-2, 145-150	83.41	0.0	0.3	0.0	0.0
1262A-8H-3, 72-74	84.18	0.1	0.8	0.0	0.0
1262A-8H-5, 72-74	85.89	0.1	0.7	0.1	0.0
1262A-9H-1, 72-74	91.93	6.1	50.7	5.9	0.0
1262A-9H-3, 72-74	94.93	10.7	89.4	10.4	0.0
1262A-9H-5, 72-74	97.93	11.1	92.8	11.0	0.0
1262A-9H-5, 145-150	98.66	9.5	79.1	9.7	0.2
1262A-10H-1, 72-74	102.33	11.3	94.3	11.3	0.0
1262B-11H-5, 140-150	103.38	11.5	95.5	11.5	0.0
1262A-10H-3, 72-74	105.33	11.4	95.0	11.0	0.0
1262A-10H-5, 72-74	108.33	11.6	96.5	11.3	0.0
1262A-11H-1, 72-74	111.77	11.5	95.6	11.4	0.0
1262A-11H-3, 72-74	114.77	11.3	94.1	11.2	0.0
1262A-11H-5, 72-74	117.77	11.0	91.4	11.0	0.0
1262A-11H-5, 145-150	118.50	10.9	91.1	10.9	0.0
1262A-12H-1, 72-74	121.83	10.9	91.1	10.8	0.0
1262A-12H-3, 72-74	124.83	10.8	90.1	11.1	0.2
1262A-12H-5, 72-74	127.83	11.2	93.2	11.1	0.0
1262A-12H-5, 140-150	128.51	11.1	92.2	11.5	0.4
1262A-13H-4, 140-150	138.01	11.1	92.6	11.1	0.0
1262A-13H-5, 1-1	138.12	11.1	92.5	ND	ND
1262A-13H-5, 10-10	138.21	11.0	91.3	ND	ND
1262A-13H-5, 20-20	138.31	11.4	94.7	ND	ND
1262A-13H-5, 30-30	138.41	11.1	92.1	ND	ND
1262A-13H-5, 40-40	138.51	11.0	91.7	ND	ND
1262A-13H-5, 50-50	138.61	11.3	94.2	ND	ND
1262A-13H-5, 60-60	138.71	11.2	93.1	ND	ND
1262A-13H-5, 70-70	138.81	10.7	89.1	ND	ND
1262A-13H-5, 80-80	138.91	11.2	93.0	ND	ND
1262A-13H-5, 90-90	139.01	11.1	92.8	ND	ND
1262A-13H-5, 100-100	139.11	11.0	91.2	ND	ND
1262A-13H-5, 110-110	139.21	11.1	92.1	ND	ND
1262A-13H-5, 120-120	139.31	11.1	92.4	ND	ND
1262A-13H-5, 130-130	139.41	10.9	91.1	ND	ND
1262A-13H-5, 140-140	139.51	11.0	91.9	ND	ND

Table T13 (continued).

Hole, core, section, interval (cm)	Depth (mcd)	Inorganic carbon (wt%)*	CaCO ₃ (wt%)*	Total carbon (wt%) [†]	Organic carbon (wt%) [‡]
1262A-13H-5, 148-148	139.59	10.7	88.9	ND	ND
1262A-13H-6, 5-5	139.66	10.7	89.1	ND	ND
1262A-13H-6, 10-10	139.71	10.8	90.1	ND	ND
1262A-13H-6, 15-15	139.76	9.5	78.9	ND	ND
1262A-13H-6, 20-20	139.81	8.2	68.1	ND	ND
1262A-13H-6, 24-24	139.85	5.8	48.7	ND	ND
1262A-13H-6, 27-27	139.88	5.2	43.2	ND	ND
1262A-13H-6, 30-30	139.91	3.3	27.7	ND	ND
1262A-13H-6, 32-32	139.93	1.4	11.4	ND	ND
1262A-13H-6, 35-35	139.96	0.1	0.8	ND	ND
1262A-13H-6, 37-37	139.98	0.1	0.8	ND	ND
1262A-13H-6, 40-40	140.01	0.1	0.4	ND	ND
1262A-13H-6, 43-43	140.04	0.1	0.5	ND	ND
1262A-13H-6, 45-45	140.06	0.1	0.7	ND	ND
1262A-13H-6, 47-47	140.08	0.1	0.7	ND	ND
1262A-13H-6, 48-48	140.09	0.1	0.8	ND	ND
1262A-13H-6, 49-49	140.10	0.1	0.8	ND	ND
1262A-13H-6, 50-50	140.11	0.1	0.7	ND	ND
1262A-13H-6, 51-51	140.12	7.1	58.8	ND	ND
1262A-13H-6, 52-52	140.13	8.6	72.0	ND	ND
1262A-13H-6, 55-55	140.16	9.2	76.9	ND	ND
1262A-13H-6, 60-60	140.21	10.0	82.9	ND	ND
1262A-13H-6, 65-65	140.26	10.1	83.7	ND	ND
1262A-13H-6, 70-70	140.31	10.2	84.6	ND	ND
1262A-13H-6, 75-75	140.36	10.6	88.0	ND	ND
1262A-13H-6, 80-80	140.41	10.3	86.0	ND	ND
1262A-13H-6, 85-85	140.46	10.8	90.0	ND	ND
1262A-13H-6, 90-90	140.51	10.9	90.5	ND	ND
1262A-13H-6, 100-100	140.61	10.6	88.5	ND	ND
1262A-13H-6, 110-110	140.71	10.4	86.5	ND	ND
1262A-13H-6, 120-120	140.81	10.8	90.1	ND	ND
1262A-14H-1, 72-74	143.44	11.4	94.6	11.3	0.0
1262A-14H-3, 72-74	146.44	11.4	94.8	11.4	0.0
1262A-14H-5, 72-74	149.44	11.1	92.2	11.1	0.0
1262A-14H-5, 140-150	150.12	11.1	92.7	10.1	0.0
1262A-15H-1, 72-74	153.88	10.6	88.3	10.5	0.0
1262A-15H-3, 72-74	156.88	10.5	87.5	10.5	0.0
1262A-15H-5, 72-74	159.88	10.8	90.0	10.8	0.0
1262A-15H-5, 140-150	160.56	11.2	93.4	10.7	0.0
1262A-16H-1, 72-74	164.18	10.5	87.4	10.5	0.0
1262A-16H-3, 72-74	167.18	10.6	87.9	10.5	0.0
1262A-16H-5, 72-74	170.18	10.1	83.9	10.0	0.0
1262A-16H-5, 140-150	170.86	10.1	84.1	9.9	0.0
1262A-17H-1, 72-74	173.11	9.9	82.4	9.9	0.0
1262A-17H-3, 72-74	176.11	10.7	89.0	10.7	0.0
1262A-17H-5, 72-74	179.11	10.7	89.3	9.4	0.0
1262B-19H-1, 72-73	179.21	10.9	91.1	10.8	0.0
1262B-19H-3, 72-73	182.21	11.2	93.6	11.1	0.0
1262B-19H-3, 140-150	182.89	10.5	87.1	10.3	0.0
1262B-19H-5, 72-73	185.21	10.5	87.1	10.5	0.1
1262B-20H-1, 72-74	189.95	10.9	90.5	11.1	0.3
1262B-20H-3, 72-74	192.95	9.0	75.2	10.1	1.1
1262B-20H-5, 72-74	195.95	11.7	97.5	10.0	0.0
1262C-11H-5, 140-150	201.42	9.5	79.0	9.6	0.2
1262B-21H-1, 72-74	202.06	11.3	93.7	9.9	0.0
1262B-21H-3, 72-74	205.06	8.8	73.6	8.9	0.1
1262B-21H-5, 72-74	208.06	9.5	79.0	9.5	0.0
1262C-12H-5, 140-150	210.18	8.2	68.3	8.4	0.2
1262B-22H-1, 72-73	212.61	7.2	59.9	7.1	0.0
1262B-22H-3, 72-73	214.37	8.7	72.6	8.3	0.0
1262B-22H-5, 72-73	217.37	7.3	60.4	9.0	1.8
1262B-22H-7, 72-73	220.37	10.2	85.1	10.2	0.0
1262B-23H-1, 72-73	224.30	10.2	84.9	10.2	0.0
1262B-23H-3, 72-73	227.30	10.0	83.3	10.3	0.3
1262B-23H-5, 72-73	230.30	8.3	69.4	9.4	1.1
1262B-23H-5, 140-150	230.98	8.9	74.2	8.2	0.0

Notes: * = measured by carbonate coulometry. † = determined by carbon-hydrogen-nitrogen-sulfur (CHNS) elemental analysis. ‡ = organic carbon values determined by subtracting inorganic carbon from total carbon.

Table T14. Chromatograph peaks identified with GC-MSD analysis of extracted hydrocarbons.

Peak number	Name of compound	Carbon number
1	3, 7, 8-trimethyldodecane	15
2	3, 7, 10-trimethyltetradecane	17
3	3, 7, 12-trimethylhexadecane	19
4	3, 7, 14-trimethyloctadecane	21
5	3, 7, 16-trimethylicosane	23
6	Dodecane	
7	Tridecane	
8	Tetradecane	14
9	Pentadecane	15
10	Hexadecane	16
11	Heptadecane	17
12	Octadecane	18
13	Nonadecane	19
14	Eicosane	20
15	Henicosane	21
16	Docosane	22
17	Tricosane	23
18	3,8-dimethyldecano	12
19	3,9-dimethylundecane	13
20	3,10-dimethyldodecane	14
21	3-methyltridecane	14
22	2,6,10-trimethyldodecane	15
23	3,11-dimethyltridecane	15
24	2,12-dimethyltetradecane	16
25	3,12-dimethyltetradecane	16
26	3-methylpentadecane	16
27	3,11-dimethylpentadecane	17
28	3,13-dimethylpentadecane	17
29	2,6,10,14-tetramethylpentadecane (Pristane)	19
30	3,14-dimethylhexadecane	18
31	3-methylheptadecane	18
32	2,6,10,14-tetramethylhexadecane (Phytane)	20
33	3,13-dimethylheptadecane	19
34	3,15-dimethylheptadecane	19
35	3,8,12-trimethylheptadecane	20
36	3,16-dimethyloctadecane	20
37	3,15-dimethylnonadecane	21
38	3,17-dimethylnonadecane	21
39	3,18-dimethylicosane	22
40	3,17-dimethylheneicosane	
41	3,19-dimethylheneicosane	

Note: GC-MSD = gas chromatography mass selective detector.

Table T15. Age-depth control points, Site 1262. (See table notes.
 Continued on next page.)

Datum	Type	Upper depth (mcd)	Lower depth (mcd)	Minimum age (Ma)	Maximum age (Ma)
T <i>Pseudoemiliania lacunosa</i>	CN	3.07	3.90	0.46	0.46
T <i>Globorotalia tosaensis</i>	PF	4.19	5.12	0.61	0.61
B <i>Gephyrocapsa parallela</i>	CN	6.05	7.04	0.98	1.03
C1n (o)	PMAG	6.15	6.47	0.781	0.781
C1r.1n (y)	PMAG	7.44	7.59	0.988	0.988
C1r.1n (o)	PMAG	7.99	8.17	1.072	1.072
T Large <i>Gephyrocapsa</i>	CN	8.74	9.52	1.22	1.26
Cobb Mountain (y)	PMAG	8.89	9.07	1.173	1.173
Cobb Mountain (o)	PMAG	9.09	9.42	1.185	1.185
B Medium <i>Gephyrocapsa</i> spp.	CN	13.49	13.84	1.69	1.71
C2n (y)	PMAG	15.46	15.56	1.785	1.775
Zone CN1 3a Assemblage	CN	16.01	17.22	1.7	1.8
B <i>Globorotalia truncatulinoides</i>	PF	16.01	22.39	2.02	2.02
C2n (o)	PMAG	16.86	16.96	1.942	1.942
Zone CN1 2aB Assemblage	CN	17.22	35.72	2.83	3.66
C2An.1n (y)	PMAG	24.18	24.39	2.582	2.582
B <i>Globorotalia tosaensis</i>	PF	25.73	31.84	3.35	3.35
T <i>Globorotalia plesiostumida</i>	PF	31.84	35.72	4.15	4.15
C2An.3n (o)	PMAG	35.41	36.61	3.596	3.596
Zone CN1 0c Assemblage	CN	35.72	46.03	4.56	5.05
B <i>Globoconella conomicoza</i>	PF	42.72	46.03	7.12	7.12
B <i>Globorotalia crassaformis</i> (s.l.)	PF	46.03	51.28	4.31	4.31
T <i>Subbotina angiporoidea</i>	PF	68.36	78.12	29.67	29.67
T <i>Ericsonia formosa</i>	CN	75.70	75.87	32.9	32.9
C13n (y)	PMAG	76.67	77.14	33.058	33.058
T <i>Discoaster saipanensis</i>	CN	78.83	79.62	34	34
T <i>Discoaster barbadiensis</i>	CN	78.83	79.62	34.2	34.2
C13n (o)	PMAG	78.92	79.07	33.545	33.545
B <i>Isthmolithus recurvus</i>	CN	81.08	81.24	36.6	36.6
T <i>Globigerinatheka index</i>	PF	83.94	87.97	34.3	34.3
B <i>Globigerinatheka semiinvoluta</i>	PF	87.97	94.13	38.4	38.4
C23n (y)	PMAG	93.01	93.31	50.778	50.778
B <i>Discoaster sublodoensis</i>	CN	93.27	93.72	49.3	49.3
T <i>Morozovella aragonensis</i>	PF	94.13	100.84	43.6	43.6
T <i>Tribrachiatus orthostylus</i>	CN	96.91	97.91	51	51
T <i>Morozovella aequa</i>	PF	104.97	111.40	52.89	52.89
T <i>Subbotina velascoensis</i>	PF	104.97	111.40	53.5	53.5
B <i>Discoaster lodoensis</i>	CN	107.67	108.11	52.4	52.4
B <i>Morozovella lensiformis</i>	PF	111.40	115.69	53.68	53.68
T <i>Subbotina triangularis</i>	PF	111.40	115.69	54.07	54.07
T <i>Discoaster multiradiatus</i>	CN	113.25	113.95	53	53
B <i>Morozovella aragonensis</i>	PF	115.69	120.29	52.3	52.3
B <i>Sphenolithus radians</i>	CN	118.04	118.94	53.3	53.3
B <i>Tribrachiatus orthostylus</i>	CN	118.04	118.94	53.4	53.4
C24n (o)	PMAG	120.42	120.52	53.347	53.347
B <i>Morozovella gracilis</i>	PF	138.01	139.49	54.46	54.46
T <i>Stensioeina beccariiformis</i>	BF	140.04	140.08	55	55
B <i>Morozovella subbotinae</i>	PF	151.93	156.65	55.9	55.9
C25n (y)	PMAG	153.21	153.31	55.904	55.904
B <i>Discoaster multiradiatus</i>	CN	153.76	155.26	56.2	56.2
T <i>Globanomalina pseudomenardii</i>	PF	156.65	161.95	55.9	55.9
T <i>Acarinina mckannai</i>	PF	156.65	161.95	56.3	56.3
B <i>Discoaster okadai</i>	CN	157.22	158.32	56.4	56.4
C25n (o)	PMAG	159.21	159.46	56.391	56.391
B <i>Acarinina soldadoensis</i>	PF	161.95	166.23	56.5	56.5
B <i>Morozovella aequa</i>	PF	161.95	166.23	56.5	56.5
B <i>Heliolithus riedelii</i>	CN	169.39	170.03	57.3	57.3
B <i>Discoaster mohleri</i>	CN	170.03	170.89	57.5	57.5
C26n (y)	PMAG	171.41	171.94	57.554	57.554
C26n (o)	PMAG	173.14	173.57	57.911	57.911
B <i>Acarinina subsphaerica</i>	PF	173.49	177.98	59.2	59.2
B <i>Heliolithus kleinpellii</i>	CN	174.39	175.39	58.2	58.2
B <i>Sphenolithus anarrhopus</i>	CN	175.39	175.89	58.4	58.4
B <i>Acarinina mckannai</i>	PF	177.98	182.36	59.1	59.1
B <i>Morozovella velascoensis</i>	PF	177.98	188.16	60	60
B <i>Heliolithus cantabriae</i>	CN	178.69	179.79	58.8	58.8
B <i>Globanomalina pseudomenardii</i>	PF	182.36	188.16	59.2	59.2
B <i>Morozovella conicotruncata</i>	PF	188.16	198.79	60.9	60.9

Table T15 (continued).

Datum	Type	Upper depth (mcd)	Lower depth (mcd)	Minimum age (Ma)	Maximum age (Ma)
B <i>Morozovella angulata</i>	PF	188.16	198.79	61	61
B <i>Fasciculithus pileatus</i>	CN	190.72	191.42	59.3	59.3
B <i>Fasciculithus</i> spp.	CN	191.66	192.57	60	60
B <i>Sphenolithus primus</i>	CN	192.43	193.33	60.6	60.6
B <i>Chiasmolithus bidens</i>	CN	195.43	196.33	60.7	60.7
C27n (y)	PMAG	195.43	195.63	60.920	60.920
C27n (o)	PMAG	197.83	198.17	61.276	61.276
B <i>Praemurica uncinata</i>	PF	198.79	210.49	61.2	61.2
C28n (y)	PMAG	204.59	204.74	62.499	62.499
C28n (o)	PMAG	209.83	210.03	63.634	63.634
B <i>Chiasmolithus danicus</i>	CN	209.94	210.49	64.2	64.2
C29n (y)	PMAG	210.98	211.08	63.976	63.976
B <i>Cruciplacolithus tenuis</i> s.s.	CN	213.61	213.98	64.5	64.5
B <i>Cruciplacolithus primus</i>	CN	213.98	214.95	64.8	64.8
B <i>Praemurica inconstans</i>	PF	214.62	215.52	63	63
B <i>Subbotina triloculinoides</i>	PF	215.52	216.00	64.5	64.5
T <i>Parvularugoglobigerina eugubina</i>	PF	216.29	216.48	64.9	64.9
B <i>Parvularugoglobigerina eugubina</i>	PF	216.48	216.58	64.97	64.97
B <i>Micula prinsii</i>	CN	221.75	223.98	65.4	65.4
C30n (y)	PMAG	224.29	224.28	65.578	65.578

Notes: T = top, B = bottom. o = oldest, y = youngest. CN = calcareous nannoplankton, PF = planktonic foraminifers, BF = benthic foraminifers, PMAG = paleomagnetic reversals. This table is also available in [ASCII](#).

Table T16. Age model, linear sedimentation rates, and mass accumulation rates, Site 1262.

Age (Ma)	Depth (mcd)	LSR	Growth Factor	Corrected LSR	Dry density (g/cm ³)	CaCO ₃ (wt%)	Total MAR (g/cm ² /k.y.)	CaCO ₃ MAR (g/cm ² /k.y.)	Noncarbonate MAR (g/cm ² /k.y.)
1	7.59	7.59	1.11	6.84	0.74	46.5	0.51	0.236	0.272
2	17.53	9.94	1.11	8.95	1.02	90.7	0.91	0.825	0.085
3	29.16	11.63	1.11	10.48	1.12	90.9	1.17	1.062	0.107
4	37.76	8.60	1.11	7.74	1.17	89.1	0.90	0.806	0.098
5	40.85	3.09	1.11	2.78	1.13	90.4	0.32	0.285	0.030
6	42.59	1.74	1.11	1.57	1.23		0.19		0.193
7	44.10	1.51	1.11	1.36	1.12	92.6	0.15	0.141	0.011
8	45.56	1.46	1.11	1.32					
9	47.00	1.44	1.11	1.30					
10	48.36	1.36	1.11	1.22	0.66	22.3	0.08	0.018	0.063
11	49.63	1.27	1.11	1.14					
12	50.85	1.22	1.11	1.10	0.92	7.3	0.10	0.007	0.094
13	52.04	1.20	1.11	1.08					
14	53.22	1.18	1.11	1.06					
15	54.39	1.17	1.11	1.05	0.91	0.6	0.10	0.001	0.095
16	55.55	1.16	1.11	1.04		0.5			
17	56.70	1.15	1.11	1.04					
18	57.85	1.15	1.11	1.04					
19	59.00	1.15	1.11	1.03	0.95	0.9	0.10	0.001	0.098
20	60.14	1.13	1.11	1.02					
21	61.25	1.11	1.11	1.00					
22	62.34	1.09	1.11	0.99	1.06	1.1	0.10	0.001	0.104
23	63.42	1.08	1.11	0.97					
24	64.48	1.06	1.11	0.95					
25	65.52	1.04	1.11	0.94	1.05	0.8	0.10	0.001	0.098
26	66.56	1.04	1.11	0.93		0.7			
27	67.59	1.03	1.11	0.93					
28	68.64	1.05	1.11	0.95	1.17		0.11		
29	69.74	1.10	1.11	0.99	1.11	42.4	0.11	0.047	0.063
30	71.00	1.26	1.11	1.13					
31	72.43	1.43	1.11	1.29	1.04	71.5	0.13	0.096	0.038
32	74.00	1.57	1.11	1.41					
33	76.51	2.51	1.11	2.26	1.18	79.3	0.27	0.211	0.055
34	79.33	2.82	1.11	2.54					
35	80.03	0.70	1.11	0.63					
36	80.74	0.70	1.11	0.63					
37	81.44	0.70	1.11	0.63	1.12	8.3	0.07	0.006	0.065
38	82.14	0.70	1.11	0.63					
39	82.83	0.69	1.11	0.62					
40	83.52	0.69	1.11	0.62		0.3			
41	84.20	0.68	1.11	0.61	1.01	0.8	0.06	0.001	0.061
42	84.88	0.68	1.11	0.61					
43	85.55	0.67	1.11	0.60					
44	86.21	0.66	1.11	0.60	0.89	0.7	0.05	0.000	0.053
45	86.87	0.66	1.11	0.59					
46	87.53	0.66	1.11	0.59					
47	88.18	0.65	1.11	0.59					
48	88.84	0.66	1.11	0.59					
49	89.53	0.69	1.11	0.62					
50	90.70	1.17	1.11	1.05					
51	97.00	6.30	1.11	5.68	1.20	70.1	0.68	0.478	0.205
52	104.62	7.62	1.11	6.87	1.27	90.4	0.87	0.786	0.083
53	113.60	8.98	1.11	8.09	1.30	95.7	1.05	1.008	0.046
54	128.62	15.02	1.11	13.54	1.30	91.9	1.76	1.615	0.143
55	140.20	11.58	1.11	10.43	1.29	92.6	1.34	1.242	0.100
56	153.84	13.64	1.11	12.29	1.23	93.6	1.51	1.414	0.097
57	165.51	11.68	1.11	10.52	1.22	89.3	1.29	1.150	0.138
58	173.78	8.27	1.11	7.45	1.25	84.6	0.93	0.787	0.144
59	183.60	9.81	1.11	8.84	1.31	89.8	1.16	1.042	0.118
60	192.12	8.52	1.11	7.67	1.28	89.5	0.98	0.877	0.103
61	196.12	4.00	1.11	3.61	1.30	86.3	0.47	0.405	0.064
62	202.13	6.01	1.11	5.41	1.26	86.3	0.68	0.591	0.093
63	207.12	5.00	1.11	4.50	1.26	73.6	0.57	0.417	0.150
64	211.12	4.00	1.11	3.60	1.30	73.6	0.47	0.344	0.123
65	216.60	5.48	1.11	4.94	1.32	66.2	0.65	0.433	0.221

Notes: LSR = linear sedimentation rate, MAR = mass accumulation rate. This table is also available in [ASCII](#).